NASA/CR-1998-206942

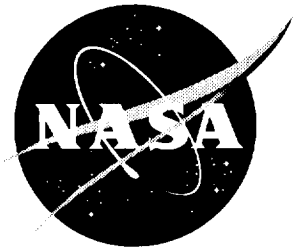

Development of a Simulation Capability for the Space Station Active Rack Isolation System

Terry L. Johnson and Robert H. Tolson
Joint Institute for Advancement of Flight Sciences
The George Washington University
Langley Research Center, Hampton, Virginia

National Aeronautics and
Space Administration

Langley Research Center
Hampton, Virginia 23681-2199

Prepared for Langley Research Center
under Cooperative Agreement NCC1-104

March 1998

Available from the following:

NASA Center for AeroSpace Information (CASI)
800 Elkridge Landing Road
Linthicum Heights, MD 21090-2934
(301) 621-0390

National Technical Information Service (NTIS)
5285 Port Royal Road
Springfield, VA 22161-2171
(703) 487-4650

Abstract

To realize quality microgravity science on the International Space Station, many microgravity facilities will utilize the Active Rack Isolation System (ARIS). Simulation capabilities incorporating ARIS will be needed to predict the microgravity environment to be realized at the various science locations. This paper discusses the development of a simulation tool for use in predicting the performance of the ARIS in attenuating disturbances with frequency content between 0.01 Hz and 10 Hz. The development of a six degree-of-freedom dynamic model of a microgravity facility, built into an International Standard Payload Rack, is presented. The derivation of this model utilizes an energy-based approach. The complete simulation includes the dynamic model of the ISPR integrated with the model for the ARIS controller so that the entire closed-loop system is simulated. Preliminary performance predictions are made for the ARIS in attenuating both off-board (station) disturbances as well as disturbances from hardware mounted onboard the microgravity facility. These predictions suggest that the ARIS does eliminate resonant behavior detrimental to microgravity experimentation. A limited comparison is made between the simulation predictions of ARIS attenuation of off-board disturbances and results from a recent ARIS flight test that was flown on the Space Shuttle. These comparisons show promise, but further tuning of the simulation is needed. The simulation capability presented in this paper is not intended to provide flight-by-flight analysis but rather a means to augment technical understanding of ARIS and to support system studies.

Table of Contents

List of Acronyms

AAA : Air Avionics Assembly

AIT : (Microgravity) Analysis Integration Team

ARIS : Active Rack Isolation System

CDR : Critical Design Review

CM : Center of Mass

DEMUX : Demultiplexer

ISPR : International Standard Payload Rack

ISS : International Space Station

LVLH : Local Vertical Local Horizontal

MIM : Microgravity Vibration Isolation Mount

MUX : Multiplexer

PSD : Power Spectral Density

RMS : Root Mean Square

REF : Rack Equilibrium Frame

RF : Rack (body-fixed) Frame

SEF : Station Equilibrium Frame

SF : Station (body-fixed) Frame

SISO : Single Input Single Output

STABLE : Suppression of Transient Acceleration by Levitation

TEA : Torque Equilibrium Attitude

List of Figures

List of Tables

List of Symbols

General Labeling Convention

If "vector a" is a position vector, then the following general convention applies:

$\bar{a}$	Vector a
$\bar{a}^{\xi}$	Vector a, with components resolved in the ξ frame
$\dot{\bar{a}}^{\xi}$, $\ddot{\bar{a}}^{\xi}$	Velocity vector a and acceleration vector a, with components measured relative to an observer in the ξ frame
$\{a^{\xi}\}$	3x1 matrix representation of $\bar{a}^{\xi}$
$\{a^{\xi}\}^{T}$	Transpose of $\{a^{\xi}\}$
$\{\dot{a}^{\xi}\}$, $\{\ddot{a}^{\xi}\}$	3x1 matrix representation of $\dot{\bar{a}}^{\xi}$, $\ddot{\bar{a}}^{\xi}$

Given the quantity described as "second order tensor A", the following general convention applies:

$\bar{\bar{A}}$	Second order tensor A
$[A]$	3x3 matrix representation of second order tensor A
$[A^{\xi}]$	Second order tensor A, resolved in the ξ frame

Specific Symbols

(All quantities are measured in English units.)

$c\theta$	$\cos\theta$
$[C_N]$	Damping matrix associated with the N^{th} damping element
$[CTOR_N]$	Torsional damping matrix associated with the N^{th} damping element
$[CTRN_N]$	Translational damping matrix associated with the N^{th} damping element
$\bar{d}_N$	Vector pointing from the center of mass of the rack to the connection point of the N^{th} elastic element on the rack
$\bar{d}_{oN}^{\xi}$	Vector $\bar{d}_N$ (resolved along frame ξ) when the system is in the equilibrium configuration
$[d_{oN}^{\xi}]$	Antisymmetric second order tensor of $\bar{d}_{oN}^{\xi}$
$\bar{D}_N$	Vector pointing from the center of mass of the station to the connection point of the N^{th} elastic element on the station
$\bar{D}_{oN}^{\xi}$	Components of the vector $\bar{D}_N$ (resolved along frame ξ) when the system is in the equilibrium configuration
$[D_{oN}^{\xi}]$	Antisymmetric second order tensor of $\bar{D}_{oN}^{\xi}$
F	Rayleigh's Dissipation Function

$F_{EXT,x,y,\text{and } z}$	Components of the external force vector along the local orbital frame
g_0	Acceleration due to gravity at Earth's sea level
G	Gravitational constant
$[I_R]$	Moment of inertia matrix of the rack
$I_{x''}, I_{y''}, I_{z''}$	Elements along the diagonal of $[I_R]$ when the inertia tensor is resolved in the rack body-fixed frame
$[K_N]$	Stiffness matrix associated with the N^{th} elastic element
$[KTOR_N]$	Torsional stiffness matrix associated with the N^{th} elastic element
$[KTRN_N]$	Translational stiffness matrix associated with the N^{th} elastic element
$[l^{R/RE}]$	Orthogonal transformation matrix between the rack equilibrium frame and the rack body-fixed frame
$[l^{RE/L}]$	Orthogonal transformation matrix between the LVLH frame and the rack equilibrium frame
$[l^{R/L}]$	Orthogonal transformation matrix between the LVLH frame and the rack body-fixed frame
$[l^{S/SE}]$	Orthogonal transformation matrix between the station equilibrium frame and the station body-fixed frame
$[l^{SE/L}]$	Orthogonal transformation matrix between the LVLH frame and the station equilibrium frame
L	Origin of the LVLH frame; also used to represent the Lagrangian
$\bar{L}_N$	Unstretched length of the N^{th} elastic element
$\{\Delta L^{\xi}_{oN}\}$	Small extension of the N^{th} umbilical element (resolved along the frame ξ) in the equilibrium condition
m_P	Mass of the P^{th} disturber onboard the rack
M_E	Mass of the Earth
M_Q	Mass of the Q^{th} disturber onboard the station
M_R	Mass of the rack
M_S	Mass of the station
M_{TOTAL}	Total mass of the system
Q_k	Generalized forces associated with the k^{th} generalized coordinate
q_k	Set of k independent generalized coordinates
δq_k	Virtual displacement of q_k
$\bar{r}$	Point where external force, $\bar{F}$, is applied
$\bar{r}_{CM}$	Position vector from center of mass of the Earth to composite center of mass of the system
r_{m_P}	Magnitude of relative position between P^{th} disturber mass and center of mass of the Earth
r_{M_Q}	Magnitude of relative position between Q^{th} disturber mass and center of mass of the Earth

$\vec{r}_P$	Position vector of the P^{th} rack disturber mass measured relative to the rack center of mass
r_R	Magnitude of relative position between rack center of mass and center of mass of the Earth
$\Delta\vec{r}_R$	Perturbed position vector of the rack center of mass, measure relative to the origin of the rack equilibrium frame
$\vec{r}_{RE}$	Position of the rack center of mass, measured relative to the origin of the LVLH frame, when the system is in its equilibrium configuration
r_S	Magnitude of relative position between station center of mass and center of mass of the Earth
$\Delta\vec{r}_S$	Perturbed position vector of the station center of mass, measure relative to the origin of the station equilibrium frame
$\vec{r}_{SE}$	Position of the station center of mass, measured relative to the origin of the LVLH frame, when the system is in its equilibrium configuration
R	Origin of the rack body-fixed frame
$\Delta\vec{R}_N$	Local translational displacement of the station at the station/rack interface
RE	Origin of the rack equilibrium frame
$\vec{R}_Q$	Position vector of the Q^{th} station disturber mass measured relative to the station center of mass
$s\theta$	$\sin\theta$
S	Origin of the station body-fixed frame
SE	Origin of the station equilibrium frame
T	Total kinetic energy of the system; also used as a superscript to denote the transpose of a matrix
T_{TRANS}	Total translational kinetic energy of the system
$\vec{v}_{m_P}$	Velocity vector of the P^{th} disturber mass onboard the rack
$\vec{v}_{M_Q}$	Velocity vector of the Q^{th} disturber mass onboard the station
$\vec{v}_S$	Velocity vector of the station center of mass
$\vec{v}_R$	Velocity vector of the rack center of mass
V	Total potential energy
$\vec{V}_N$	Translational velocity of the connection point of the N^{th} elastic element on the station
$V_{ELASTIC}$	Total elastic energy stored in the system
V_{GRAV}	Total gravitational potential energy of the system
δW	Virtual work
$\{\Delta X_N\}$	Extension (translational and rotational) of the N^{th} elastic element from its unstretched state
$\Delta\vec{X}_N$	Translational displacement of the connection point of the N^{th} elastic element on the station
x,y,z	Orthogonal axes of the LVLH frame
x', y', z'	Orthogonal axes of the rack equilibrium frame
x'', y'', z''	Orthogonal axes of the rack body-fixed frame
X,Y,Z	Orthogonal axes of the inertial frame

Greek Symbols

ε_{ijk}	Permutation symbol
μ_E	Gravitational constant for the Earth
$\theta_1, \theta_2, \theta_3$	Three consecutive small-angle rotations that bring the rack equilibrium frame into alignment with the rack body-fixed frame
$\Delta\vec{\theta}_R$	Small-angle displacement vector representing the deflection of the rack body-fixed frame from the rack equilibrium frame
$\Delta\vec{\theta}_S$	Small-angle displacement vector representing the deflection of the station body-fixed frame from the station equilibrium frame
$\left\{\Delta\theta^{\xi}_{oN}\right\}$	Components of the angular extension of the N^{th} umbilical or actuator assembly, resolved along frame ξ, when the system is in the equilibrium configuration
$\Delta\theta_{x''}, \Delta\theta_{y''}, \Delta\theta_{z''}$	Components of $\Delta\vec{\theta}_R$ resolved along the rack body-fixed frame
$\vec{\omega}_{PERT}$	Perturbed angular velocity of the rack about its center of mass
$\vec{\omega}_R$	Total angular velocity vector of the rack about its center of mass
$\vec{\omega}_S$	Total angular velocity vector of the station about its center of mass
$\vec{\Omega}$	Orbital rate vector
$\Omega_{x'}, \Omega_{y'}, \Omega_{z'}$	Components of the orbital rate vector about the orthogonal axes of the rack equilibrium frame

1. Introduction

One of the primary missions of the International Space Station (ISS) will be to support scientific research in a microgravity environment. This mission statement implies that an environment must be established and maintained on ISS in which body forces on the various microgravity experiments are reduced to acceptable levels. Many of the physical processes that will be investigated in these experiments are very sensitive to body force disturbances. If the proper environment is not realized, the experiment objective will be compromised. Due to the inherent disturbances on any manned space platform, realizing this environment on the station poses a technical challenge that will require on-orbit vibration isolation of the experiments.

The planned strategy for providing an acceptable environment for ISS experiments currently involves the Active Rack Isolation System (ARIS), under development by the Boeing Defense and Space Group. The ARIS is a Space Station subsystem that provides an isolated platform on which microgravity experiments may be mounted. In its most common configuration, the system utilizes an International Standard Payload Rack (ISPR) as the mounting platform and a combination of acceleration, stiffness compensation and position control loops for active isolation of the ISPR from unwanted disturbances.

In order that the ARIS be utilized to its full potential, an understanding of system performance among microgravity payload developers, research management, and the microgravity community is important. Since the ARIS represents a new technology that has not yet been utilized for vibration isolation, many questions related to ARIS

performance remain unanswered. An understanding of the impact of payload configuration to ARIS performance, for example, may lead to methods that can improve the microgravity environment to be realized on orbit. One of the ways to augment such technical knowledge of the ARIS is through computer-based simulation.

The major objective of this research is to build and validate a simulation capability for the ARIS. To meet this major objective, a number of smaller objectives must be realized. Firstly, a firm understanding of the rigid-body dynamics of an ISPR, or microgravity rack, must be established. This is accomplished through a detailed analytical treatment, leading to the subsequent derivation of the rigid-body equations of motion for a microgravity rack in orbit about the Earth. The dynamic model of the ISPR used in the simulation presented in this paper is very similar to that used in a Boeing ARIS simulation. However, to the author's knowledge, such a comprehensive and detailed treatment of the microgravity rack dynamics has not been documented previously.

A second important step in building the current simulation capability is the implementation of an ARIS controller simulation that is then integrated with the dynamic model for the microgravity rack. The simulation tool presented in this paper is based heavily on an ARIS simulation capability currently used by the Boeing Defense and Space Group. In developing the simulation capability presented in this paper, an effort was made to replicate the Boeing controller simulation to the greatest extent possible. This effort represents a first important step in acquiring a valid simulation tool because it lays the groundwork for a simulation architecture that can be utilized to carry out system

studies. Using such a simulation, end users of the ARIS can augment their knowledge of the system and assess the impact of unique facility configurations to ARIS performance.

To validate the current simulation capability, results from the simulation are compared to results from a Boeing ARIS simulation as well as to real performance data from an ARIS flight experiment (flown on a recent shuttle mission). Comparison to results from the Boeing simulation helps to ensure that all of the important control elements are simulated. Comparison of results with real flight data is the final word on whether the simulation is an adequate predictor of ARIS performance.

This paper is divided into ten chapters. After the introduction in Chapter 1, Chapter 2 discusses reasons that vibration isolation is needed if quality microgravity science is to be realized on ISS. Chapter 3 provides a basic problem statement for vibration isolation on orbit, a discussion of general isolation strategies, and a detailed description of the ARIS configuration. Chapter 4 describes the system to be modeled, the application of the energy method as it relates specifically to the system under consideration, and a first step in formulating the quantities needed to derive the system equations of motion. In Chapter 5 the orbital equations of motion for the composite center of mass are derived, and shown to take the form of the familiar set of equations for the two-body problem, with the addition of a forcing function. Chapter 6 discusses the choice of generalized coordinates to describe the local perturbed motion of the microgravity rack, and expands energy functions formulated in Chapter 4 in terms of these generalized coordinates. In Chapter 7 the perturbed equations of motion for the microgravity rack are derived. This chapter provides a detailed description of all terms appearing in the equations of motion and ways to rewrite and simplify these equations.

Chapter 8 introduces the computerized version of the simulation. Details of the ARIS controller simulation are given in this chapter and predictions of the steady state response for the system (in the form of transfer functions) are shown for both the passive system (ARIS inactive) and the active system (ARIS active). Chapter 9 describes the ARIS Risk Mitigation Experiment (RME), an ARIS flight experiment conducted on a recent Space Shuttle mission. The simulation version used to simulate the RME configuration is described and a limited comparison between simulation results and actual flight data is shown. Concluding remarks that summarize the model development and simulation results are given in Chapter 10.

Figure 1 shows a flowchart for the information presented in this paper. The blocks in bold outline represent each of the ten chapters (with the appendices also represented) and the arrows represent the flow of information from one chapter to the next. A brief description of the most significant information passed between chapters is also given.

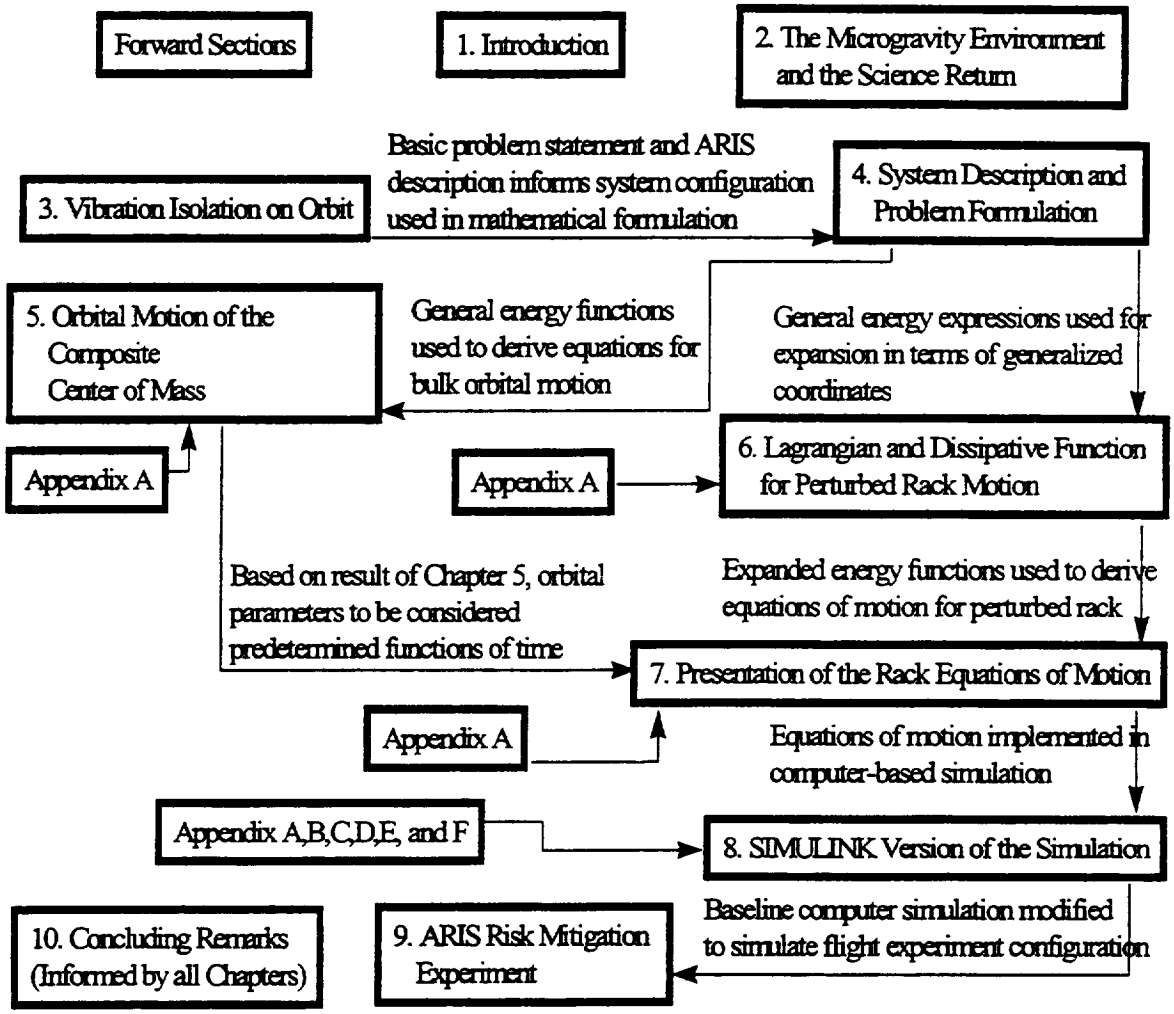

Figure 1: Organization of the Paper

2. The Microgravity Environment and the Science Return

In the this paper, and consistent with the definition in reference 3, the term microgravity environment does not denote a gravity environment at one particular g-level. Instead, the term is used to refer to a general, low-gravity environment, such as that realized on any orbiting space platform. To address the feasibility of microgravity science on ISS, the expected microgravity environment must be characterized and compared to a microgravity requirement deemed suitable for the planned scientific activities. The following discussion describes the typical environment on current manned orbiters and shows that the ISS environment will need to be enhanced if quality microgravity science is to be realized.

2.1 Typical Environment on Manned Orbiters

Although the environment inside orbiting bodies such as the Space Shuttle is many times described as weightless, the acceleration of objects rigidly mounted to the space platform's structure exceeds levels conducive to microgravity science activities. Mounted accelerometers flown on the Space Shuttle and Skylab have recorded accelerations with magnitudes on the order of 10^{-2} g_0 [1]. The symbol g_0 denotes the acceleration due to gravity at the earth's surface. These unsatisfactory acceleration levels are a result of body force disturbances that are always present on the vehicle and have ultimately reduced the value of the science return on past missions [2].

The acceleration levels seen in the space platform's structure are the result of disturbance sources inherent to the vehicle and its orbit. These disturbance sources can

be divided into three major groups [1,3]. One group consists of sudden, transient-type disturbances, which include propulsive maneuvers, the closing of a hatch by a crew member, and other similar events. Another group includes vibratory disturbances – disturbance sources that last for a duration of time and oscillate with frequencies in the range of 0.01 Hz to 300 Hz. Among other things, vibratory disturbance sources include treadmills and other rotating machinery mounted onboard the vehicle. The third group consists of the quasi-steady disturbances – disturbances acting on the vehicle at a sustained force level for a duration of minutes. The major disturbances in this third group are atmospheric drag and gravity gradient. These various disturbance sources transmit forces into the vehicle, which ultimately results in an unacceptable environment in which to conduct microgravity science activities. The primary concern of this study is the prediction of the vibratory disturbance attenuation capability of the ARIS.

2.2 The Microgravity Requirement for Vibratory Disturbances

The microgravity requirement for steady state vibratory acceleration disturbances is shown in Figure 2 (reference 4). The requirement is defined according to the needs of the scientific community. The requirement curve is the result of a compilation of individual requirements for microgravity experimentation across several disciplines.

The current requirement effectively restricts the vibrational disturbance energy that may be present in the environment onboard the vehicle. The requirement consists of forty-five points located at the center frequencies of 1/3 octave bands, which span the frequency spectrum from 0.01 Hz to 300 Hz. The requirement sets a limit on the RMS level of the cumulative disturbance environment across finite frequency intervals of 1/3

octave. To meet the requirement within a given 1/3 octave band, the RMS level of the cumulative oscillatory disturbance in that band cannot exceed the value of the requirement at the center frequency of the given 1/3 octave band.

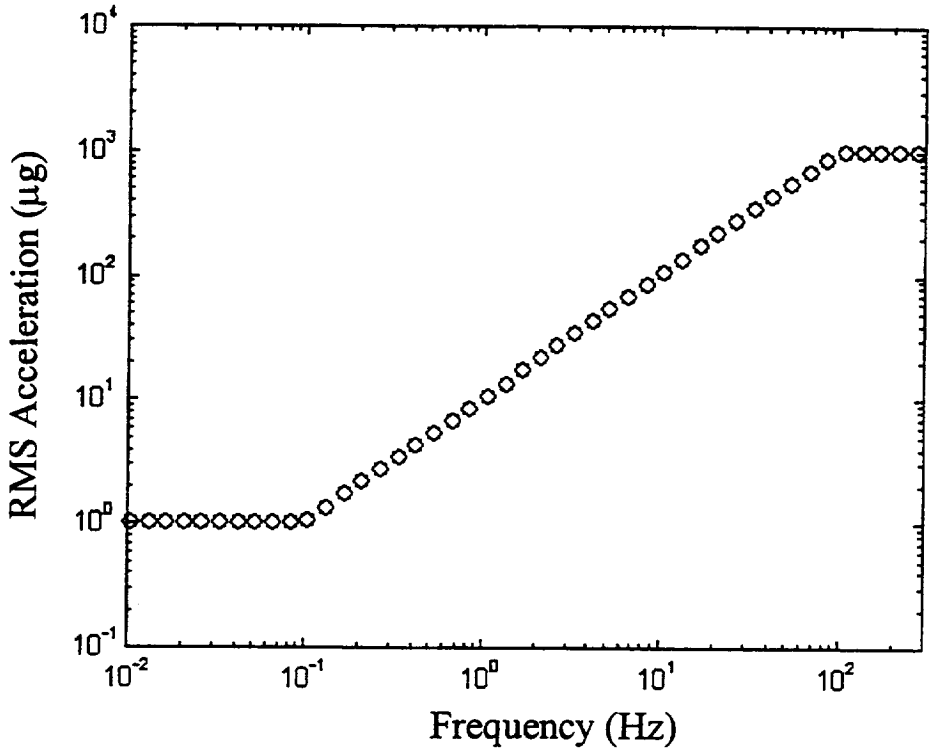

Figure 2: Vibratory RMS Acceleration Limit for Microgravity Experiments per 1/3 Octave Band

Generally the physical processes important to microgravity experiments are most sensitive to acceleration disturbances in the low frequency range [1]. Therefore, the microgravity requirement is most stringent at low frequencies, demanding that the RMS level of the cumulative disturbance to which the experiment is subjected be no greater than 1 micro-g. The increase in the allowable acceleration disturbance with increasing frequency reflects the higher tolerance of the physical processes to high frequency

disturbances. At frequencies of 100 Hz and above, experiments can be subjected to RMS levels of one milli-g.

2.3 Predicted ISS Vibratory Environment

In order to compare the predicted ISS environment to the requirement in Figure 2, a 1/3 octave band RMS representation of the ISS environment must be generated. The formulation of this representation begins with a prediction of the acceleration environment in the time domain. An ISS acceleration environment prediction is currently generated through a NASTRAN model, at the NASA Johnson Space Center, that incorporates the structural and rigid body dynamics of ISS and the various disturbance sources that will be present on orbit. By utilizing the power spectral density (PSD) of the ISS acceleration prediction, an RMS, 1/3 octave band representation is generated (private communication, Steve Del Basso, Microgravity Analysis Integration Team (AIT), June, 1996).

Figure 3 shows the projected ISS (US Lab) acceleration environment in the 1/3 octave band representation (reference 5), plotted with the requirement shown in Figure 2. Also shown is the projected environment at the science location when the ARIS is utilized to attenuate the station disturbances. The projected environment takes into account the major disturbance sources from U.S. on-orbit operations. Note that disturbances from equipment used by international partners are not included in the environment prediction. Figure 3 clearly shows that the ISS acceleration environment is expected to exceed the microgravity requirement, making the use of vibration isolation at the science locations necessary.

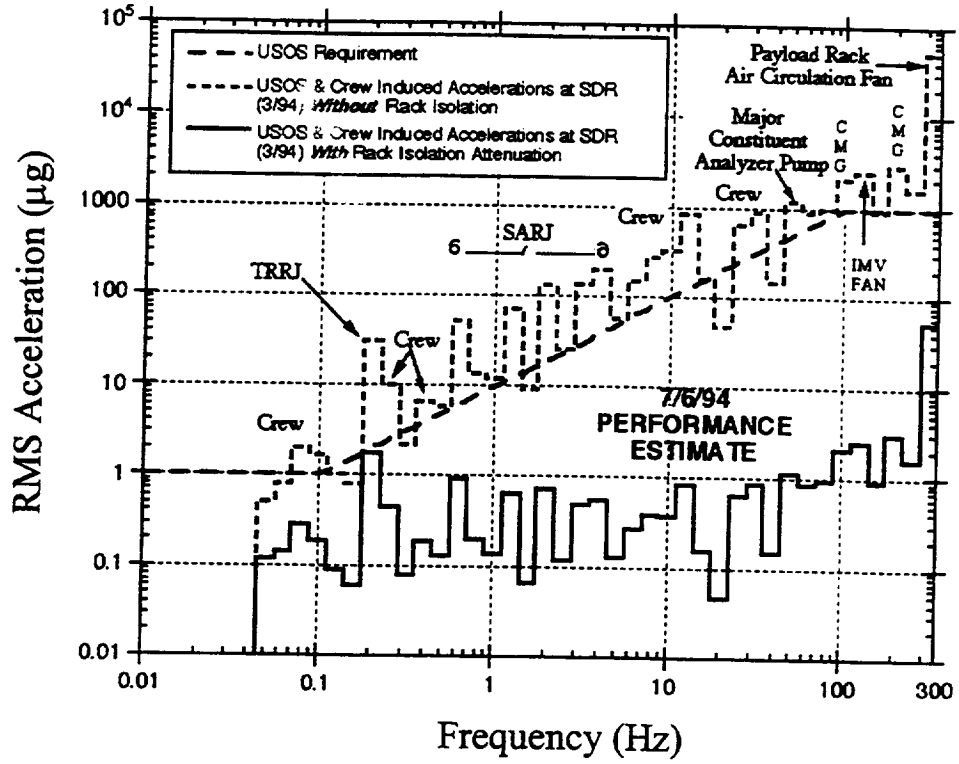

Figure 3: Projected Vibratory Environment Resulting from U.S. On-Orbit Disturbers

3. Vibration Isolation on Orbit

Since the predicted ISS microgravity environment exceeds NASA's microgravity requirement, a strategy for isolating the experiments from ISS must be formulated. Several different systems intended for vibration isolation of experiments on orbit have been developed. Generally these systems attempt to create an acceptable environment inside a rigid-walled container (such as a rack or box) that houses one or more microgravity experiments. The position of the science container is maintained with respect to the station within an allowable sway space. In most cases these systems employ active feedback control to reject the detrimental disturbances that would otherwise degrade the microgravity environment inside of the container.

Examples of isolation systems for use on orbit (other than the ARIS) include the Suppression of Transient Accelerations by Levitation Evaluation (STABLE) system and the Microgravity Vibration Isolation Mount (MIM). The STABLE system was designed and built in a joint effort between McDonnell Douglas Aerospace (circa 1996) and NASA Marshall Space Flight Center. Development of the MIM is headed by the Canadian Space Agency. Both isolation systems employ electromagnetic actuators and active control to isolate the scientific payload [6].

3.1 General Isolation Strategies

The general strategy for vibration isolation from a space platform is shown in Figure 4. The Space Station and the science container are shown as two rigid bodies that are in orbit about the Earth. In the general case, numerous science containers could be

utilized on ISS, ranging from foot-locker-sized boxes to payload-rack-sized facilities. Therefore, the general situation for vibration isolation on orbit involves more than the simple two-body problem illustrated here.

The Space Station and science container are passively coupled via an umbilical assembly as well as by actuators, which are used to control the container motion. In some systems, such as those employing magnetic levitation for control of the container, the passive actuator coupling between the station and the container is not present. The umbilical assembly coupling is generally present, however, in the form of power cords, data transfer cables, vacuum hoses, and other required connections.

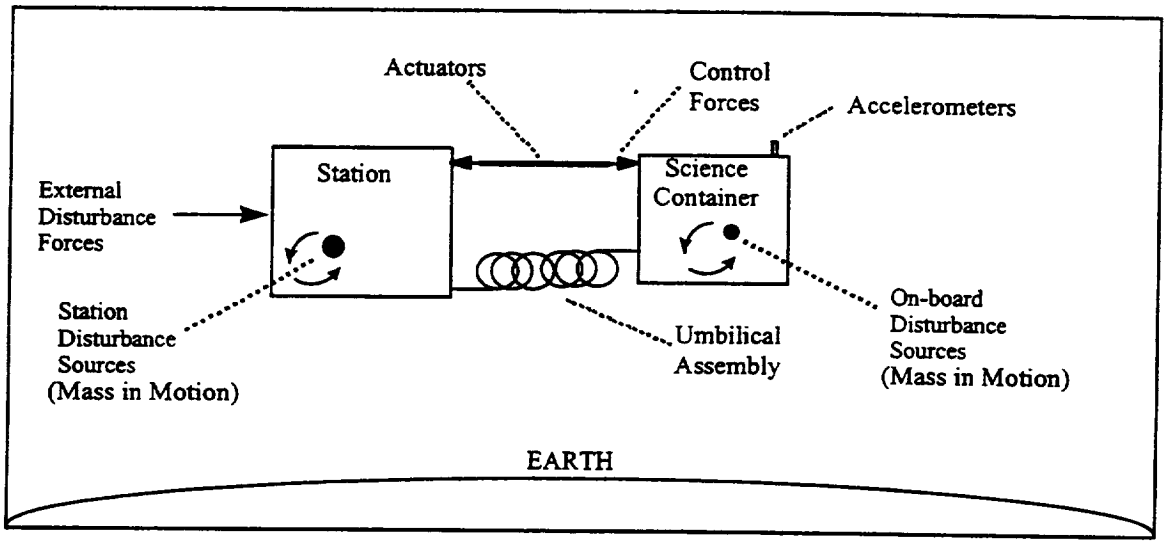

Figure 4: Vibration Isolation on Orbit

The microgravity container must be isolated from two broad classes of disturbances – off-board disturbances, which act on the Space Station, and onboard disturbances, which act directly on the container itself. The off-board disturbances affect the environment inside the container via the umbilical and actuator assemblies, which provide a path by which station body forces can be transmitted. Internal disturbances act

on the container through the hardware mounting interfaces, which are assumed to provide rigid connections between the onboard equipment and the container.

The group of off-board disturbances includes forces external to the station/rack system (such as aerodynamic drag) as well as forces induced by mass in motion inside of the system (such the station's rotating machinery). Onboard disturbances generally result from the science facility's mechanical hardware. These sources may include cooling fans, fluid pumps, tape drive data recorders, and a myriad of other devices with moving parts. The off-board and onboard disturbances sources are represented in Figure 4.

Another source of disturbance, not depicted in Figure 4, is the gravity gradient force. The gravity gradient force arises from the spatial separation between the science container and the composite center of mass of the system. The science container prefers to be in an orbit that is different than that of the composite center of mass of the system but it is tethered to the station via the umbilical assembly. An additional acceleration is therefore induced on the container via the umbilical connection as the container is dragged along by the station [3,7].

To counter the effects of the disturbance sources, a control force (which reacts against the station) is applied to the container. Although passive isolation strategies have been contemplated for the on-orbit isolation problem, active control of the container has been the most popular strategy. The justification for employing an active control system is the ability of such a system to provide a low effective stiffness to isolate against low frequency off-board disturbances, without need for large swayspaces, while also providing high effective stiffness for isolation from disturbances originating within the payload [8]. A passive isolation system cannot adapt itself to provide the same quality of

isolation that can be realized with active control. Passive isolation systems normally have a preset stiffness that cannot be varied in real time. For an isolation problem in which largely contrasting stiffness properties are needed to combat different types of disturbances, this fixed stiffness represents a true shortfall. Further, low stiffness materials (needed for isolation against low frequency disturbances) do not provide sufficient damping [8], which results in large oscillatory amplitudes of the microgravity container when it is subjected to low frequency disturbances. These large amplitudes may result in bumping between the container and the station, which would certainly compromise the environment within the container.

3.2 Description of the Active Rack Isolation System (ARIS)

The ARIS is a state-of-the-art vibration isolation system. The ARIS kit consists of a set of actuators, snubbers, acceleration and position sensors, and controller electronics that interface with an ISPR. The ISPR serves as the science container, on which the various microgravity experiments are mounted. In future sections of this document, the ISPR is many times referred to simply as "the rack".

Figure 5 shows a diagram of the ARIS hardware components interfaced with an ISPR. The production version of the ARIS employs a total of nine accelerometers mounted in three accelerometer assemblies. Two accelerometer triad assemblies (ACCELEROMETER #1 and ACCELEROMETER #2) are located in the bottom portion of the ISPR and another assembly (ACCELEROMETER #3) is mounted on the top of the rack. The orientations of the accelerometers were chosen so that redundancy is built into the system in case of a single or double accelerometer failure.

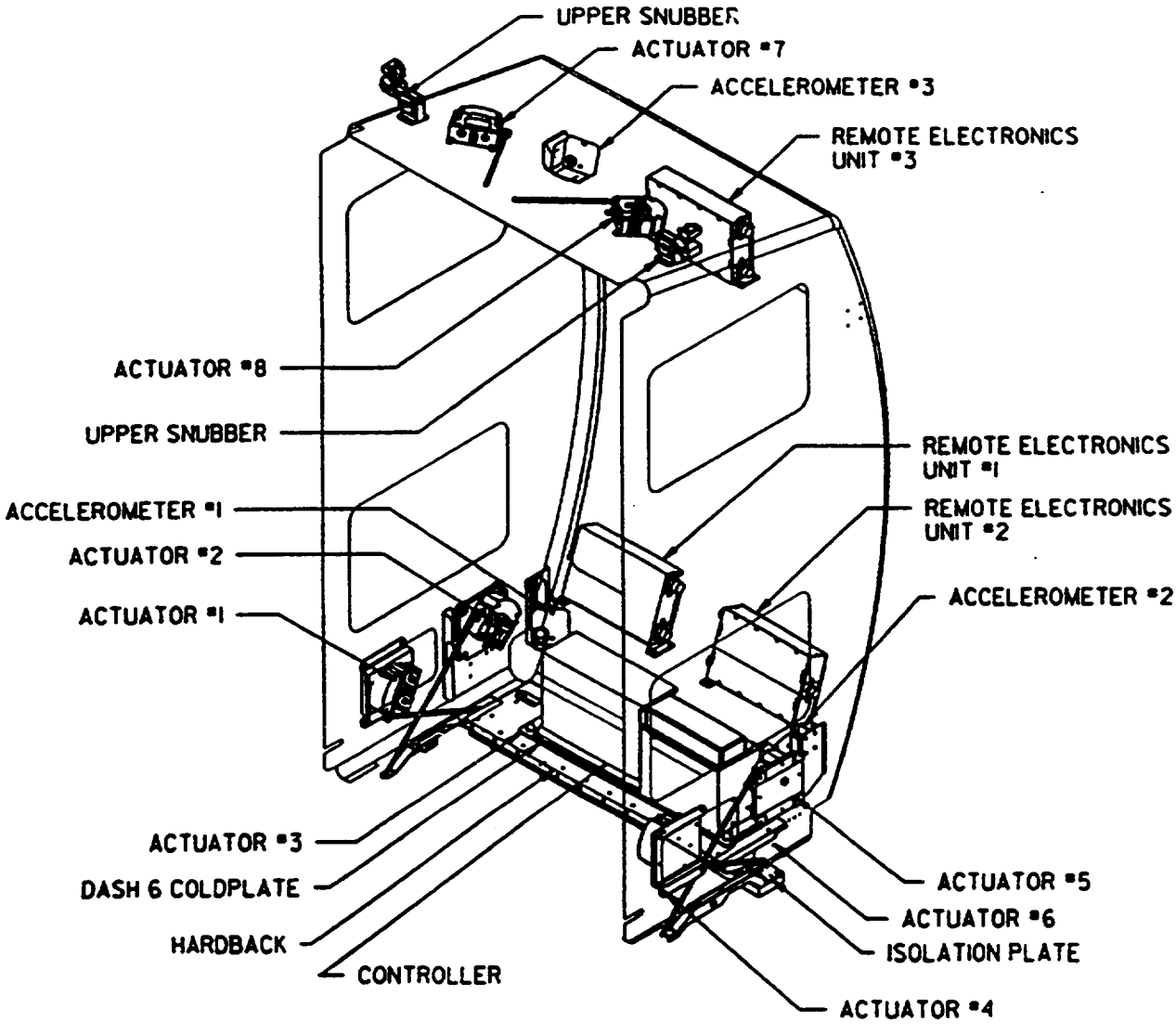

Figure 5: Major Components of the ARIS Mounted on an ISPR

(Source: ARIS Critical Design Review, Huntsville, AL, November 1996)

The ARIS employs eight actuators, also arranged to increase system redundancy. The actuator assemblies consist of a pushrod connected to a voice coil that receives actuation commands from the ARIS controller. An optical position measurement device is built into each actuator mechanism. The position measurements are used by ARIS to maintain the swayspace between the rack and the station wall.

Although estimates of system parameters will be made prior to the launch of the various microgravity facilities, there will be uncertainty in these parameters. To enhance ARIS performance, the design incorporates a payload evaluator, which is a system capable of estimating and updating parameters on orbit. Using known force inputs, accelerometer data and position data are used to accurately determine ISPR mass, CM location, and umbilical stiffness properties in the low-gravity environment. The ARIS controller parameters can then be updated to account for any differences between the parameters measured on orbit and estimates made for those parameters prior to launch.

Another hardware component used in each microgravity facility is the umbilical assembly, shown in Figures 6 and 7. The umbilical assembly connects to the ISPR via a mounting plate that is situated so as not to interfere with the ARIS hardware components. As mentioned before, the umbilical assembly is necessary to provide power, data links, and resources to the microgravity experiments and it is also the main path via which station disturbances are transmitted to the rack. Since the presence of the umbilical assembly greatly affects the dynamic behavior of the rack, the umbilical properties must be modeled correctly if the rack behavior is to be successfully simulated.

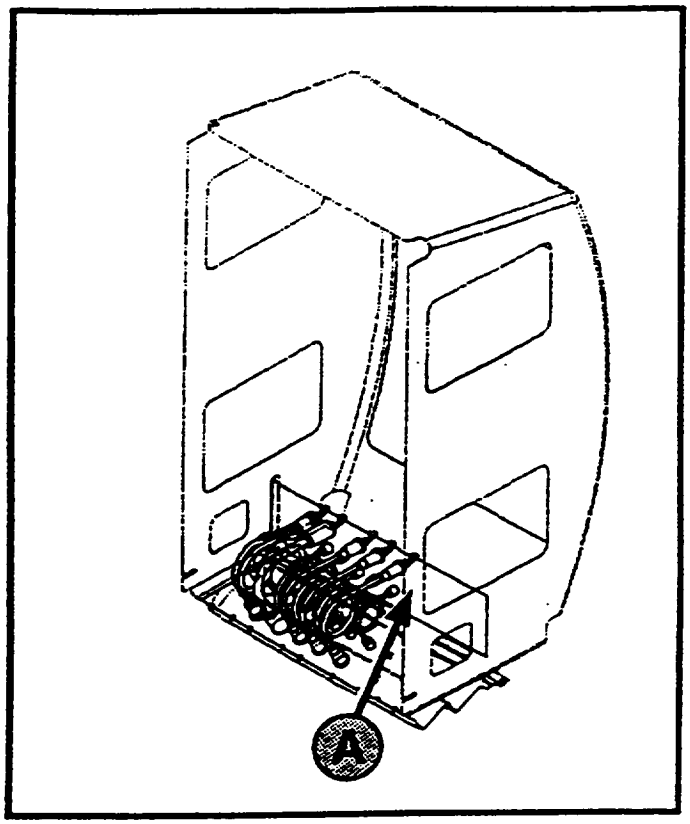

Figure 6: Location and Configuration of the Umbilical Assembly

(Source: LP/S Phase 1 IPT Status Review, August 1995)

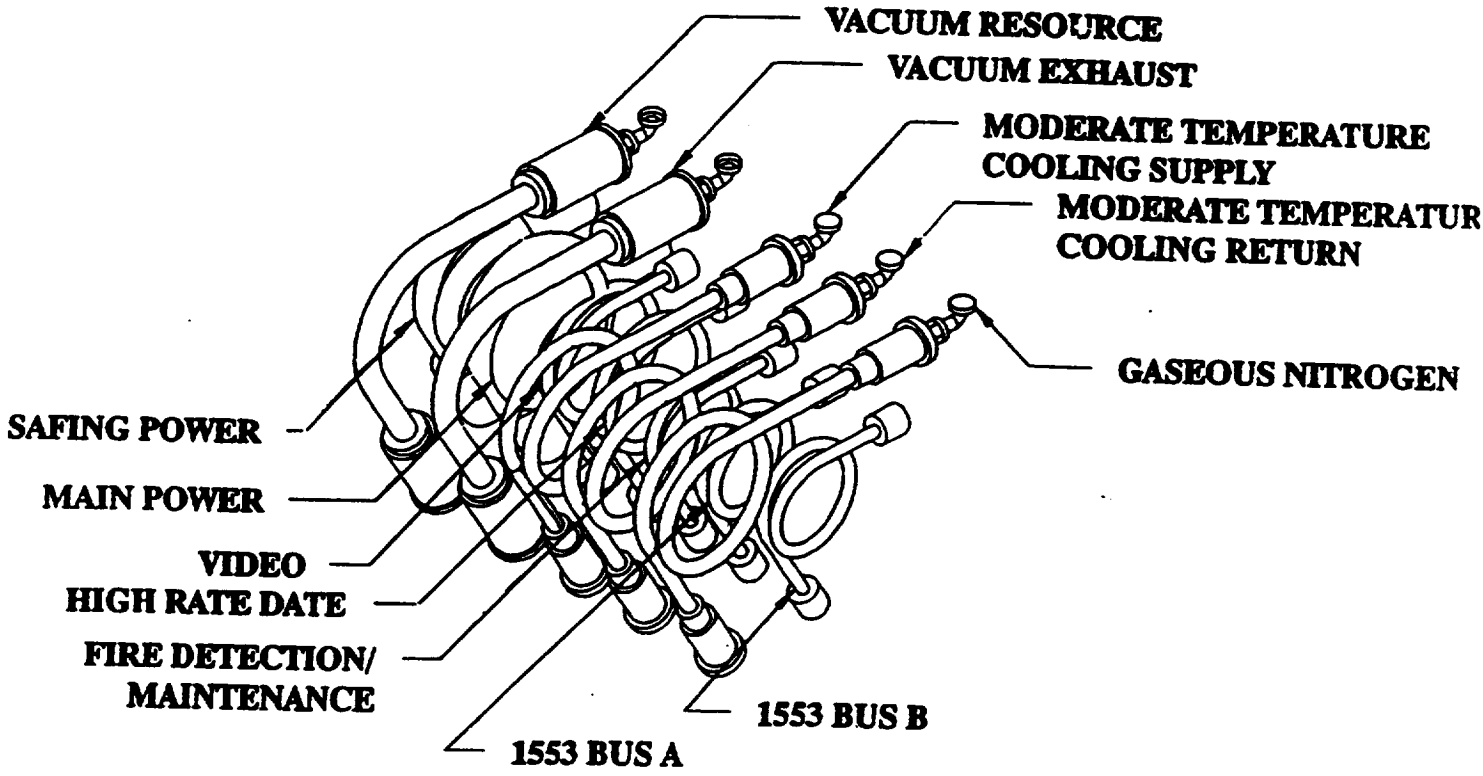

Figure 7: Detailed Diagram of the Umbilical Assembly

(Source: ARIS In-Process Review, Seattle, WA, May 1995)

4. System Description and Problem Formulation

The purpose of this chapter is to provide a description of the station/rack system that is suitable for the subsequent derivation of rigid body equations of motion. In Chapters 5 and 7 of this paper, a Lagrangian approach is used to derive the equations. This approach is an energy-based method that is well suited to problems involving systems with multiple degrees-of-freedom.

4.1 System Configuration

Figure 8 provides a basic description of the system, which is assumed to consist of the station, the rack, a set of disturber masses, and a collection of elastic and dissipative elements. Figure 8 is conceptually similar to Figure 4, but provides a more detailed description of the system. The Space Station is represented by two figures in the left portion of the diagram and the science container is represented by two figures in the right portion. The science container is assumed to be an ARIS rack, although the description given here can be extended to other isolation systems. The set of Q disturber masses onboard the station (M_Q) and the P disturber masses onboard the rack (m_P) represent small point-mass imbalances in rotating equipment such as the ISS centrifuge and the Air Avionics Assembly (commonly known as the AAA fan). The elastic and dissipative elements represent the umbilical assembly and control system actuators through which the rack is tethered to the station.

Figure 8 shows the station/rack system in two different configurations. The figures shown in dashed outlines represent the *equilibrium* configuration of the system.

The equilibrium state is defined as the state of the system in a circular orbit whose orbital rate coincides with the mean angular motion of the actual ISS orbit under consideration. The altitude of the orbit associated with the equilibrium state is taken as the mean of the apoapsis and periapsis altitudes for the actual orbit. In this equilibrium condition, it is assumed that quasi-steady forces (such as aerodynamic drag and gravity gradient) are active on the system and are of constant magnitude and direction over the time interval of interest. No other disturbance sources are active when the system is in this state. External quasi-steady forces actually result in orbit decay and increasing orbit rates over time, but these effects are negligible over the time intervals of interest so that this idealized equilibrium condition can be used. In the equilibrium condition, the station, rack, and all disturber masses are stationary with respect to the center of mass of the composite system (point L) and therefore are stationary with respect to one another. The N^{th} umbilical or (passive) actuator assembly is shown as a spring/damper element with an effective stiffness, $[K_N]$, and an effective damping, $[C_N]$. The spring element connecting the dashed outlines of the station and rack is assumed to be stretched so that the cumulative force in all of the elastic assemblies balances with the quasi-steady forces of the circular orbit.

The scenario depicted by the solid outlines of the two bodies represents the system when vibratory disturbances are active. The station and rack have been displaced to a perturbed state but the center of mass of the system still coincides with point L. In Chapter 5 of this paper, the perturbed motion is decoupled from the predetermined, bulk orbital motion of the system.

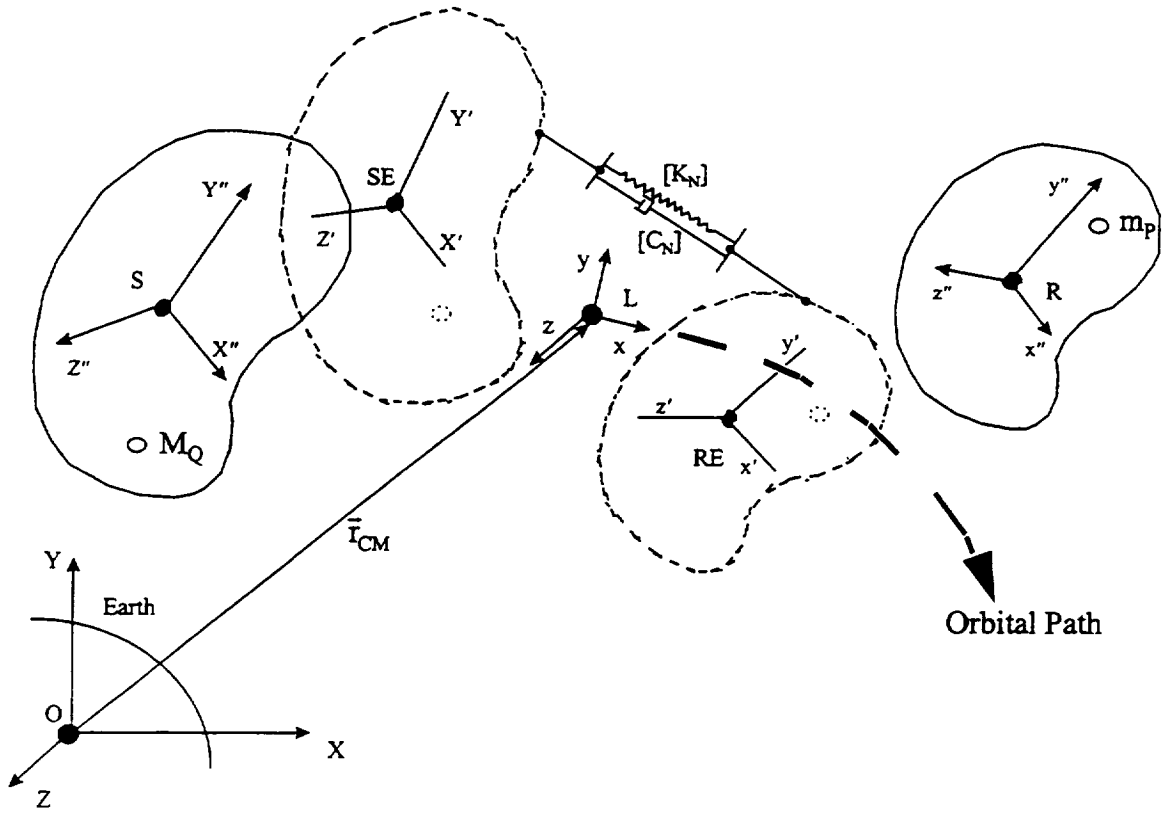

Figure 8: Diagram for Analytic Treatment of the Station/Rack Problem

(Note: To avoid complexity in the diagram, the spring/damper element is not shown connecting the station and rack in the perturbed state; however, the two bodies are always assumed to be connected via this mechanism.)

This analysis employs several different reference frames, which are shown in Figure 8. Reference frame OXYZ has an origin at the center of the Earth and its axes are fixed on distant stars. For the purpose of this study, reference frame OXYZ is considered an inertial frame. A second frame is the local vertical local horizontal (LVLH) frame, which is defined with respect to the system orbit. The origin of the LVLH frame (L) is located at the composite center of mass, with one axis (z) pointing toward the center of the Earth (nadir direction) and another axis (y) perpendicular to the orbital plane. A third frame is the station equilibrium frame (SEF) whose origin (point SE) marks the position

of the center of mass of the station when the system is in the equilibrium configuration and whose orientation represents the nominal orientation of the station's body-fixed axes relative to the LVLH frame. The station is oriented in a Torque Equilibrium Attitude (TEA) in which the body-fixed axis system is not aligned with LVLH. A fourth reference frame is the station body-fixed frame (SF) whose origin (point S) is fixed to the center of mass of the Space Station. The axes of the SF represent the principal axes for the station. When the system is in the equilibrium condition, the axes of the SF are aligned with the axes of the SEF. The rack equilibrium frame (REF) is the counterpart of the SEF and the RF is the counterpart of the SF. However, the axes of the RF do not necessarily coincide with the principal axes of the rack.

4.2 Application of Analytical Mechanics to the Station/Rack System

The purpose of this section is to introduce general expressions for the fundamental quantities necessary in the application of analytical mechanics to the station/rack system. Whereas the vector formulation of the equations of motion relies on the use of vector quantities such as force and momentum, the analytical mechanics approach formulates the problem in terms of quantities such as kinetic and potential energy and work. These quantities are then used in a general form of Lagrange's equations to derive the equations of motion for the system.

For the purpose of this formulation, a general form of the Lagrange equation is introduced as the following [7],

$$\frac{d}{dt}\left(\frac{\partial L}{\partial \dot{q}_k}\right) - \frac{\partial L}{\partial q_k} + \frac{\partial F}{\partial \dot{q}_k} = Q_k \qquad (1)$$

where L is known as the Lagrangian, defined as

$$L = T - V \tag{2}$$

T represents the total kinetic energy of the system and V represents the total potential energy. In Eq. (1) Rayleigh's dissipation function is represented as F and accounts for the velocity-dependent dissipative forces of the system. The symbol q_k represents a set of k independent generalized coordinates, and Q_k represents the generalized forces associated with q_k.

The total kinetic energy of the system shown in Figure 8 is expressed as the sum of the translational and rotational kinetic energies [7],

$$\begin{aligned} T = {} & \frac{1}{2}M_S(\vec{v}_S \bullet \vec{v}_S) + \frac{1}{2}M_R(\vec{v}_R \bullet \vec{v}_R) + \frac{1}{2}\sum_Q M_Q(\vec{v}_{M_Q} \bullet \vec{v}_{M_Q}) + \frac{1}{2}\sum_P m_P(\vec{v}_{m_P} \bullet \vec{v}_{m_P}) \\ & + \frac{1}{2}\{\omega_S\}^T[I_S]\{\omega_S\} + \frac{1}{2}\{\omega_R\}^T[I_R]\{\omega_R\} \end{aligned} \tag{3}$$

where all velocity vectors are measured relative to the inertial reference frame (OXYZ) and the dot symbol ($\bullet$) denotes the inner vector product. Vectors $\vec{v}_S$ and $\vec{v}_R$ are the velocity vectors of the center of mass of the station and the rack, respectively. The quantities $\{\omega_S\}$ and $\{\omega_R\}$ are 3x1 matrices containing components of the angular velocity vectors of the bodies about their own centers of mass. The T superscript denotes the transpose of the matrix. The scalars M_S and M_R represent the mass of the station and rack and $[I_S]$ and $[I_R]$ are 3x3 matrices representing the moment of inertia tensors of each body. Vectors $\vec{v}_{M_Q}$ and $\vec{v}_{m_P}$ are the velocity vectors of the disturber masses,

which are assumed to be predetermined functions of time in the body-fixed frames of the station and rack respectively. The quantities M_Q and m_P are the masses of the Q^{th} station disturber mass and the P^{th} rack disturber mass, respectively. Note that since the disturber masses are considered point masses, they have no rotational kinetic energy about their own centers of mass.

The total potential energy of the system is a combination of the energy stored in the various elastic elements as well as the potential energy due to the position of the system in the Earth's gravitational field. The general expression for the elastic energy stored in the system is

$$V_{ELASTIC} = \frac{1}{2}\sum_N \{\Delta X_N\}^T [K_N]\{\Delta X_N\} \tag{4}$$

where $\{\Delta X_N\}$ is the column vector representing the extension (translational and rotational) of the N^{th} elastic element from its unstretched state and $[K_N]$ is the stiffness matrix associated with this element.

The general expression for the gravitational potential energy is

$$V_{GRAV} = -\mu_E\left(\frac{M_S}{r_S} + \frac{M_R}{r_R} + \sum_Q \frac{M_Q}{r_{M_Q}} + \sum_P \frac{m_P}{r_{m_P}}\right) \tag{5}$$

in which r_S, r_R, r_{M_Q}, and r_{m_P} are the magnitudes of the relative position vectors between the center of mass of the Earth and the centers of mass of the various bodies in the system [9]. Since the mass of the station/rack system is negligible in comparison to the mass of the Earth, the parameter μ_E is

$$\mu_E \approx GM_E \tag{6}$$

where G is the gravitational constant and M_E is the mass of the Earth.

The dissipative function F of Eq. (1) accounts for the dissipative forces in the system that are proportional to the velocities of the bodies. In the case of the station/rack system, these dissipative forces result from the damping effect inherent in the umbilical and passive actuator assemblies. Since the same physical elements are responsible for the elastic and dissipative forces, the form of F appears similar to that of the potential function $V_{ELASTIC}$, and is

$$F = \frac{1}{2}\sum_{N}\left\{\Delta\dot{x}_N\right\}^T\left[C_N\right]\left\{\Delta\dot{x}_N\right\} \tag{7}$$

where $\left\{\Delta\dot{x}_N\right\}$ is the column vector representing the time rate of change of the extension (translational and rotational) of the N^{th} element and $\left[C_N\right]$ is the damping matrix associated with this element [7].

The calculation of the generalized forces Q_k is based on the principle of virtual work. An expression for the virtual work is

$$\delta W = \sum_{k=1}^{n}\left(\sum_{j=1}^{p}\vec{F}_j \bullet \frac{\partial\vec{r}_j}{\partial q_k}\right)\delta q_k \tag{8}$$

where p is total number of forces acting on the system, n is the total number of generalized coordinates, $\vec{F}_j$ is the j^{th} force vector, $\vec{r}_j$ is the point where $\vec{F}_j$ is applied, q_k is the k^{th} generalized coordinate (as in Eq. (1)), and δq_k is the virtual displacement of q_k [7].

The virtual work can also be expressed as the result of the generalized forces Q_k acting over the virtual displacements δq_k

$$\delta W = \sum_{k=1}^{n} Q_k \, \delta q_k \tag{9}$$

so that, by comparison of the previous two equations, the set of generalized forces can be calculated as

$$Q_k = \sum_{j=1}^{p} \bar{F}_j \cdot \frac{\partial \bar{r}_j}{\partial q_k} \tag{10}$$

In the case of the station/rack system, the generalized forces include external forces, such as aerodynamic drag, that are not derivable from a potential function [7].

4.3 Breakdown of System Motion

One of the most important steps in the analytical mechanics approach is choosing a suitable set of generalized coordinates to describe the system motion. The purpose of this section is to introduce a vector breakdown of the translational motion of the system from which a partial set of generalized coordinates may be chosen. The angular coordinates used in the formulation are discussed in Sections 4.4 and 4.5, where a breakdown of the total angular motion of the system is presented. The velocity vectors $\bar{v}_R$, $\bar{v}_{m_P}$, $\bar{v}_S$, and $\bar{v}_{M_Q}$, of Eq. (3), account for the total translational motion of the system as seen by an observer in the inertial frame. This motion can be expressed mathematically as the sum of the motion of the system's center of mass and a perturbed motion of the individual bodies about their respective equilibrium positions.

Figure 9 shows the set of position vectors that are used in this analysis. In this figure the dashed outlines of the bodies in the equilibrium configuration have been omitted to increase the clarity of the diagram. Vector $\vec{r}_{CM}$ points from the center of mass of the Earth to the center of mass of the composite system. The equations of motion for the composite center of mass are derived in Section 5.2 and $\vec{r}_{CM}$ is shown to be a suitable vector for tracking the orbital motion of the system. Vectors $\vec{r}_{SE}$ and $\vec{r}_{RE}$ are fixed in the LVLH frame and represent the position vectors of the origins of the SEF and REF measured from the center of mass of the composite system. Vectors $\Delta\vec{r}_S$ and $\Delta\vec{r}_R$ measure the perturbed displacements of the station and rack from the points SE and RE respectively. Vectors $\vec{R}_Q$ and $\vec{r}_P$ point from the center of mass of the station and rack to the Q^{th} and P^{th} disturber masses. Vectors $\vec{D}_N$ and $\vec{d}_N$ point from the centers of mass of the station and rack to the connection points of the N^{th} umbilical (or actuator) assembly on the respective bodies.

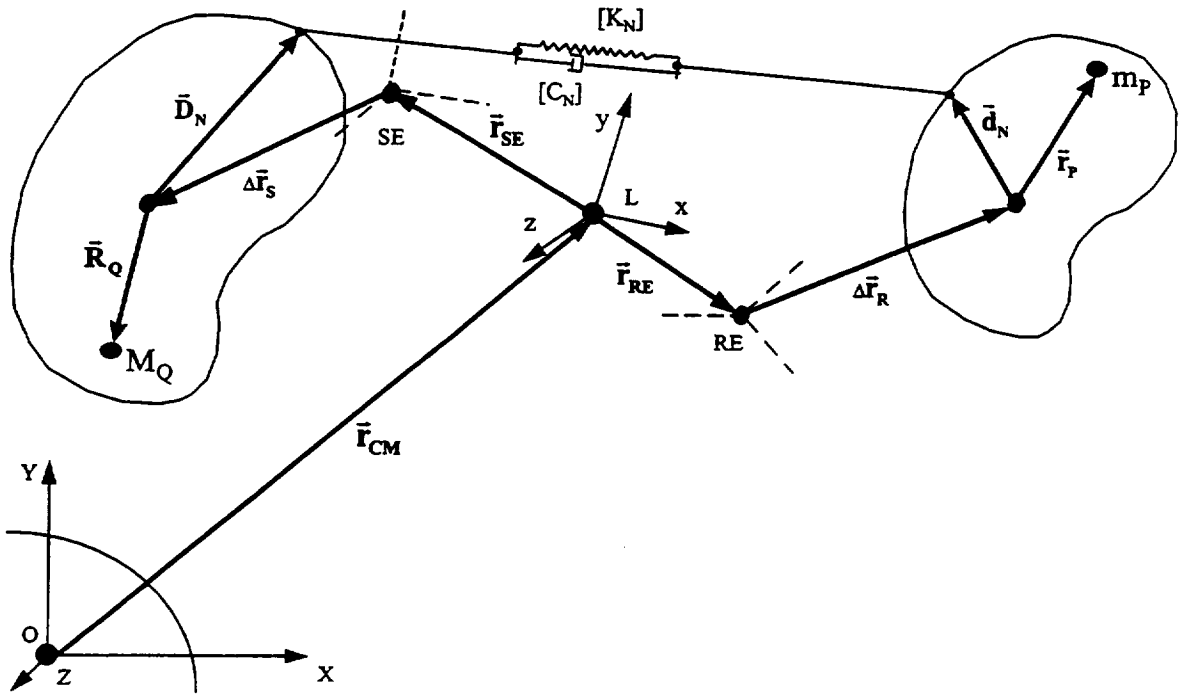

Figure 9: Vectors for Measuring System Motion

4.4 System Kinetic Energy

The purpose of this section is to present a formulation of the kinetic energy expression in terms of motion measured by a local observer (fixed in the LVLH frame). For the system considered in this paper, the composite center of mass is accelerating due to its orbital motion about the Earth. Furthermore, the inertial observer is considered to be fixed in a frame in which a once-per-orbit bulk rotation of the system about its own center of mass is observed. A description of the system motion from the standpoint of a local (noninertial) observer can still be obtained, however, as long as the proper transformations of the inertially measured velocities are performed. This section, along with Sections 4.4, 4.5, and 4.6, set the stage for the subsequent derivation of the equations of motion for the composite center of mass of the system (Section 5.2) as well as the equations of motion for perturbed rack motion (Sections 7.1 and 7.2).

Translational Kinetic Energy

The translational velocity vectors of Eq. (3) may be expressed as the time rate of change of the position vectors shown in Figure 9. The velocity vector for the center of mass of the rack, for example, may be expressed as

$$\vec{v}_R = \dot{\vec{r}}_{CM} + \dot{\vec{r}}_{RE} + \Delta\dot{\vec{r}}_R \tag{11}$$

where all time derivatives in Eq. (11) are calculated in the inertial frame. Similar expressions can be written for the vectors $\vec{v}_{m_p}$, $\vec{v}_S$, and $\vec{v}_{M_Q}$.

A truly local description of the system motion is that motion seen by an observer fixed in the local orbital frame. (The local orbital frame will be denoted by the symbol L

from this point forward.) Although the velocity vectors in Eq. (3) are measured relative to the inertial frame (denoted with the symbol O from this point forward), they may be rewritten as vectors measured relative to a rotating frame by applying the following general transformation,

$$\dot{\bar{x}} = \dot{\bar{x}}' + \bar{\omega} \times \bar{x}' \tag{12}$$

where $\dot{\bar{x}}$ is the time rate of change of any vector measured in the inertial frame and $\dot{\bar{x}}'$ is the rate of change of the vector as measured by an observer in the rotating frame, and $\bar{\omega}$ is the angular velocity of the rotating frame measured relative to inertial space.

To avoid confusion, a new notation will be introduced in the form of a superscript that denotes the frame in which vector and tensor quantities are measured. The superscript will be appended to the vector notation in the following fashion,

$$\bar{x} = \bar{x}^{\xi} \tag{13}$$

Using this notation, the vectors given in Eq. (3) would all take an O superscript. (Further information regarding vector and tensor notation is given in the List of Symbols.)

Applying Eq. (12) to Eq. (11), the rack velocity is written as

$$\bar{v}_R^O = \dot{\bar{r}}_{CM}^L + \bar{\Omega} \times \bar{r}_{CM}^L + \dot{\bar{r}}_{RE}^L + \bar{\Omega} \times \bar{r}_{RE}^L + \Delta\dot{\bar{r}}_R^L + \bar{\Omega} \times \Delta\bar{r}_R^L \tag{14}$$

where vector notation such as $\Delta\dot{\bar{r}}_R^L$ implies the time derivative of the components only, as if the base vectors of L were constant, and notation such as $\Delta\bar{r}_R^L$ simply implies that the components of this position vector have been resolved along the local orbital frame. The symbol $\bar{\Omega}$ is the orbital rate vector. Note that the quantity $\bar{\Omega}$ represents a special case because it is measured by an inertial observer, but the components of this vector are

assumed to be resolved along the local orbital frame so that the cross products of Eq. (14) may be carried out.

Noting that $\dot{\bar{r}}_{RE}^{L} = \bar{0}$, the total translational kinetic energy of the rack and its disturber masses is rewritten in the L frame as

$$\begin{aligned} T_{TRANS,RACK} = & \frac{1}{2} M_R \left(\dot{\bar{r}}_{OM}^{L} + \Delta\dot{\bar{r}}_{R}^{L} + \bar{\Omega} \times \left(\bar{r}_{OM}^{L} + \bar{r}_{RE}^{L} + \Delta\bar{r}_{R}^{L} \right) \right) \cdot \\ & \left(\dot{\bar{r}}_{OM}^{L} + \Delta\dot{\bar{r}}_{R}^{L} + \bar{\Omega} \times \left(\bar{r}_{OM}^{L} + \bar{r}_{RE}^{L} + \Delta\bar{r}_{R}^{L} \right) \right) \\ & + \frac{1}{2} \sum_{P} m_P \left(\dot{\bar{r}}_{OM}^{L} + \Delta\dot{\bar{r}}_{R}^{L} + \dot{\bar{r}}_{P}^{L} + \bar{\Omega} \times \left(\bar{r}_{OM}^{L} + \bar{r}_{RE}^{L} + \Delta\bar{r}_{R}^{L} + \bar{r}_{P}^{L} \right) \right) \cdot \\ & \left(\dot{\bar{r}}_{OM}^{L} + \Delta\dot{\bar{r}}_{R}^{L} + \dot{\bar{r}}_{P}^{L} + \bar{\Omega} \times \left(\bar{r}_{OM}^{L} + \bar{r}_{RE}^{L} + \Delta\bar{r}_{R}^{L} + \bar{r}_{P}^{L} \right) \right) \end{aligned} \tag{15}$$

A similar expression can be written for the kinetic energy of the station and its set of disturber masses.

Rotational Kinetic Energy

The rotation of the station and rack about their respective centers of mass consists of one complete revolution every orbit plus small angle rotations from the equilibrium orientations. The orientation of the station's body-fixed frame (SF) deviates from that of the SEF but attitude requirements limit these deviations to 3.5 degrees, peak-to-peak (private communication, Alan Henry, Microgravity AIT, January, 1997). The rack also rotates through perturbed angular displacements as it oscillates about its equilibrium orientation. However, the stiffness of the umbilical and actuator assemblies limits these deflections to small angle rotations.

The total angular velocity of the rack can be written as the sum of the bulk orbital motion and the perturbed motion,

$$\vec{\omega}_R = \vec{\Omega} + \vec{\omega}_{PERT} \tag{16}$$

where $\vec{\omega}_{PERT}$ is the angular velocity due to perturbed motion. The angular rates given in Eq. (16) must be measured inertially if they are to be substituted into Eq. (3). An expression similar to that of Eq. (16) can also be written for the total angular velocity of the station.

The components of the inertia tensors given in the last two terms of Eq. (3) are time varying-quantities except in the case in which they are resolved in their respective body-fixed frames. If the rotational kinetic energy is to be expressed in terms of the moments of inertia measured in the body-fixed frames, the angular velocities must also be resolved along these frames. It is assumed that the components of the orbital rate vector are known in the local orbital frame so that the total angular velocity of the rack can be expressed in the body-fixed frame through the following transformation,

$$\left\{\omega_R^R\right\} = \left[l^{R/L}\right]\left\{\Omega^L\right\} + \left\{\omega_{PERT}^R\right\} \tag{17}$$

The L and R superscripts denote that the orbit rate and the perturbed angular velocity are resolved in the LVLH and rack body-fixed frame respectively, although these quantities are measured relative to an observer in the inertial frame. The quantity $\left[l^{R/L}\right]$ is an orthogonal transformation matrix that transforms vector components from the L frame to the rack body-fixed frame. Using Eq. (17) the total rotational kinetic energy of the rack can be expressed in matrix notation as the following:

$$T_{ROT,RACK} = \left(\left[l^{R/L}\right]\left\{\Omega^L\right\} + \left\{\omega_{PERT}^R\right\}\right)^T \left[I_R^R\right]\left(\left[l^{R/L}\right]\left\{\Omega^L\right\} + \left\{\omega_{PERT}^R\right\}\right) \tag{18}$$

A similar expression can be written for the rotational kinetic energy of the station.

4.5 System Potential Energy

The total potential energy stored in the station/rack system is the sum of the elastic and gravitational energies given in Eqs. (4) and (5) respectively. The purpose of this section is to rewrite the general expressions given in these equations in terms of the vector quantities shown in Figure 9 and a set of perturbed angular displacement coordinates. The angular displacement coordinates are used to account for the torsional elastic energy stored in the umbilical and actuator assemblies.

Elastic Potential Energy

The elastic elements that tether the rack and the station are assumed to possess a translational stiffness property as well as a torsional stiffness property. Therefore, the total elastic potential energy given in Eq. (4) must include the energy stored due to both of these mechanisms. This energy is accounted for by splitting the quantity represented in Eq. (4) into two parts.

Using the position vectors shown in Figure 9, the energy stored due to the translational stiffness can be written in matrix form as

$$V_{TRN} = \frac{1}{2}\sum_{N}\left(\left\{r_{RE}^{L}\right\}+\left\{\Delta r_{R}^{L}\right\}+\left\{d_{N}^{L}\right\}-\left\{r_{SE}^{L}\right\}-\left\{\Delta r_{S}^{L}\right\}-\left\{D_{N}^{L}\right\}-\left\{L_{N}^{L}\right\}\right)^{T}\cdot \left[KTRN_{N}^{L}\right]\cdot \left(\left\{r_{RE}^{L}\right\}+\left\{\Delta r_{R}^{L}\right\}+\left\{d_{N}^{L}\right\}-\left\{r_{SE}^{L}\right\}-\left\{\Delta r_{S}^{L}\right\}-\left\{D_{N}^{L}\right\}-\left\{L_{N}^{L}\right\}\right) \tag{19}$$

where the small dot symbol denotes matrix multiplication. The L superscript implies that the elements of the matrix quantities are vector and tensor components resolved along the local orbital frame. The quantity $\left\{L_{N}^{L}\right\}$ represents the unstretched length of the N^{th} elastic

element. The matrix quantity $\left[\mathrm{KTRN}_N^L\right]$ is the 3x3 translational stiffness matrix of the N^{th} elastic element.

When the perturbed angular motion of the rack and station are sufficiently small, the angular rates associated with this motion are integrable into components of small angle rotation vectors that measure the deflection of the station and rack body-fixed coordinate systems (SF and RF) from the station and rack equilibrium coordinate systems (SEF and REF). Further details concerning this assumption are given in Chapter 6. Under the assumption of small angle rotations, the stored energy due to pure angular extension of the N^{th} elastic element is

$$V_{TOR} = \frac{1}{2}\sum_N \left(\left\{\Delta\theta_R^L\right\} - \left\{\Delta\theta_S^L\right\} + \left\{\Delta\theta_{oN}^L\right\}\right)^T \left[\mathrm{KTOR}_N^L\right] \left(\left\{\Delta\theta_R^L\right\} - \left\{\Delta\theta_S^L\right\} + \left\{\Delta\theta_{oN}^L\right\}\right) \qquad (20)$$

where the quantities $\left\{\Delta\theta_S^L\right\}$ and $\left\{\Delta\theta_R^L\right\}$ represent the components of the small angle displacement vectors for the station and the rack and $\left\{\Delta\theta_{oN}^L\right\}$ represents the angular extension of the N^{th} umbilical or actuator assembly when the system is in the equilibrium configuration. In the equilibrium configuration, quasi-steady orbital forces are active on the rack and steady-state torques are induced about the rack CM. These torques are partially counteracted by the torsional stiffness property of the elastic elements via the angular displacements $\left\{\Delta\theta_{oN}^L\right\}$. The quantity $\left[\mathrm{KTOR}_N^L\right]$ is the 3x3 torsional stiffness matrix.

Gravitational Potential Energy

The gravitational potential energy of the rack and the set of rack disturber masses is taken from Eq. (5). Using the position vectors from Figure 9, the gravitational potential energy for the rack and its disturber masses is rewritten as

$$V_{GRAV,RACK} = -\mu_E \left(\frac{M_R}{\left| \bar{r}_{CM}^L + \bar{r}_{RE}^L + \Delta\bar{r}_R^L \right|} + \sum_P \frac{m_P}{\left| \bar{r}_{CM}^L + \bar{r}_{RE}^L + \Delta\bar{r}_R^L + \bar{r}_P^L \right|} \right) \tag{21}$$

A similar set of expressions is derivable for the gravitational potential energy of the station and its disturber masses.

4.6 Rayleigh's Dissipation Function

The method used to construct the dissipation function is very similar to that used for the elastic potential energy function. The umbilicals and actuators are assumed to possess a translational damping property as well as a torsional damping property. The dissipation function, represented in Eq. (7), is split into two parts that include contributions from the translational and torsional resistance to motion.

Using the vectors shown in Figure 9, the dissipated energy due to the relative translational velocity of the bodies is written as

$$F_{TRN} = \frac{1}{2} \sum_N \left(\left\{ \Delta\dot{r}_R^L \right\} + \left\{ \dot{d}_N^L \right\} - \left\{ \Delta\dot{r}_S^L \right\} - \left\{ \dot{D}_N^L \right\} \right)^T \left[CTRN_N^L \right] \left(\left\{ \Delta\dot{r}_R^L \right\} + \left\{ \dot{d}_N^L \right\} - \left\{ \Delta\dot{r}_S^L \right\} - \left\{ \dot{D}_N^L \right\} \right) \tag{22}$$

where the L superscript implies that the elements of the matrix quantities are vector components measured in the local orbital frame. The matrix quantity $\left[CTRN_N^L \right]$ is the translational damping matrix of the N^{th} damper element, resolved in the L frame.

The energy dissipated due to pure angular motion of the N^{th} damper element is assumed to be

$$F_{TOR} = \frac{1}{2}\sum_{N}\left(\left\{\Delta\dot{\theta}_R^L\right\} - \left\{\Delta\dot{\theta}_S^L\right\}\right)^T \left[CTOR_N^L\right] \left(\left\{\Delta\dot{\theta}_R^L\right\} - \left\{\Delta\dot{\theta}_S^L\right\}\right) \tag{23}$$

where the quantities $\left\{\Delta\dot{\theta}_S^L\right\}$ and $\left\{\Delta\dot{\theta}_R^L\right\}$ are the time rates of change of the angular displacements given in Eq. (20). The matrix quantity $\left[CTOR_N^L\right]$ is the torsional damping matrix.

5. Orbital Motion of the Composite Center of Mass

5.1 Lagrange's Equations and Indicial Quantities

As a first application of Eq. (1), the equations of motion for the curvilinear translation of the center of mass of the composite system are derived. The set of generalized coordinates chosen for this derivation are the components of the vector $\bar{r}_{CM}$ resolved along the local orbital frame. For this derivation, Eq. (1) is written as

$$\frac{d}{dt}\left(\frac{\partial L}{\partial \dot{r}^L_{CM,\lambda}}\right) - \frac{\partial L}{\partial r^L_{CM,\lambda}} + \frac{\partial F}{\partial \dot{r}^L_{CM,\lambda}} = Q_\lambda \tag{24}$$

where λ is an indicial counter that takes the integer values of 1, 2, and 3 assigned to correspond to the directions x, y, and z (respectively) of the axes of the local orbital frame. In this special case, the generalized coordinates corresponding to $\lambda = 1$ and $\lambda = 2$ are zero because the vector $\bar{r}^L_{CM}$ has a nonzero component only along the z (nadir) direction.

The translational kinetic energy and the gravitational potential energy of the system are the only quantities in the Lagrangian that are functions of the components of $\bar{r}^L_{CM}$ and/or $\dot{\bar{r}}^L_{CM}$. These quantities have been given for the microgravity rack and its disturber masses in Eqs. (15) and (21). The kinetic and gravitational energies of the station and its disturbers have a very similar form. By inspection of Eqs. (19) and (20) it can be seen that the elastic energy stored in the system is a function of the relative displacements between the connection points of the elastic elements on the station and the

rack, and does not depend on the set of generalized coordinates $\left\{r_{CM}^{L}\right\}$. A similar statement can be made for energy dissipated in the umbilical and actuator assemblies in that the dissipation function F includes no elements of the set $\left\{r_{CM}^{L}\right\}$ or $\left\{\dot{r}_{CM}^{L}\right\}$. Likewise, the rotational kinetic energies contain no components of the set $\left\{r_{CM}^{L}\right\}$ or $\left\{\dot{r}_{CM}^{L}\right\}$. Thus, Eq. (24) can be rewritten as

$$\frac{d}{dt}\left(\frac{\partial(T_{TRANS})}{\partial\dot{r}_{CM,\lambda}^{L}}\right)-\frac{\partial(T_{TRANS}-V_{GRAV})}{\partial r_{CM,\lambda}^{L}}=Q_{\lambda} \tag{25}$$

where T_{TRANS} is the total translational kinetic energy of the system and V_{GRAV} is the total gravitational potential energy of the system. These quantities are

$$\begin{aligned}
T_{TRANS} = &\frac{1}{2}M_R\left(\dot{\bar{r}}_{CM}^{L}+\Delta\dot{\bar{r}}_{R}^{L}+\bar{\Omega}\times\left(\bar{r}_{CM}^{L}+\bar{r}_{RE}^{L}+\Delta\bar{r}_{R}^{L}\right)\right)\cdot \\
&\left(\dot{\bar{r}}_{CM}^{L}+\Delta\dot{\bar{r}}_{R}^{L}+\bar{\Omega}\times\left(\bar{r}_{CM}^{L}+\bar{r}_{RE}^{L}+\Delta\bar{r}_{R}^{L}\right)\right) \\
&+\frac{1}{2}\sum_{P}m_P\left(\dot{\bar{r}}_{CM}^{L}+\Delta\dot{\bar{r}}_{R}^{L}+\dot{\bar{r}}_{P}^{L}+\bar{\Omega}\times\left(\bar{r}_{CM}^{L}+\bar{r}_{RE}^{L}+\Delta\bar{r}_{R}^{L}+\bar{r}_{P}^{L}\right)\right)\cdot \\
&\left(\dot{\bar{r}}_{CM}^{L}+\Delta\dot{\bar{r}}_{R}^{L}+\dot{\bar{r}}_{P}^{L}+\bar{\Omega}\times\left(\bar{r}_{CM}^{L}+\bar{r}_{RE}^{L}+\Delta\bar{r}_{R}^{L}+\bar{r}_{P}^{L}\right)\right) \\
&+\frac{1}{2}M_S\left(\dot{\bar{r}}_{CM}^{L}+\Delta\dot{\bar{r}}_{S}^{L}+\bar{\Omega}\times\left(\bar{r}_{CM}^{L}+\bar{r}_{SE}^{L}+\Delta\bar{r}_{S}^{L}\right)\right)\cdot \\
&\left(\dot{\bar{r}}_{CM}^{L}+\Delta\dot{\bar{r}}_{S}^{L}+\bar{\Omega}\times\left(\bar{r}_{CM}^{L}+\bar{r}_{SE}^{L}+\Delta\bar{r}_{S}^{L}\right)\right) \\
&+\frac{1}{2}\sum_{Q}M_Q\left(\dot{\bar{r}}_{CM}^{L}+\Delta\dot{\bar{r}}_{S}^{L}+\dot{\bar{R}}_{Q}^{L}+\bar{\Omega}\times\left(\bar{r}_{CM}^{L}+\bar{r}_{SE}^{L}+\Delta\bar{r}_{S}^{L}+\bar{R}_{Q}^{L}\right)\right)\cdot \\
&\left(\dot{\bar{r}}_{CM}^{L}+\Delta\dot{\bar{r}}_{S}^{L}+\dot{\bar{R}}_{Q}^{L}+\bar{\Omega}\times\left(\bar{r}_{CM}^{L}+\bar{r}_{SE}^{L}+\Delta\bar{r}_{S}^{L}+\bar{R}_{Q}^{L}\right)\right)
\end{aligned} \tag{26}$$

and

$$V_{GRAV} = \frac{-\mu_e M_R}{\left|\bar{r}^L_{CM} + \bar{r}^L_{RE} + \Delta\bar{r}^L_R\right|} + \sum_P \frac{-\mu_e m_P}{\left|\bar{r}^L_{CM} + \bar{r}^L_{RE} + \Delta\bar{r}^L_R + \bar{r}^L_P\right|}$$

$$+ \frac{-\mu_e M_S}{\left|\bar{r}^L_{CM} + \bar{r}^L_{SE} + \Delta\bar{r}^L_S\right|} + \sum_Q \frac{-\mu_e M_Q}{\left|\bar{r}^L_{CM} + \bar{r}^L_{SE} + \Delta\bar{r}^L_S + \bar{R}^L_Q\right|} \tag{27}$$

The generalized forces are calculated from Eq. (10) as

$$\begin{aligned} Q_1 &= Q_x = F_{EXT,x} \\ Q_2 &= Q_y = F_{EXT,y} \\ Q_3 &= Q_z = F_{EXT,z} \end{aligned} \tag{28}$$

where $F_{EXT,x,y,\text{and } z}$ represent the components of the total external forces (not derivable from a potential function) that are acting on the system.

Given the developments up to this point, all of the information needed to derive the equations of motion (from Eq. (25)) has been collected. As a bookkeeping tool, indicial notation is employed to reduce the number of calculations that must be performed. The expressions for the kinetic and potential energies given in Eqs. (26) and (27) can be rewritten in indicial notation as follows:

$$\begin{aligned} T_{TRANS} = \; & \frac{1}{2} M_R \left[\dot{r}^L_{CM,i} + \Delta\dot{r}^L_{R,i} + \varepsilon_{ijk}\Omega_j\left(r^L_{CM,k} + r^L_{RE,k} + \Delta r^L_{R,k}\right)\right] \cdot \\ & \left[\dot{r}^L_{CM,i} + \Delta\dot{r}^L_{R,i} + \varepsilon_{imn}\Omega_m\left(r^L_{CM,n} + r^L_{RE,n} + \Delta r^L_{R,n}\right)\right] \\ & + \frac{1}{2}\sum_P m_P \left[\dot{r}^L_{CM,i} + \Delta\dot{r}^L_{R,i} + \dot{r}^L_{P,i} + \varepsilon_{ijk}\Omega_j\left(r^L_{CM,k} + r^L_{RE,k} + \Delta r^L_{R,k} + r^L_{P,k}\right)\right] \cdot \\ & \left[\dot{r}^L_{CM,i} + \Delta\dot{r}^L_{R,i} + \dot{r}^L_{P,i} + \varepsilon_{imn}\Omega_m\left(r^L_{CM,n} + r^L_{RE,n} + \Delta r^L_{R,n} + r^L_{P,n}\right)\right] \\ & + \frac{1}{2} M_S \left[\dot{r}^L_{CM,i} + \Delta\dot{r}^L_{S,i} + \varepsilon_{ijk}\Omega_j\left(r^L_{CM,k} + r^L_{SE,k} + \Delta r^L_{S,k}\right)\right] \cdot \\ & \left[\dot{r}^L_{CM,i} + \Delta\dot{r}^L_{S,i} + \varepsilon_{imn}\Omega_m\left(r^L_{CM,n} + r^L_{SE,n} + \Delta r^L_{S,n}\right)\right] \end{aligned}$$

$$+\frac{1}{2}\sum_{Q} M_Q\left[\dot{r}^L_{CM,i}+\Delta\dot{r}^L_{S,i}+\dot{R}^L_{Q,i}+\varepsilon_{ijk}\Omega_j\left(r^L_{CM,k}+r^L_{SE,k}+\Delta r^L_{S,k}+R^L_{Q,k}\right)\right]\cdot \tag{29}$$

$$\left[\dot{r}^L_{CM,i}+\Delta\dot{r}^L_{S,i}+\dot{R}^L_{Q,i}+\varepsilon_{imn}\Omega_m\left(r^L_{CM,n}+r^L_{SE,n}+\Delta r^L_{S,n}+R^L_{Q,n}\right)\right]$$

To avoid confusion, subscripts used to identify the vector are in capital letters and have been separated from the indicial notation with a comma. Therefore, all subscripts to the right of the comma are indices that count from 1 to 3. In terms where one index appears twice, a summation across this index is implied. The quantity ε_{ijk} is the permutation symbol defined in Appendix A.

The indicial expression for the gravitational potential energy is

$$V_{GRAV} =$$

$$-\mu_E M_R\left[r^L_{CM,i}r^L_{CM,i}+r^L_{RE,i}r^L_{RE,i}+\Delta r^L_{R,i}\Delta r^L_{R,i}+2r^L_{CM,i}r^L_{RE,i}+2r^L_{CM,i}\Delta r^L_{R,i}+2r^L_{RE,i}\Delta r^L_{R,i}\right]^{-\frac{1}{2}}$$

$$-\mu_E\sum_P m_P\left[r^L_{CM,i}r^L_{CM,i}+r^L_{RE,i}r^L_{RE,i}+\Delta r^L_{R,i}\Delta r^L_{R,i}+r^L_{P,i}r^L_{P,i}\right.$$

$$\left.+2r^L_{CM,i}r^L_{RE,i}+2r^L_{CM,i}\Delta r^L_{R,i}+2r^L_{CM,i}r^L_{P,i}+2r^L_{RE,i}\Delta r^L_{R,i}+2r^L_{RE,i}r^L_{P,i}+2\Delta r^L_{R,i}r^L_{P,i}\right]^{-\frac{1}{2}}$$

$$-\mu_E M_R\left[r^L_{CM,i}r^L_{CM,i}+r^L_{SE,i}r^L_{SE,i}+\Delta r^L_{S,i}\Delta r^L_{S,i}+2r^L_{CM,i}r^L_{SE,i}+2r^L_{CM,i}\Delta r^L_{S,i}+2r^L_{SE,i}\Delta r^L_{S,i}\right]^{-\frac{1}{2}}$$

$$-\mu_E\sum_Q M_Q\left[r^L_{CM,i}r^L_{CM,i}+r^L_{SE,i}r^L_{SE,i}+\Delta r^L_{S,i}\Delta r^L_{S,i}+R^L_{Q,i}R^L_{Q,i}\right.$$

$$\left.+2r^L_{CM,i}r^L_{SE,i}+2r^L_{CM,i}\Delta r^L_{S,i}+2r^L_{CM,i}R^L_{Q,i}+2r^L_{SE,i}\Delta r^L_{S,i}+2r^L_{SE,i}R^L_{Q,i}+2\Delta r^L_{S,i}R^L_{Q,i}\right]^{-\frac{1}{2}} \tag{31}$$

5.2 Equations of Motion

The equations of motion for the composite center of mass are obtained by applying Eq. (25) to the quantities in Eqs. (29) and (31). In presenting the equations of motion, indicial notation is retained but conversion of the equations of motion to vector form is straightforward. The equations of motion are as follows:

$$M_R\Big[\ddot{r}^L_{CM,\lambda}+\Delta\ddot{r}^L_{R,\lambda}+\varepsilon_{\lambda jk}\dot{\Omega}_j\left(r^L_{CM,k}+r^L_{RE,k}+\Delta r^L_{R,k}\right)+2\varepsilon_{\lambda jk}\Omega_j\left(\dot{r}^L_{CM,k}+\Delta\dot{r}^L_{R,k}\right)$$
$$+\varepsilon_{\lambda ji}\Omega_j\varepsilon_{imn}\Omega_m\left(r^L_{CM,n}+r^L_{RE,n}+\Delta r^L_{R,n}\right)\Big]$$

$$+\sum_P m_P\Big[\ddot{r}^L_{CM,\lambda}+\Delta\ddot{r}^L_{R,\lambda}+\ddot{r}^L_{P,\lambda}+\varepsilon_{\lambda jk}\dot{\Omega}_j\left(r^L_{CM,k}+r^L_{RE,k}+\Delta r^L_{R,k}+r^L_{P,k}\right)+2\varepsilon_{\lambda jk}\Omega_j\left(\dot{r}^L_{CM,k}+\Delta\dot{r}^L_{R,k}+\dot{r}^L_{P,k}\right)$$
$$+\varepsilon_{\lambda ji}\Omega_j\varepsilon_{imn}\Omega_m\left(r^L_{CM,n}+r^L_{RE,n}+\Delta r^L_{R,n}+r^L_{P,n}\right)\Big]$$

$$+M_S\Big[\ddot{r}^L_{CM,\lambda}+\Delta\ddot{r}^L_{S,\lambda}+\varepsilon_{\lambda jk}\dot{\Omega}_j\left(r^L_{CM,k}+r^L_{SE,k}+\Delta r^L_{S,k}\right)+2\varepsilon_{\lambda jk}\Omega_j\left(\dot{r}^L_{CM,k}+\Delta\dot{r}^L_{S,k}\right)$$
$$+\varepsilon_{\lambda ji}\Omega_j\varepsilon_{imn}\Omega_m\left(r^L_{CM,n}+r^L_{SE,n}+\Delta r^L_{S,n}\right)\Big]$$

$$+\sum_Q M_Q\Big[\ddot{r}^L_{CM,\lambda}+\Delta\ddot{r}^L_{S,\lambda}+\ddot{R}^L_{Q,\lambda}+\varepsilon_{\lambda jk}\dot{\Omega}_j\left(r^L_{CM,k}+r^L_{SE,k}+\Delta r^L_{S,k}+R^L_{Q,k}\right)+2\varepsilon_{\lambda jk}\Omega_j\left(\dot{r}^L_{CM,k}+\Delta\dot{r}^L_{R,k}+\dot{R}^L_{Q,k}\right)$$
$$+\varepsilon_{\lambda ji}\Omega_j\varepsilon_{imn}\Omega_m\left(r^L_{CM,n}+r^L_{SE,n}+\Delta r^L_{S,n}+R^L_{Q,n}\right)\Big]$$

$$+\frac{\mu_E M_R}{|\vec{r}_{CM}|^3}\left[1+2\frac{|\vec{r}_{RE}+\Delta\vec{r}_R|\cos\alpha}{|\vec{r}_{CM}|}+\left(\frac{|\vec{r}_{RE}+\Delta\vec{r}_R|}{|\vec{r}_{CM}|}\right)^2\right]^{-\frac{3}{2}}\left(r^L_{CM,\lambda}+r^L_{RE,\lambda}+\Delta r^L_{R,\lambda}\right)$$

$$+\sum_P \frac{\mu_E m_P}{|\vec{r}_{CM}|^3}\left[1+2\frac{|\vec{r}_{RE}+\Delta\vec{r}_R+\vec{r}_P|\cos\theta_P}{|\vec{r}_{CM}|}+\left(\frac{|\vec{r}_{RE}+\Delta\vec{r}_R+\vec{r}^{\,L}_P|}{|\vec{r}_{CM}|}\right)^2\right]^{-\frac{3}{2}}\left(r^L_{CM,\lambda}+r^L_{RE,\lambda}+\Delta r^L_{R,\lambda}+r^L_{P,\lambda}\right)$$

$$+\frac{\mu_E M_S}{|\vec{r}_{CM}|^3}\left[1+2\frac{|\vec{r}_{SE}+\Delta\vec{r}_S|\cos\beta}{|\vec{r}_{CM}|}+\left(\frac{|\vec{r}_{SE}+\Delta\vec{r}_S|}{|\vec{r}_{CM}|}\right)^2\right]^{-\frac{3}{2}}\left(r^L_{CM,\lambda}+r^L_{SE,\lambda}+\Delta r^L_{S,\lambda}\right)$$

$$+\sum_Q \frac{\mu_E M_Q}{|\vec{r}_{CM}|^3}\left[1+2\frac{|\vec{r}_{SE}+\Delta\vec{r}_S+\vec{R}_Q|\cos\phi_Q}{|\vec{r}_{CM}|}+\left(\frac{|\vec{r}_{SE}+\Delta\vec{r}_S+\vec{R}_Q|}{|\vec{r}_{CM}|}\right)^2\right]^{-\frac{3}{2}}\left(r^L_{CM,\lambda}+r^L_{RE,\lambda}+\Delta r^L_{R,\lambda}+R^L_{Q,\lambda}\right)$$

$$= F_{EXT,\lambda} \qquad (32)$$

Here the symbol α denotes the angle between the vectors $\vec{r}_{CM}$ and the vector resulting from $\vec{r}_{RE}+\Delta\vec{r}_R$. Note that the $\cos\alpha$ derives from the inner vector (dot) product of $\vec{r}_{CM}$ and the resultant of $\vec{r}_{RE}+\Delta\vec{r}_R$. The angle θ_P is between $\vec{r}_{CM}$ and the resultant of $\vec{r}_{RE}+\Delta\vec{r}_R+\vec{r}_P$ (a vector pointing to the P^{th} disturber mass). The angles β and ϕ_Q have similar definitions but apply to the station and its disturber masses.

Each of the last four (gravitational) terms in Eq. (32) can be expanded in a Taylor series of the following form,

$$f(x) = \left(1 + ax + x^2\right)^{-\frac{3}{2}} \approx 1 - 3ax \tag{33}$$

where, in the first of these terms,

$a = 2\cos\alpha$

and

$$x = \frac{\left|\vec{r}_{RE} + \Delta\vec{r}_R\right|}{\left|\vec{r}_{CM}\right|}$$

so that all higher order terms in $\frac{\left|\vec{r}_{RE} + \Delta\vec{r}_R\right|}{\left|\vec{r}_{CM}\right|}$ are neglected. This approximation is reasonable, given that the rack and station are tethered via umbilical and actuator assemblies that hold the bodies' centers of mass in proximity to the center of mass of the composite system.

The application of Eq. (33) to the first of the gravitational terms in Eq. (32) gives

$$\frac{\mu_E M_R}{\left|\vec{r}_{CM}\right|^3}\left[1 + 2\frac{\left|\vec{r}_{RE} + \Delta\vec{r}_R\right|\cos\alpha}{\left|\vec{r}_{CM}\right|} + \left(\frac{\left|\vec{r}_{RE} + \Delta\vec{r}_R\right|}{\left|\vec{r}_{CM}\right|}\right)^2\right]^{-\frac{3}{2}}\left(r^L_{CM,\lambda} + r^L_{RE,\lambda} + \Delta r^L_{R,\lambda}\right)$$

$$\approx \frac{\mu_E M_R}{\left|\vec{r}_{CM}\right|^3}\left[1 - 3\frac{\left|\vec{r}_{RE} + \Delta\vec{r}_R\right|\cos\alpha}{\left|\vec{r}_{CM}\right|}\right]\left(r^L_{CM,\lambda} + r^L_{RE,\lambda} + \Delta r^L_{R,\lambda}\right)$$

$$\approx \frac{\mu_E M_R r^L_{CM,\lambda}}{\left|\vec{r}_{CM}\right|^3} + \frac{\mu_E M_R\left(r^L_{RE,\lambda} + \Delta r^L_{R,\lambda}\right)}{\left|\vec{r}_{CM}\right|^3} \qquad \text{for} \quad \lambda = 1,2$$

$$\approx \frac{\mu_E M_R r^L_{CM,\lambda}}{\left|\vec{r}_{CM}\right|^3} - \frac{2\mu_E M_R\left(r^L_{RE,\lambda} + \Delta r^L_{R,\lambda}\right)}{\left|\vec{r}_{CM}\right|^3} \qquad \text{for} \quad \lambda = 3$$

(34)

where higher order terms have again been eliminated. Expansions similar to that shown in Eq. (34) can be carried out for the other gravitational terms in Eq. (32).

Since the point L (to which the vector $\bar{r}_{CM}$ points) is located at the composite center of mass of the system, a special relationship exists for the positions of the centers of mass of the various bodies relative to this point. Referring to Figure 9, this relationship can be expressed as the following:

$$M_R\left(\bar{r}_{RE}+\Delta\bar{r}_R\right)+\sum_P m_P\left(\bar{r}_{RE}+\Delta\bar{r}_R+\bar{r}_P\right)+M_S\left(\bar{r}_{SE}+\Delta\bar{r}_S\right)+\sum_Q M_Q\left(\bar{r}_{SE}+\Delta\bar{r}_S+\bar{R}_Q\right)=\bar{0} \tag{35}$$

From Eq. (35) the following relation is derived.

$$M_R\left(\ddot{\bar{r}}^O_{RE}+\Delta\ddot{\bar{r}}^O_R\right)+\sum_P m_P\left(\ddot{\bar{r}}^O_{RE}+\Delta\ddot{\bar{r}}^O_R+\ddot{\bar{r}}^O_P\right)+M_S\left(\ddot{\bar{r}}^O_{SE}+\Delta\ddot{\bar{r}}^O_S\right)+\sum_Q M_Q\left(\ddot{\bar{r}}^O_{SE}+\Delta\ddot{\bar{r}}^O_S+\ddot{\bar{R}}^O_Q\right)=\bar{0} \tag{36}$$

Eqs. (35) and (36) can be used to eliminate a number of terms in Eq. (32).

The acceleration vectors of Eq. (36) can be transformed using the relation

$$\ddot{\bar{x}}^O=\ddot{\bar{x}}^L+2\bar{\Omega}\times\dot{\bar{x}}^L+\dot{\bar{\Omega}}\times\bar{x}^L+\bar{\Omega}\times\left(\bar{\Omega}\times\bar{x}^L\right) \tag{37}$$

where Eq. (37) is derivable from the transformation given in Eq. (12). If Eq. (36) is transformed according to Eq. (37) and substituted (along with Eq. (35)) into Eq. (32), the vector equation of motion for the composite center of mass becomes

$$\ddot{\bar{r}}_{CM}+\frac{\mu_E\bar{r}_{CM}}{\left|\bar{r}_{CM}\right|^3}=\frac{\bar{F}_{EXT}}{M_{TOTAL}} \tag{38}$$

where all vector quantities are measured and resolved in the inertial frame.

The homogeneous form of the differential equation given in Eq. (38) is the well-known equation of motion of the two-body problem. One of the bodies is the Earth and the other is the entire station/rack system. In this case, the mass of the Earth is so large

compared to that of the station/rack system that the homogeneous form of Eq. (38) reflects the central-force motion of the station/rack system in orbit. The term on the right-hand side of Eq. (38) is the total disturbing acceleration due to any force not included in the central force term (e.g. drag and solar pressure).

Although Eq. (38) is nonlinear, general analytical solutions of the homogeneous form of the equation are attainable [9]. Furthermore, well-known methods are available for dealing with the case in which disturbing forces are present. For the purpose of this study, the orbital motion of the composite center of mass of the station/rack system is considered a predetermined function of time. One advantage of making this assumption is that the equations for the orbital motion need not be integrated in order to solve for the station and rack motion, leaving only the local perturbed motion of the system as unknown. Although orbital coupling terms still appear in the equations for the perturbed motion, these terms are either quasi-steady in nature or they are small enough to disregard. Accurate estimations of the quasi-steady terms can be made through knowledge of the ISS orbital parameters. These predetermined, quasi-steady orbital terms can be treated as DC signals over the time interval of interest, which, when considering vibratory behavior, is usually of 100 second duration or less.

6. Lagrangian and Dissipative Function for Perturbed Rack Motion

The purpose of this chapter is to present a suitable choice of generalized coordinates to be used in deriving rigid body equations of motion for the microgravity rack and to rewrite the Lagrangian in terms of these generalized coordinates and quantities that are assumed to be predetermined functions of time. In the previous chapter, the equations of motion for translation of the composite center of mass were derivable from a general form of the Lagrangian. Unknown quantities appearing in the Lagrangian did not preclude the derivation of Eq. (38). Examples of these quantities include the elements of the P^{th} disturber mass velocity $\left\{\dot{r}_P^L\right\}$, which appear indicially in Eq. (29). As before, the notation $\left\{\dot{r}_P^L\right\}$ represents the components of the disturber mass velocity measured by an observer in the LVLH (L) frame. The disturbing equipment is assumed to be hard mounted to the rigid chassis of the rack and the motion of the P^{th} disturber mass is assumed to be a known function of time in the rack body-fixed frame only. As the rack tilts from its equilibrium orientation, it carries with it the disturber masses. Since this perturbed motion of the rack is unknown, the quantity $\left\{\dot{r}_P^L\right\}$ is also unknown. In retrospect Eq. (38) shows that the coordinates $\left\{r_{CM}\right\}$ are independent of the system's internal mass motion, so that detailed information about internal motion is unnecessary in deriving equations of motion for the composite center of mass.

The primary issue addressed in this paper is the vibratory disturbance attenuation capability of the ARIS. The vibratory behavior of the rack is primarily a function of the characteristics of the umbilical and actuator assemblies, the vibratory acceleration

environment onboard the station, and the forces induced by disturber mass motion. Therefore, detailed descriptions of umbilical and actuator parameters and internal mass motion are required.

6.1 Choice of Generalized Coordinates

The methodology employed in Chapter 4, in which the system motion is broken into the bulk motion of the composite system and a perturbed motion of the individual bodies, reveals an adequate description from which a set of generalized coordinates can be chosen. The minimum number of independent generalized coordinates needed to describe the motion of a given system is

$$n = N - c \tag{39}$$

where N is the number of degrees of freedom of the unconstrained system and c is the number of kinematic constraints [7].

For the remainder of this paper, the motion of the station is considered a predetermined function of time that remains unaffected by the motion of the rack. This assumption is justified by the large mass ratio between the two bodies. In the assembly-complete configuration, the station mass is 500 times greater than that of the most massive microgravity facility. Therefore, the only motion that is assumed unknown is the perturbed motion of the microgravity rack. (The bulk orbital motion of the rack is assumed to be given in Eq. (38)). Since the rack has six degrees of freedom as a rigid body, N = 6. Since no kinematic constraints have been placed on its perturbed motion, c=0; thus n=6.

From the standpoint of an observer in the local orbital frame, the perturbed motion of the rack may be considered oscillatory motion about a position of equilibrium. The perturbed motion results in small translational excursions as well as small attitude deviations of the rack body-fixed frame from the rack equilibrium frame. The perturbed translational displacement is measured with the set of components $\{\Delta r_R\}$, while the attitude deviation is contained in the transformation matrix $[l^{R/L}]$ given in Eq. (18). The components of the displacement vector $\Delta\vec{r}_R$, resolved along a chosen set of axes, represent a suitable choice of generalized coordinates for translational motion. In the special case in which the angular motion of the body is small, the perturbed angular velocity vector $\vec{\omega}_{PERT}$ is integrable into an angular displacement vector, and Lagrange's equation may be applied directly [7]. This small-angle assumption was applied to the potential energy expression in Eq. (20) and can be used to choose a suitable set of generalized coordinates to represent the rotational degrees of freedom of the rack.

For the purpose of this study, the generalized coordinates are chosen to be the perturbed translational displacements of the rack resolved along the local orbital frame and the perturbed angular displacements resolved along the rack body-fixed frame. The reason for choosing the angular displacements resolved along the RF is that the moments of inertia for the rack are time invariant in that frame. The translational displacements are represented by the set $\{\Delta r_R^L\}$, which tracks the motion of the rack center of mass. The rotational displacements are represented by the set $\{\Delta\theta_R^R\}$, which measures the angular deflection of the rack body-fixed frame from the rack equilibrium frame.

6.2 Approximating Expression for the Lagrangian

With regard to the application of Eq. (1) to derive the equations for perturbed rack motion, suitable approximations of the kinetic and potential energy functions are realized through a Taylor expansion of the exact expressions for these functions. Since application of Lagrange's equation reduces the order of the energy functions by one in the generalized coordinates, linear equations of motion are realized by retaining quadratic terms in the generalized coordinates.

The general expression for the Taylor expansion in n variables $(q_1,q_2,...,q_n)$ is

$$\begin{aligned} f(q_1,q_2,...,q_n) = f(c_1,c_2,...,c_n) &+ \sum_{r=1}^{n}\left(\frac{\partial f}{\partial q_r}\right)(q_r - c_r) \\ &+ \frac{1}{2!}\sum_{r}^{n}\sum_{s}^{n}\left(\frac{\partial^2 f}{\partial q_r \partial q_s}\right)(q_r - c_r)(q_s - c_s) \\ &+ \frac{1}{3!}\sum_{r}^{n}\sum_{s}^{n}\sum_{i}^{n}\left(\frac{\partial^3 f}{\partial q_r \partial q_s \partial q_i}\right)(q_r - c_r)(q_s - c_s)(q_i - c_i)+... \end{aligned} \tag{40}$$

where $c_1,c_2,...,c_n$ represent the point about which the expansion is carried out. For the purpose of this study, the point $c_1,c_2,...,c_n$ is taken to correspond to the equilibrium position. Note that the partial derivatives are evaluated at the point $q_1 = c_1$, $q_2 = c_2$, etc. [10].

Rotational Kinetic Energy

The rotational kinetic energy of the rack was given in Eq. (18) as

$$T_{ROT,RACK} = \left(\left[I^{R/L}\right]\left\{\Omega^L\right\} + \left\{\omega^R_{PERT}\right\}\right)^T \left[I^R_R\right]\left(\left[I^{R/L}\right]\left\{\Omega^L\right\} + \left\{\omega^R_{PERT}\right\}\right)$$

The transformation matrix $\left[l^{R/L}\right]$ can be interpreted as being composed of two parts. The first part represents a (large angle) time-invariant transformation from the L frame to the rack equilibrium frame, and the second part represents a time varying transformation from the REF to the RF so that

$$\left[l^{R/L}\right]=\left[l^{R/RE}\right]\left[l^{RE/L}\right] \tag{41}$$

where the transformation matrix $\left[l^{R/RE}\right]$ is

$$\left[l^{R/RE}\right]=\begin{bmatrix} c\theta_2 c\theta_3 & c\theta_1 s\theta_3 + s\theta_1 s\theta_2 c\theta_3 & s\theta_1 s\theta_3 - c\theta_1 s\theta_2 c\theta_3 \\ -c\theta_2 s\theta_3 & c\theta_1 c\theta_3 - s\theta_1 s\theta_2 s\theta_3 & s\theta_1 c\theta_3 + c\theta_1 s\theta_2 s\theta_3 \\ s\theta_2 & -s\theta_1 c\theta_2 & c\theta_1 c\theta_2 \end{bmatrix} \tag{42}$$

Here θ_1, θ_2, and θ_3 represent three consecutive (small-angle) rotations that bring the REF axis system into alignment with the RF axes. Under the assumption of small angle rotations the angles θ_1, θ_2, and θ_3 are the same as those represented by the set of generalized coordinates $\left\{\Delta\theta_R^R\right\}$. The notation $s\theta$, $c\theta$ is used to represent $\sin\theta$ and $\cos\theta$, respectively. The transformation matrix $\left[l^{RE/L}\right]$ transforms the components of a vector resolved in the L frame into components resolved along the REF. The elements of $\left[l^{RE/L}\right]$ have the same functional form as those of $\left[l^{R/RE}\right]$ but the perturbed rotations θ_1, θ_2, and θ_3 from Eq. (42) are replaced with a set of time-invariant large-angle rotations.

The components of the perturbed angular velocity, resolved along the rack body-fixed frame, can be expressed in terms of the angles θ_1, θ_2, and θ_3 and their time rates of change. The angular velocity components are given as

$$\begin{Bmatrix} \omega_{PERT,x''} \\ \omega_{PERT,y''} \\ \omega_{PERT,z''} \end{Bmatrix} = \begin{bmatrix} c\theta_2 c\theta_3 & s\theta_3 & 0 \\ -c\theta_2 s\theta_3 & c\theta_3 & 0 \\ s\theta_2 & 0 & 1 \end{bmatrix} \begin{Bmatrix} \dot{\theta}_1 \\ \dot{\theta}_2 \\ \dot{\theta}_3 \end{Bmatrix} \tag{43}$$

where x'', y'', and z'' denote directions along the RF axes. Substitution of Eqs. (42) and (43) into the kinetic energy expression given in Eq. (18) still results in an exact expression for the rotational kinetic energy. Starting with this expression, a Taylor expansion about the equilibrium orientation $(\theta_1 = \theta_2 = \theta_3 = 0)$ can be carried out using the expression given in Eq. (40).

Retaining second-order terms in the Taylor expansion from the sets $\{\theta_1, \theta_2, \theta_3\}$ and $\{\dot{\theta}_1, \dot{\theta}_2, \dot{\theta}_3\}$ results in first order (linear) equations of motion in the generalized coordinates. Since the angles θ_1, θ_2, and θ_3 are considered sufficiently small to retain only second order terms in the expansion, these angles are considered components of the angular displacement vector designated as $\Delta\vec{\theta}_R^R$. As mentioned before, consistent with the choice of generalized coordinates $\{\Delta\theta_R^R\}$, these angular components are the angular displacements of the rack about the orthogonal set of rack body-fixed axes. The symbols for the components θ_1, θ_2, and θ_3 become $\Delta\theta_{x''}$, $\Delta\theta_{y''}$, and $\Delta\theta_{z''}$.

With respect to only those terms involving coupling between the orbital and perturbed motion (terms involving components from both $\vec{\Omega}$ or $\dot{\vec{\Omega}}$ and $\Delta\vec{\theta}_R$ or $\Delta\dot{\vec{\theta}}_R$), the expansion of the rotational kinetic energy function is presented as if the rack body-fixed axes are principal axes. The justification for this assumption is explained in Section 7.2 where the rotational equations of motion for the rack are discussed. Coupling terms between the orbital and perturbed motions appear in these equations of motion, but it is

concluded that these terms have minimal impact on the microgravity environment inside the rack. This conclusion applies to coupling terms involving elements taken from the diagonal of the inertia matrix, and it applies even more so to coupling terms involving elements from the off-diagonal because the off-diagonal elements of the inertia matrix are small compared to the diagonal elements (see Appendix B).

Under the condition just stated, the expansion of the rotational kinetic energy is

$$
\begin{aligned}
T_{\text{ROTATION}} \approx\ & \Omega_{y'}\Omega_{z'}\left(I_{y''}-I_{z''}\right)\Delta\theta_{x''}+\Omega_{x'}\Omega_{z'}\left(I_{z''}-I_{x''}\right)\Delta\theta_{y''} \\
& +\Omega_{x'}\Omega_{y'}\left(I_{x''}-I_{y''}\right)\Delta\theta_{y''} \\
& +\frac{1}{2}\left(\Omega_{y'}^2-\Omega_{z'}^2\right)\left(I_{z''}-I_{y''}\right)\Delta\theta_{x''}^2+\frac{1}{2}\left(\Omega_{z'}^2-\Omega_{x'}^2\right)\left(I_{x''}-I_{z''}\right)\Delta\theta_{y''}^2 \\
& +\frac{1}{2}\left(\Omega_{x'}^2-\Omega_{y'}^2\right)\left(I_{y''}-I_{x''}\right)\Delta\theta_{z''}^2 \\
& +\Omega_{y'}\Omega_{z'}\left(I_{x''}-I_{z''}\right)\Delta\theta_{x''}\Delta\theta_{y''}+\Omega_{x'}\Omega_{z'}\left(I_{x''}-I_{y''}\right)\Delta\theta_{x''}\Delta\theta_{z''} \\
& +\Omega_{y'}\Omega_{z'}\left(I_{y''}-I_{x''}\right)\Delta\theta_{y''}\Delta\theta_{z''} \\
& +\Omega_{x'}I_{x''}\Delta\dot{\theta}_{x''}+\Omega_{y'}I_{y''}\Delta\dot{\theta}_{y''}+\Omega_{z'}I_{z''}\Delta\dot{\theta}_{z''} \\
& +\Omega_{z'}I_{y''}\Delta\dot{\theta}_{y''}\Delta\theta_{x''}-\Omega_{y'}I_{z''}\Delta\dot{\theta}_{z''}\Delta\theta_{x''} \\
& +\Omega_{z'}\left(I_{z''}-I_{x''}\right)\Delta\dot{\theta}_{x''}\Delta\theta_{y''}+\Omega_{x'}I_{z''}\Delta\dot{\theta}_{z''}\Delta\theta_{y''} \\
& +\Omega_{y'}\left(I_{x''}-I_{y''}\right)\Delta\dot{\theta}_{x''}\Delta\theta_{z''}+\Omega_{x'}\left(I_{x''}-I_{y''}\right)\Delta\dot{\theta}_{y''}\Delta\theta_{z''} \\
& +\frac{1}{2}\Delta\dot{\theta}_{R,i}^{R}I_{R,ij}^{R}\Delta\dot{\theta}_{R,j}^{R}
\end{aligned}
\tag{44}
$$

where the subscripts x', y', and z' denote directions along the REF axes. Note that in the expansion given in Eq. (44) all terms of order three (and above) in the generalized coordinates have been omitted. Furthermore, although the orbital coupling terms involving the cross moments of inertia have been omitted in the above expression, the final term is written indicially and can include the cross moments of inertia.

Translational Kinetic Energy

The translational kinetic energy expression given in Eq. (15) contains the vectors $\bar{r}_P^L$ and $\dot{\bar{r}}_P^L$, which represent the position and velocity of the P^{th} disturber mass relative to the rack center of mass with components resolved along and measured in the local orbital frame. The disturber mass motion is assumed to be known only in the rack body-fixed frame because the disturbing hardware is assumed to be hard mounted (bolted) to the rack structure. Therefore, transformation of the components of $\bar{r}_P^L$ and $\dot{\bar{r}}_P^L$ is necessary.

Transformation of the components of the relative position vector is accomplished through the following:

$$\left\{r_P^L\right\} = \left[l^{L/RE}\right]\left[l^{RE/R}\right]\left\{r_P^R\right\} \tag{45}$$

The matrix $\left[l^{RE/R}\right]$ represents a transformation between the RF and REF and is simply the transpose of the matrix given in Eq. (42). The matrix $\left[l^{L/RE}\right]$ is the transpose of $\left[l^{RE/L}\right]$, also given in Eq. (42).

Transformation of the components of the velocity vector $\dot{\bar{r}}_P^L$ is partially accomplished with the relation given in Eq. (12). The transformation takes the following form,

$$\dot{\bar{r}}_P^L = \dot{\bar{r}}_P^R + \vec{\omega}_{PERT} \times \bar{r}_P^R \tag{46}$$

where $\vec{\omega}_{PERT}$ is the perturbed angular velocity of rack, resolved along the RF. The vector expression on the right-hand side of Eq. (46) has unit vectors in the RF that require components to be transformed to the L frame for substitution into the kinetic energy

expression given in Eq. (15). The matrix expression for the transformation of the vector components is then given as

$$\left\{\dot{r}_P^L\right\} = \left[l^{L/RE}\right]\left[l^{RE/R}\right]\left(\left\{\dot{r}_P^R\right\} + \left[\omega_{PERT}\right]\left\{r_P^R\right\}\right) \tag{47}$$

where $\left[\omega_{PERT}\right]$ is the antisymmetric second order tensor of $\vec{\omega}_{PERT}$.

The matrix quantities $\left[l^{RE/R}\right]$ and $\left[\omega_{PERT}\right]$ can be written in terms of the angles θ_1, θ_2, and θ_3 (and their rates of change) through the relations given in Eqs. (42) and (43). Exact expressions for the components of the position and velocity vectors of the P^{th} disturber mass, in terms of the generalized coordinates, can then be obtained. By substituting these expressions into the disturber mass velocity (given in Eq. (15)), a Taylor expansion of the velocity about the equilibrium orientation ($\theta_1 = \theta_2 = \theta_3 = 0$) can be carried out. The expansion is obtained using Eq. (40).

For the purpose of this study, quadratic terms (and terms of higher order) in the coordinates θ_1, θ_2, and θ_3, as well as in $\dot{\theta}_1$, $\dot{\theta}_2$, and $\dot{\theta}_3$, are omitted. The reason for omitting these terms is that they are multiplied by the small disturber mass quantity, m_P. These quadratic terms then become third-order terms in magnitude in the kinetic energy expression. Applying the expansion in Eq. (40), the velocity components of the P^{th} disturber mass are given as

$$\begin{aligned} v_{m_P} \approx\ & \dot{r}_{CM,i}^L + \Delta\dot{r}_{R,i}^L + l_{ij}^{L/RE}\left(\dot{r}_{P,j}^R + \varepsilon_{jmk}\Delta\dot{\theta}_{R,m}^R r_{P,k}^R + \varepsilon_{jmk}\Delta\theta_{R,m}^R \dot{r}_{P,k}^R\right) \\ & + \varepsilon_{ijk}\Omega_j\left(r_{CM,k}^L + r_{RE,k}^L + \Delta r_{R,k}^L + l_{km}^{L/RE} r_{P,m}^R + l_{km}^{L/RE}\varepsilon_{mnp}\Delta\theta_{R,n}^R r_{P,p}^R\right) \end{aligned} \tag{48}$$

where, consistent with earlier developments, the perturbed angular displacements are considered sufficiently small so that the components $\dot{\theta}_1$, $\dot{\theta}_2$, and $\dot{\theta}_3$ can be integrated

into components of a small angle displacement vector resolved along the orthogonal axes of the RF.

Elastic Potential Energy

The elastic potential energy function given in Eq. (19) contains the quantities $\{d_N^L\}$ and $\{D_N^L\}$. These quantities represent components of the position vectors of the connection point of the N^{th} elastic element on the rack and station respectively (see Figure 9) resolved along the L (LVLH) frame. Because the station and rack are rigid bodies, the components of these vectors are time invariant in their respective body-fixed frames. However, owing to the perturbed angular motion of the bodies, the components of these vectors vary in time relative to the axes of the L frame.

The elements of the column vector $\{d_N^L\}$ may be expressed in terms of the time-invariant body-fixed components through a transformation like that given in Eq. (45):

$$\{d_N^L\} = [l^{L/RE}][l^{RE/R}]\{d_N^R\} \tag{49}$$

A similar transformation can be used for the quantity $\{D_N^L\}$. Substituting the transformations for $\{d_N^L\}$ and $\{D_N^L\}$ into the displacement vector given in Eq. (19), the translational stretching displacement of the N^{th} elastic element becomes

$$\{\Delta r_N^L\} = \{r_{RE}^L\} + \{\Delta r_R^L\} + [l^{L/RE}][l^{RE/R}]\{d_N^R\} - \{r_{SE}^L\} - \{\Delta r_S^L\} - [l^{L/SE}][l^{SE/S}]\{D_N^S\} - \{L_N^L\} \tag{50}$$

Note that Eq. (50) represents an exact expression for the displacement of the N^{th} elastic element.

The relation given in Eq. (50) can be expanded about the equilibrium orientations for both the station and the rack. This expansion is obtained with Eq. (40) as

$$\left\{\Delta r_N^L\right\} \approx \left\{r_{RE}^L\right\} + \left\{d_{oN}^L\right\} - \left\{r_{SE}^L\right\} - \left\{D_{oN}^L\right\} - \left\{L_N^L\right\} + \left\{\Delta r_R^L\right\} + \left[l^{L/RE}\right]\left[\Delta\Theta_R^R\right]\left\{d_{oN}^{RE}\right\} - \left\{\Delta r_S^L\right\} - \left[l^{L/SE}\right]\left[\Delta\Theta_S^S\right]\left\{D_{oN}^{SE}\right\} \tag{51}$$

where the quantities $\left\{d_{oN}^L\right\}$ and $\left\{D_{oN}^L\right\}$ are the time-invariant components of the position vectors $\bar{d}_N$ and $\bar{D}_N$, resolved in the L frame, when the rack and station are in their equilibrium orientations. The quantities $\left\{d_{oN}^{RE}\right\}$ and $\left\{D_{oN}^{SE}\right\}$ have the same definition but are components resolved in the REF and SEF respectively. Note that the components of $\left\{d_{oN}^{RE}\right\}$ and $\left\{D_{oN}^{SE}\right\}$ are equal to the components of $\bar{d}_N$ and $\bar{D}_N$ resolved in their respective body-fixed frames. The matrix quantities $\left[\Delta\Theta_R^R\right]$ and $\left[\Delta\Theta_S^S\right]$ represent the antisymmetric tensors of the vectors $\Delta\bar{\theta}_R^R$ and $\Delta\bar{\theta}_S^S$ respectively. With regard to the equilibrium condition, the resultant of the vector sum of the first five terms of Eq. (51) is

$$\left\{r_{RE}^L\right\} + \left\{d_{oN}^L\right\} - \left\{r_{SE}^L\right\} - \left\{D_{oN}^L\right\} - \left\{L_N^L\right\} = \left\{\Delta L_{oN}^L\right\} \tag{52}$$

where $\left\{\Delta L_{oN}^L\right\}$ is the small extension of the N^{th} umbilical assembly when the system is in equilibrium. The approximation for $\left\{\Delta r_N^L\right\}$ is then rewritten as

$$\left\{\Delta r_N^L\right\} \approx \left\{\Delta L_{oN}^L\right\} + \left\{\Delta r_R^L\right\} + \left[l^{L/RE}\right]\left[\Delta\Theta_R^R\right]\left\{d_{oN}^{RE}\right\} - \left\{\Delta r_S^L\right\} - \left[l^{L/SE}\right]\left[\Delta\Theta_S^S\right]\left\{D_{oN}^{SE}\right\} \tag{53}$$

In this case the expansion of $\left\{\Delta r_N^L\right\}$ has only been carried out through the first order terms. Eq. (52) shows that the large displacement vectors cancel out due to the equilibrium condition, leaving only small terms in the expression for $\left\{\Delta r_N^L\right\}$. According to Eq. (4), the displacement vector is multiplied by itself (via the stiffness matrix) in the

potential energy function. If second-order terms were included in Eq. (53), the only additional terms that would appear in the potential energy function would be third and fourth order terms. Therefore, for the purpose of this study, the expansion given in Eq. (53) is considered sufficient.

The indicial expression for the relation given in Eq. (53) is

$$\Delta r^{L}_{N,i} \approx \Delta L^{L}_{oN,i} + \Delta r^{L}_{R,i} + l^{L/RE}_{ij}\Delta\Theta^{R}_{R,jk}\, d^{RE}_{oN,k} - \Delta r^{L}_{S,i} - l^{L/SE}_{ij}\Delta\Theta^{S}_{S,jk}\, D^{SE}_{oN,k} \tag{54}$$

which can be rewritten as

$$\Delta r^{L}_{N,i} \approx \Delta L^{L}_{oN,i} + \Delta r^{L}_{R,i} - \mathbf{d}^{L}_{oN,ij} l^{L/RE}_{jk}\Delta\theta^{R}_{R,k} - \Delta r^{L}_{S,i} + \mathbf{D}^{L}_{oN,ij} l^{L/SE}_{jk}\Delta\theta^{S}_{S,k} \tag{55}$$

where $\mathbf{d}^{L}_{oN,ij}$ and $\mathbf{D}^{L}_{oN,ij}$ are the elements of the second-order tensors $\bar{\bar{\mathbf{d}}}^{L}_{oN}$ and $\bar{\bar{\mathbf{D}}}^{L}_{oN}$. The elements of these tensors are defined as

$$\mathbf{d}^{L}_{oN,ij} = \varepsilon_{jik} d^{L}_{oN,k}$$

and

$$\mathbf{D}^{L}_{oN,ij} = \varepsilon_{jik} D^{L}_{oN,k}$$

The quantities $d^{L}_{oN,k}$ and $D^{L}_{oN,k}$ are the k^{th} components of $\left\{d^{L}_{oN}\right\}$ and $\left\{D^{L}_{oN}\right\}$, described above. An approximation for the elastic potential energy due to translation is obtained by substituting the approximation for displacement given in Eq. (55) for the total displacement vector in Eq. (19). The resulting expression is shown in the Lagrangian given in Appendix A.

The translational and torsional stiffness parameters, contained in the quantities $\left[\mathrm{KTRN}_{N}\right]$ and $\left[\mathrm{KTOR}_{N}\right]$, appear in Eqs. (19) and (20). The parameters were measured in the rack body-fixed frame and require transformation if they are to be resolved in any

other frame of reference. The transformation of the stiffness quantities between the RF and the REF involves small angle correction terms from the transformation matrix $\left[l^{RE/R}\right]$. Therefore, these correction terms include the small angle displacements $\left\{\Delta\theta_R^R\right\}$. These correction terms are omitted in the transformation of the stiffness tensors because if the correction terms are substituted into the potential energy expression, along with the expansion given in Eq. (55), the terms that result are third order (and higher). For this reason, the transformation of the stiffness tensors takes the form

$$\left[K_N^L\right] \approx \left[l^{RE/L}\right]^T \left[K_N^R\right] \left[l^{RE/L}\right] \tag{56}$$

where $\left[K_N^L\right]$ represents either $\left[KTRN_N^L\right]$ or $\left[KTOR_N^L\right]$. For the purpose of substitution into the potential energy function, Eq. (56) states that the stiffness quantities are considered invariant under transformation between the RF and the REF.

If third-order terms are ignored in the torsional potential energy given in Eq. (20), the potential energy due to the torsional stiffness property of the umbilical and actuator assemblies can be rewritten as

$$V_{TOR} = \frac{1}{2}\sum_N \left(\left\{\Delta\theta_R^R\right\} - \left\{\Delta\theta_S^R\right\} - \left\{\Delta\theta_{oN}^R\right\}\right)^T \left[KTOR_N^R\right] \left(\left\{\Delta\theta_R^R\right\} - \left\{\Delta\theta_S^R\right\} - \left\{\Delta\theta_{oN}^R\right\}\right) \tag{57}$$

All of the quantities in this equation have been resolved in the RF because this will become the preferred frame of reference for the final form of the equations of motion. Just as in the other expansions presented to this point, all third-order terms in Eq. (57) have been excluded. Consistent with the exclusion of these terms, small-angle correction terms for the transformation of the quantity $\left[KTOR_N\right]$ between the RF and the REF have been omitted, as stated in Eq. (56).

Gravitational Potential Energy

The second term of the potential energy function given in Eq. (27) contains the vector $\vec{r}_P^{\,L}$. As described above, the position of the P^{th} disturber mass at some given time is known only in the rack body-fixed frame. The position vector of the P^{th} disturber mass can be expanded about the equilibrium orientation using Eq. (40). Just as in the case of the kinetic energy expression for the disturber masses, terms of second order and higher in the coordinates θ_1, θ_2, and θ_3 are omitted because these terms are multiplied by the small disturber mass quantity m_P. Because of this multiplier, second-order terms in the angular coordinates would be considered third-order terms in magnitude relative to other terms in the Lagrangian. Applying Eq. (40) to the position vector of the P^{th} disturber results in

$$R_{P,i}^{L} \approx r_{CM,i}^{L} + \Delta r_{R,i}^{L} + r_{RE,i}^{L} + l_{ij}^{L/RE} r_{P,j}^{R} + l_{ij}^{L/RE} \varepsilon_{jmk} \Delta\theta_{R,m}^{R} r_{P,k}^{R} \tag{58}$$

The approximation for the position of the P^{th} disturber mass is substituted into the gravitational potential energy expression for the P^{th} disturber mass and used to form the Lagrangian given in Appendix A.

6.3 Dissipation Function

The dissipation function given in Eq. (22) contains the quantities $\left\{\dot{d}_N^L\right\}$ and $\left\{\dot{D}_N^L\right\}$. These quantities are time varying relative to an observer in the local orbital frame, due to the perturbed angular motion of the rack and station. The elements of the vector $\left\{\dot{d}_N^L\right\}$ transform in a manner identical to the transformation given in Eq. (47).

Since the components of the vector $\bar{d}_N$ are time invariant when resolved in the rack body-fixed frame, the transformation is

$$\left\{\dot{d}_N^L\right\} = \left[l^{L/RE}\right]\left[l^{RE/R}\right]\left(\left[\omega_{PERT}\right]\left\{d_N^R\right\}\right) \tag{59}$$

The quantity $\left\{\dot{D}_N^L\right\}$ can be transformed in a similar fashion.

The expression given in Eq. (59) can be substituted, along with the transformation for $\left\{\dot{D}_N^L\right\}$, into the (relative) velocity term from Eq. (22). If these substitutions are made and the velocity is expanded using Eq. (40), the resulting approximation for the relative velocity between the rack and the station is

$$\Delta\dot{r}_{N,i}^L = \Delta\dot{r}_{R,i}^L + d_{oN,ij}^L l_{jk}^{L/RE}\Delta\dot{\theta}_{R,k}^R - \Delta\dot{r}_{S,i}^L - D_{oN,ij}^L l_{jk}^{L/SE}\Delta\dot{\theta}_{R,k}^S \tag{60}$$

Since the relative velocity term is multiplied by itself (via the damping matrix) in the dissipation function, the expansion given above has only been carried out through the first-order terms. Inclusion of higher order terms would result in third- and fourth- order terms in the dissipation function. Therefore, the expansion given in Eq. (60) is considered sufficient for the purpose of this study. Furthermore, inclusion of small angle correction terms for the transformation of the quantities $\left[\mathrm{CTRN}_N\right]$ and $\left[\mathrm{CTOR}_N\right]$ results in third order terms in the dissipation function and these terms are therefore omitted. The final form of the dissipation function is given in Appendix A.

7. Presentation of the Rack Equations of Motion

7.1 Translational Equations of Motion

For the purpose of deriving the equations for the perturbed motion of the rack, the Lagrangian and dissipative function are formed from those energy expressions that include the set of generalized coordinates $\left\{\Delta r_R^L\right\}$ and $\left\{\Delta\theta_R^R\right\}$. Substituting the expansions given in the previous chapter, a suitable form of the Lagrangian and dissipation function is derived so that Eq. (1) may be directly applied. Lagrange's equations for the translational motion of the rack are then given as

$$\frac{d}{dt}\left(\frac{\partial L}{\partial \Delta \dot{r}_{R,\lambda}^L}\right) - \frac{\partial L}{\partial \Delta r_{R,\lambda}^L} + \frac{\partial F}{\partial \Delta \dot{r}_{R,\lambda}^L} = 0 \tag{61}$$

where λ counts from 1 to 3 and all forces acting on the rack are derivable from the Lagrangian and the dissipative function so that $Q_\lambda = 0$ for all λ. The final forms of the Lagrangian and the dissipative function used in Eq. (61) are included in Appendix A so that the origin of specific terms appearing in the final equations of motion may be traced. Indicial form is retained in the equations of motion so that the progression from Eq. (61) to the terms appearing in these equations may be followed.

Carrying out Eq. (61) yields the following indicial terms:

$$\frac{d}{dt}\left(\frac{\partial L}{\partial \Delta \dot{r}_{R,\lambda}^L}\right) - \frac{\partial L}{\partial \Delta r_{R,\lambda}^L} + \frac{\partial F}{\partial \Delta \dot{r}_{R,\lambda}^L} =$$

$$M_R\left(\ddot{r}_{CM,\lambda}^L + \varepsilon_{\lambda jk}\dot{\Omega}_j r_{CM,k}^L + 2\varepsilon_{\lambda jk}\Omega_j \dot{r}_{CM,k}^L + \varepsilon_{\lambda jk}\Omega_j \varepsilon_{kmn}\Omega_m r_{CM,n}^L\right) \tag{a}$$

$$+ M_R \left(\varepsilon_{\lambda jk} \dot{\Omega}_j r^L_{RE,k} + \varepsilon_{\lambda jk} \Omega_j \varepsilon_{kmn} \Omega_m r^L_{RE,n} \right) \quad \text{(b)}$$

$$+ M_R \left(\Delta\ddot{r}^L_{R,\lambda} + \varepsilon_{\lambda jk} \dot{\Omega}_j \Delta r^L_{R,k} + 2\varepsilon_{\lambda jk} \Omega_j \Delta\dot{r}^L_{R,k} + \varepsilon_{\lambda jk} \Omega_j \varepsilon_{kmn} \Omega_m \Delta r^L_{R,n} \right) \quad \text{(c)}$$

$$+ \sum_P m_P \left(\ddot{r}^L_{CM,\lambda} + \varepsilon_{\lambda jk} \dot{\Omega}_j r^L_{CM,k} + 2\varepsilon_{\lambda jk} \Omega_j \dot{r}^L_{CM,k} + \varepsilon_{\lambda jk} \Omega_j \varepsilon_{kmn} \Omega_m r^L_{CM,n} \right) \quad \text{(d)}$$

$$+ \sum_P m_P \left(\varepsilon_{\lambda jk} \dot{\Omega}_j r^L_{RE,k} + \varepsilon_{\lambda jk} \Omega_j \varepsilon_{kmn} \Omega_m r^L_{RE,n} \right) \quad \text{(e)}$$

$$+ \sum_P m_P \left(\Delta\ddot{r}^L_{R,\lambda} + \varepsilon_{\lambda jk} \dot{\Omega}_j \Delta r^L_{R,k} + 2\varepsilon_{\lambda jk} \Omega_j \Delta\dot{r}^L_{R,k} + \varepsilon_{\lambda jk} \Omega_j \varepsilon_{kmn} \Omega_m \Delta r^L_{R,n} \right) \quad \text{(f)}$$

$$+ \sum_P m_P \, l^{L/RE}_{\lambda j} \left(\ddot{r}^R_{P,j} + \varepsilon_{jmk} \Delta\ddot{\theta}^R_{R,m} r^R_{P,k} + 2\varepsilon_{jmk} \Delta\dot{\theta}^R_{R,m} \dot{r}^R_{P,k} + \varepsilon_{jmk} \Delta\theta^R_{R,m} \ddot{r}^R_{P,k} \right) \quad \text{(g)}$$

+ Additional forces on rack due to coupling between orbital motion and motion of disturbers relative to the rack center of mass (h)

$$+ \sum_N \mathrm{KTRN}^L_{N,\lambda i} \left(\Delta r^L_{R,i} - \Delta r^L_{S,i} \right) \quad \text{(i)}$$

$$- \sum_N \mathrm{KTRN}^L_{N,\lambda i} \, \mathbf{d}^L_{oN,ij} \, l^{L/RE}_{jk} \, \Delta\theta^R_{R,k} \quad \text{(j)}$$

$$+ \sum_N \mathrm{KTRN}^L_{N,\lambda i} \, \mathbf{D}^L_{oN,ij} \, l^{L/SE}_{jk} \, \Delta\theta^S_{S,k} \quad \text{(k)}$$

$$+ \sum_N \mathrm{KTRN}^L_{N,\lambda i} \, \Delta L^L_{oN,i} \quad \text{(l)}$$

$$+ \sum_N \mathrm{CTRN}^L_{N,\lambda i} \left(\Delta\dot{r}^L_{R,i} - \Delta\dot{r}^L_{S,i} \right) \quad \text{(m)}$$

$$- \sum_N \mathrm{CTRN}^L_{N,\lambda i} \, \mathbf{d}^L_{oN,ij} \, l^{L/RE}_{jk} \, \Delta\dot{\theta}^R_{R,k} \quad \text{(n)}$$

$$+ \sum_N \mathrm{CTRN}^L_{N,\lambda i} \, \mathbf{D}^L_{oN,ij} \, l^{L/SE}_{jk} \, \Delta\dot{\theta}^S_{S,k} \quad \text{(o)}$$

$$+ \frac{\mu_E M_R \left(r^L_{RE,\lambda} + \Delta r^L_{R,\lambda} \right)}{\left| \bar{r}_{CM} \right|^3} + \frac{\mu_E \sum_P m_P \left(r^L_{RE,\lambda} + \Delta r^L_{R,\lambda} + r^L_{P,\lambda} + l^{L/RE}_{\lambda j} \left(r^R_{P,j} + \varepsilon_{kjm} \Delta\theta^R_{R,m} r^R_{P,k} \right) \right)}{\left| \bar{r}_{CM} \right|^3} \quad \text{(p)}$$

for $\lambda = 1,2$

$$+ \frac{\mu_E M_R r^L_{CM,\lambda}}{\left| \bar{r}_{CM} \right|^3} + \frac{\mu_E \sum_P m_P r^L_{CM,\lambda}}{\left| \bar{r}_{CM} \right|^3} - \frac{2\mu_E M_R \left(r^L_{RE,\lambda} + \Delta r^L_{R,\lambda} \right)}{\left| \bar{r}_{CM} \right|^3}$$

for $\lambda = 3$ (q)

$$- \frac{2\mu_E \sum_P m_P \left(r^L_{RE,\lambda} + \Delta r^L_{R,\lambda} + l^{L/RE}_{\lambda j} \left(r^R_{P,j} + \varepsilon_{kjm} \Delta\theta^R_{R,m} r^R_{P,k} \right) \right)}{\left| \bar{r}_{CM} \right|^3}$$

Discussion of Terms

In the following discussion, the terms (a) through (m) (presented above) are discussed individually. Physical interpretations of the terms are given along with a discussion of the significance of the terms in the context of the microgravity environment or their relative size in comparison to other terms. In cases where, based on an order of magnitude study, a given term is found to have negligible impact on the microgravity environment inside the rack or is sufficiently small in comparison to other terms, the term is omitted from the final equations of motion, which will appear in Eq. (73). When practicable, the equivalent vector or matrix expressions are given for the indicial expressions.

(a)

$$M_R\left(\ddot{r}^L_{CM,\lambda} + \varepsilon_{\lambda jk}\dot{\Omega}_j r^L_{CM,k} + 2\varepsilon_{\lambda jk}\Omega_j \dot{r}^L_{CM,k} + \varepsilon_{\lambda jk}\Omega_j \varepsilon_{kmn}\Omega_m r^L_{CM,n}\right)$$
$$\Rightarrow M_R\left(\ddot{\vec{r}}^L_{CM} + \dot{\vec{\Omega}} \times \vec{r}^L_{CM} + 2\vec{\Omega} \times \dot{\vec{r}}^L_{CM} + \vec{\Omega} \times \left(\vec{\Omega} \times \vec{r}^L_{CM}\right)\right)$$

The terms in parentheses represent the total acceleration of the composite center of mass measured inertially but transformed to the local orbital frame. Eq. (38) shows that if the external forces on the station are small, the inertial acceleration of the system in orbit is nearly canceled by the acceleration due to gravity given in the first term of (q).

(b)

$$M_R\left(\varepsilon_{\lambda jk}\dot{\Omega}_j r^L_{RE,k} + \varepsilon_{\lambda jk}\Omega_j\varepsilon_{kmn}\Omega_m r^L_{RE,n}\right) \Rightarrow M_R\left(\dot{\bar{\Omega}}\times\bar{r}^L_{RE} + \bar{\Omega}\times\left(\bar{\Omega}\times\bar{r}^L_{RE}\right)\right)$$

The spatial separation of the rack from the composite center of mass results in the quasi-steady forces given in (b). The first term in the parentheses is the tangential acceleration, which is negligible due to the small magnitude of $\dot{\bar{\Omega}}$. The two factors contributing to the rate of change of the orbit rate are the orbital eccentricity and the external forces such as aerodynamic drag. However, the effect of the external forces on $\dot{\bar{\Omega}}$ is negligible compared to the effect from the orbital eccentricity. Typical eccentricities of the Space Shuttle and the MIR Space Station ($e \approx 0.001$) result in magnitudes of $\dot{\bar{\Omega}}$ that are on the order of 10^{-9} rad/sec^2. Using this value for the magnitude of $\dot{\bar{\Omega}}$, and considering that the maximum distance of any ARIS-fitted rack from the composite center of mass of the system is approximately forty feet, maximum accelerations of only about 10^{-9} g_0 would be experienced at the science location due to the tangential acceleration effect. Since the eccentricity of the typical ISS orbit is expected to be even smaller than the typical Space Shuttle and MIR orbits, the tangential effect can be omitted.

The second term in (b) represents the centripetal acceleration that is due to the (once per orbit) revolution of the rack about the system's composite center of mass. The centripetal acceleration is a significant factor in the quasi-steady acceleration environment at the science location. An order of magnitude study shows that centripetal acceleration can

result in accelerations at the science location of $1.2 \times 10^{-7}\ g_o$ for every meter of separation between the microgravity rack and the system's composite center of mass. Because of swayspace limitations, isolation of the experiments from this type of disturbance is not achievable.

(c)

$$M_R\left(\Delta\ddot{r}^L_{R,\lambda} + \varepsilon_{\lambda jk}\dot{\Omega}_j \Delta r^L_{R,k} + 2\varepsilon_{\lambda jk}\Omega_j \Delta\dot{r}^L_{R,k} + \varepsilon_{\lambda jk}\Omega_j \varepsilon_{kmn}\Omega_m \Delta r^L_{R,n}\right)$$

$$\Rightarrow \quad M_R\left(\Delta\ddot{\vec{r}}^L_R + \dot{\vec{\Omega}} \times \Delta\vec{r}^L_R + 2\vec{\Omega} \times \Delta\dot{\vec{r}}^L_R + \vec{\Omega} \times \left(\vec{\Omega} \times \Delta\vec{r}^L_R\right)\right)$$

The terms in parentheses represent the inertially measured, perturbed acceleration of the rack, transformed to the local orbital frame. The first term is the linear acceleration of the rack. The second, third, and fourth terms represent the tangential, Coriolis, and centripetal accelerations respectively. Although orbital forces are many times thought of as quasi-steady disturbances, the terms represented in (c) can operate in the vibratory frequency range. The tangential acceleration is negligible due to the small magnitude of $\dot{\vec{\Omega}}$. The centripetal acceleration arising from the perturbed motion of the rack is most significant at quasi-steady frequencies, where the pitch, yaw and roll of the station carry the rack a maximum distance from the equilibrium position. Assuming nominal operating conditions on the station, order of magnitude estimates for the centripetal acceleration represented in (c) show that the upper limit of this term is approximately $3.4 \times 10^{-8}\ g_o$. This value represents a small portion of the microgravity acceleration allowance in the quasi-steady frequency range and is therefore omitted from the final equations of motion presented in this paper.

The Coriolis term deserves consideration because it does impact the simulation results presented in this paper. In the Coriolis term, the set of coefficients $2M_R\varepsilon_{\lambda jk}\Omega_j$ are multiplied by the perturbed velocity states $\Delta\dot{r}^L_{R,k}$ so that, in the equations of motion, these coefficients would be added directly to the off-diagonal elements of the aggregate damping matrix $\sum_N \left[\text{CTRN}_N\right]$ given in term (m) above. Depending on the orientation of the ARIS rack under consideration, the largest Coriolis coefficient could be a full order of magnitude larger than the various off-diagonal damping coefficients. Using the estimation for the damping matrix given in this paper (see Appendix D) and assuming a full set of umbilicals, the Coriolis coefficients will always be a full order of magnitude less than the eigenvalues of $\sum_N \left[\text{CTRN}_N\right]$. Although the Coriolis term is not included in the final equations of motion presented in this paper, the possible impact of this term to the simulation results should be noted. Further discussion regarding the effect of the Coriolis term is given in Section 8.4, where closed-loop ARIS attenuation results are presented.

(d)

$$\sum_P m_P \left(\ddot{r}^L_{CM,\lambda} + \varepsilon_{\lambda jk}\dot{\Omega}_j r^L_{CM,k} + 2\varepsilon_{\lambda jk}\Omega_j \dot{r}^L_{CM,k} + \varepsilon_{\lambda jk}\Omega_j \varepsilon_{kmn}\Omega_m r^L_{CM,n}\right)$$

$$\Rightarrow \sum_P m_P \left(\ddot{\bar{r}}^L_{CM} + \dot{\bar{\Omega}} \times \bar{r}^L_{CM} + 2\bar{\Omega} \times \dot{\bar{r}}^L_{CM} + \bar{\Omega} \times \left(\bar{\Omega} \times \bar{r}^L_{CM}\right)\right)$$

This expression accounts for the force induced on the disturber masses due to the orbital motion of the composite center of mass. This force is nearly balanced by the force due to

gravity at the composite center of mass (second term in (q)). Note that any force on the disturber masses results in an equal and opposite reaction force on the rack and is, therefore, present in the equations of motion for the rack. Since all of the quantities in (d) are assumed known, these forces could be moved to the right-hand side of the equations of motion, to become forcing functions of opposite sign (direction).

(e)

$$\sum_{P} m_P \left(\varepsilon_{\lambda jk} \dot{\Omega}_j r^L_{RE,k} + \varepsilon_{\lambda jk} \Omega_j \varepsilon_{kmn} \Omega_m r^L_{RE,n} \right) \Rightarrow \sum_{P} m_P \left(\dot{\bar{\Omega}} \times \bar{r}^L_{RE} + \bar{\Omega} \times \left(\bar{\Omega} \times \bar{r}^L_{RE} \right) \right)$$

These terms account for the quasi-steady tangential and centripetal forces acting on the disturber masses due to their spatial separation from the composite center of mass. The tangential effect is negligible because of (among other reasons) the small magnitude of $\dot{\bar{\Omega}}$. The more significant force is the centripetal force. Assuming a full complement of disturbers, the maximum acceleration that the centripetal force term in (e) could induce in a rack is several orders of magnitude less than the micro-g level. Considering that the disturber mass is normally taken to be 0.5% of the mass of the rotating part (see Appendix C), the mass ratio between the disturber masses and the rack mass is very small. Therefore, the terms in (e) can also be neglected based on a comparison with the terms in (b), given above.

(f)

$$\sum_P m_P \left(\Delta\ddot{r}^L_{R,\lambda} + \varepsilon_{\lambda jk}\dot{\Omega}_j \Delta r^L_{R,k} + 2\varepsilon_{\lambda jk}\Omega_j \Delta\dot{r}^L_{R,k} + \varepsilon_{\lambda jk}\Omega_j \varepsilon_{kmn}\Omega_m \Delta r^L_{R,n} \right)$$

$$\Rightarrow \sum_P m_P \left(\Delta\ddot{\vec{r}}^L_R + \dot{\vec{\Omega}} \times \Delta\vec{r}^L_R + 2\vec{\Omega} \times \Delta\dot{\vec{r}}^L_R + \vec{\Omega} \times \left(\vec{\Omega} \times \Delta\vec{r}^L_R \right) \right)$$

The expression (f) represents the forces induced on the disturber masses due to perturbed motion of the rack. These terms are negligible in comparison to the terms in (c) because the masses of the disturbers are small compared to the mass of the rack (see Appendix C).

(g)

$$\sum_P m_P \, l^{L/RE}_{\lambda j} \left(\ddot{r}^R_{P,j} + \varepsilon_{jmk}\Delta\ddot{\theta}^R_{R,m} r^R_{P,k} + 2\varepsilon_{jmk}\Delta\dot{\theta}^R_{R,m}\dot{r}^R_{P,k} + \varepsilon_{jmk}\Delta\theta^R_{R,m}\ddot{r}^R_{P,k} \right)$$

where

$$\ddot{r}^R_{P,j} + \varepsilon_{jmk}\Delta\ddot{\theta}^R_{R,m} r^R_{P,k} + 2\varepsilon_{jmk}\Delta\dot{\theta}^R_{R,m}\dot{r}^R_{P,k} + \varepsilon_{jmk}\Delta\theta^R_{R,m}\ddot{r}^R_{P,k} \Rightarrow$$

$$\ddot{\vec{r}}^R_P + \Delta\ddot{\vec{\theta}}^R_R \times \vec{r}^R_P + 2\Delta\dot{\vec{\theta}}^R_R \times \dot{\vec{r}}^R_P + \Delta\vec{\theta}^R_R \times \vec{r}^R_P$$

The first term in parentheses represents the linear acceleration of the disturber masses measured relative to an observer in the rack body-fixed frame. The second and third terms in (g) are the tangential and Coriolis terms respectively and result from the rotation of the disturber masses about the rack center of mass due to the perturbed rotational motion of the rack. Of these two terms, the Coriolis term is the most significant. Assuming a standard compliment of onboard disturbers, the Coriolis term is estimated to be at least one order of magnitude smaller than the first term in (g). The final term in (g) represents a first order transformation of the disturber force from the RF to the REF.

Assuming a standard complement of onboard disturbers, all in phase with each other and operating at peak force input, the forces represented by the last term in (g) are at least one order of magnitude smaller than the forces induced by the umbilical and actuator assemblies due to perturbed rotation of the rack (given in (j)). For the purpose of this study, only the first term in (g) is retained in the final equations of motion presented in Eq. (73). Regarding the terms in (g), the vector equivalent of the indicial terms in parentheses is given but the subsequent transformation denoted as $l_{\lambda j}^{L/RE}$ would be otherwise represented as a matrix multiplication.

(h)

Additional forces on the rack due to coupling between orbital motion and motion of disturbers relative to the rack center of mass.

Because disturber masses are located at some distance (no greater than one meter) from the center of mass of the rack and have velocity relative to the rack CM, they experience rotationally induced forces due to orbital motion that are different from those experienced at the center of mass of the rack. An example of one of the terms in (h) is the centripetal force on the P^{th} disturber mass due to its spatial separation from the rack center of mass, given as

$$\sum_{P} m_P\left(\bar{\Omega}\times\left(\bar{\Omega}\times\bar{r}_P\right)\right)$$

The force terms in (h) can be neglected because the magnitudes of the reaction forces on the rack are several orders smaller than the forces induced by the rapid rotation of the disturber masses inside the rotating equipment (given in the first term of (g)).

(i)

$$\sum_{N} \mathrm{KTRN}^{L}_{N,\lambda i}\left(\Delta r^{L}_{R,i} - \Delta r^{L}_{S,i}\right) \;\Rightarrow\; \sum_{N} \left[\mathrm{KTRN}^{L}_{N}\right]\left\{\Delta r^{L}_{R} - \Delta r^{L}_{S}\right\}$$

The terms in (i) represent the restoring forces in the elastic elements arising from the relative perturbed displacement between the rack and station.

(j)

$$-\sum_{N} \mathrm{KTRN}^{L}_{N,\lambda i}\, \mathbf{d}^{L}_{oN,ij}\, l^{L/RE}_{jk}\, \Delta\theta^{L}_{R,k} \;\Rightarrow\; -\sum_{N} \left[\mathrm{KTRN}^{L}_{N}\right]\left[\mathbf{d}^{L}_{oN}\right]\left[l^{L/RE}\right]\left\{\Delta\theta^{R}_{R}\right\}$$

Expression (j) accounts for the elastic forces arising from the rotation of the rack about its own center of mass. This rotation results in translation of the umbilical and actuator connection points that induces a restoring force in the elastic elements.

(k)

$$\sum_{N} \mathrm{KTRN}^{L}_{N,\lambda i}\, \mathbf{D}^{L}_{oN,ij}\, l^{L/SE}_{jk} \Delta\theta^{S}_{S,k} \;\Rightarrow\; \sum_{N} \left[\mathrm{KTRN}^{L}_{N}\right]\left[\mathbf{D}^{L}_{oN}\right]\left[l^{L/SE}\right]\left\{\Delta\theta^{S}_{S}\right\}$$

Expression (k) is similar to (j) but applies to station rotation about its own center of mass.

(l)

$$\sum_{N} \mathrm{KTRN}^{L}_{N,\lambda i}\, \Delta L^{L}_{oN,i} \;\Rightarrow\; \sum_{N} \left[\mathrm{KTRN}^{L}_{N}\right]\left\{\Delta L^{L}_{oN}\right\}$$

The term (l) represents a small elastic force that counteracts the orbital forces on the rack in the equilibrium configuration.

(m), (n), (o)

These terms are similar to (i), (j), and (k) but represent forces induced by the damping effect of the umbilical and actuator assemblies.

(p)

$$\frac{\mu_E M_R \left(r^L_{RE,\lambda} + \Delta r^L_{R,\lambda} \right)}{\left| \bar{r}_{CM} \right|^3} + \frac{\mu_E \sum_P m_P \left(r^L_{RE,\lambda} + \Delta r^L_{R,\lambda} + l^{L/RE}_{\lambda j} \left(r^R_{P,j} + \varepsilon_{kjm} \Delta\theta^R_{R,m} r^R_{P,k} \right) \right)}{\left| \bar{r}_{CM} \right|^3}$$

for $\lambda = 1$ or 2

The terms in (p) are gravity gradient terms that result from the spatial separation of the rack and the disturber masses from the composite center of mass of the system. The terms in (p) are given for the cases in which λ takes the value of either 1 or 2, which correspond to the x and y directions of the L frame respectively. Just like the centripetal force described in (b), the gravity gradient force is a significant factor in the quasi-steady environment at the science location. The gravity gradient force arising from the perturbed displacement of the rack can be omitted in the final equations of motion because this force results in rack accelerations that are small compared to the micro-g level. The entire second term in (p) is negligible because it results in accelerations in the rack that are of the same order of magnitude as the centripetal term given in (e) (several orders of magnitude less than the micro-g level).

(q)

$$\frac{\mu_E M_R r^L_{CM,\lambda}}{\left|\bar{r}_{CM}\right|^3} + \frac{\mu_E \sum_P m_P r^L_{CM,\lambda}}{\left|\bar{r}_{CM}\right|^3}$$

$$- \frac{2\mu_E M_R \left(r^L_{RE,\lambda} + \Delta r^L_{R,\lambda}\right)}{\left|\bar{r}_{CM}\right|^3} - \frac{2\mu_E \sum_P m_P \left(r^L_{RE,\lambda} + \Delta r^L_{R,\lambda} + l^{L/RE}_{\lambda j}\left(r^R_{P,j} + \varepsilon_{kjm}\Delta\theta^R_{R,m} r^R_{P,k}\right)\right)}{\left|\bar{r}_{CM}\right|^3}$$

for $\lambda = 3$

For the case in which λ takes the value of 3 (corresponding to the nadir direction) the central gravitational force terms appear in the equations of motion. These first two terms are nearly balanced by the terms given in (a) and (d). The last two terms represent the gravity gradient force along the z direction. Consistent with the result in reference 3, the magnitude of the gravity gradient force along z is twice that of the x and y directions. Just as in (p), the entire last term in (q) can be omitted and the gravity gradient force arising from the perturbed displacement of the rack is also negligible.

Force per Unit Mass at the Composite Center of Mass

Utilizing the equations of motion given in vector Eq. (38), the terms in (a) and (d) along with the central force terms of (q) can be combined to give

$$
\begin{aligned}
&M_R\left(\ddot{r}^L_{CM,\lambda}+\varepsilon_{\lambda jk}\dot{\Omega}_j r^L_{CM,k}+2\varepsilon_{\lambda jk}\Omega_j \dot{r}^L_{CM,k}+\varepsilon_{\lambda jk}\Omega_j\varepsilon_{kmn}\Omega_m r^L_{CM,n}\right)\\
&+\sum_P m_P\left(\ddot{r}^L_{CM,\lambda}+\varepsilon_{\lambda jk}\dot{\Omega}_j r^L_{CM,k}+2\varepsilon_{\lambda jk}\Omega_j \dot{r}^L_{CM,k}+\varepsilon_{\lambda jk}\Omega_j\varepsilon_{kmn}\Omega_m r^L_{CM,n}\right)\\
&+\frac{\mu_E M_R r^L_{CM,\lambda}}{\left|\bar{r}_{CM}\right|^3}+\frac{\mu_E\sum_P m_P r^L_{CM,\lambda}}{\left|\bar{r}_{CM}\right|^3}\\
&=\left(M_R+\sum_P m_P\right)\frac{F^L_{EXT,\lambda}}{M_{TOTAL}}
\end{aligned}
\tag{62}
$$

where $\frac{F^L_{EXT,\lambda}}{M_{TOTAL}}$ is recognized as the acceleration of the composite center of mass due to forces external to the station/rack system. For the purpose of this study, the external forces are considered to be quasi-steady in nature and of constant magnitude and direction over the time interval of interest. This assumption is justified because the vibratory microgravity environment, which is the main subject of this paper, includes oscillatory behavior with a frequency content only as low as 0.01 Hz. The implication is that the longest time window of interest is about 100 seconds, which is a small fraction of the 5,400 second orbital period. Assuming a low eccentricity orbit, the station altitude changes little during this 100-second time interval, and the system covers only a small portion of the total orbital distance. Therefore, parameters such as atmospheric density and solar radiation incidence are assumed to remain constant over this time interval.

Equilibrium Force Balance

To this point in the paper, it has been assumed that the orbital path of the composite system could deviate from the nominal circular orbit that defines the equilibrium configuration of the system. When reboost maneuvers for ISS are performed, a circular orbit will be targeted, but this orbit can only be realized to within a certain

tolerance. Although external forces result in orbit decay and increasing orbit rates, it has been assumed that the altitude and orbit rate of the system remain unchanged due to these factors over the time intervals of interest. The assumption that the ISS orbit will not be perfectly circular after reboost results in tangential acceleration terms in the equations of motion because the time rate of change of the orbit rate is assumed to be non-zero. However, the tolerance on reboost altitude is small enough that the time rate of change of the orbit rate due to orbital eccentricity is very small (see explanation for term (b) above).

Because the deviation of the station's low eccentricity orbit from that defined for the equilibrium state (see Section 4.1) is so small, it is permissible that the altitude, orbit rate, and external forces for the equilibrium orbit be used to estimate the quasi-steady forces encountered in the actual station orbit. The dominant quasi-steady forces can be accounted for by using the parameters from this idealized orbit. Furthermore, consistent with the discussion of terms in the translational equations of motion, the orbitally induced forces on the small disturber masses are negligible because the accelerations induced in the rack due to these forces are several orders smaller than the micro-g level.

Given the assumptions stated above, several terms can be omitted from the equations of motion. Those omitted include any term containing components of the vector $\dot{\bar{\Omega}}$, all of the terms in (e), (f), and (h), and the disturber mass gravity gradient terms in (p) and (q). Using steady-state parameters from the equilibrium orbit to estimate the quasi-steady forces leads to an equilibrium balance of force terms that cancel out of the equations of motion. The equilibrium condition can be stated as

$$\sum_N KTRN^L_{N,\lambda i}\,\Delta L^L_{oN,i} + M_R\left(\varepsilon_{\lambda jk}\Omega_j\varepsilon_{kmn}\Omega_m r^L_{RE,n}\right) + \frac{\mu_E M_R r^L_{RE,\lambda}}{\left|\vec{r}_{CM}\right|^3} + \frac{M_R F_{EXT,\lambda}}{M_{TOTAL}} = 0 \qquad (63)$$

(for $\lambda = 1$ or 2)

For the case in which $\lambda = 3$, the third term takes a multiplier of -2, as in (q).

Mapping Station Motion to the Station/Rack Interface

The sum of the second term in (i) and the term in (k) is

$$-\sum_N KTRN^L_{N,\lambda i}\left(\Delta r^L_{S,i} - \mathbf{D}^L_{oN,ij}\, l^{L/SE}_{jk}\Delta\theta^S_{S,k}\right) \qquad (64)$$

If the second-order terms resulting from the transformation of the components $\left\{\Delta\theta^S_S\right\}$ from the SF to the SEF are neglected, then the vector expression associated with the terms in parentheses in Eq. (64) is

$$\Delta r^L_{S,i} - \mathbf{D}^L_{oN,ij}\,\Delta\theta^L_{S,j} \Rightarrow \Delta\vec{r}_S + \Delta\vec{\theta}_S \times \vec{D}_{oN} = \Delta\vec{X}_N \qquad (65)$$

The relation given in Eq. (65) is recognized as a first-order approximation of the displacement of the connection point of the N^{th} elastic element on the station due to rigid body motion.

The calculation of certain parameters in the equations of motion for the rack is made easier by introducing the vector $\vec{d}_{oN}$ into Eq. (65) in the following fashion:

$$\Delta r^L_{S,i} - \mathbf{D}^L_{oN,ij}\,\Delta\theta^L_{S,j} = \Delta r^L_{S,i} + \varepsilon_{ijk}\Delta\theta^L_{S,j}\left(D^L_{oN,k} - d^L_{oN,k}\right) + \varepsilon_{ijk}\Delta\theta^L_{S,j}d^L_{oN,k} = \Delta X^L_{N,i} \qquad (66)$$

where the first two terms to the right of the first equal sign are combined as

$$\Delta r^L_{S,i} + \varepsilon_{ijk}\Delta\theta^L_{S,j}\left(D^L_{oN,k} - d^L_{oN,k}\right) = \Delta X^L_{N,i} - \varepsilon_{ijk}\Delta\theta^L_{S,j}d^L_{oN,k} = \Delta R^L_{N,i} \qquad (67)$$

The components $\Delta R^L_{N,i}$ represent a first-order approximation of the displacement of a point in the vicinity of the rack as if that point were rigidly attached to the station. In future discussions, the set of points tracked by the position vectors $\Delta\vec{R}^L_N$ are collectively referred to as the station/rack interface because they are in the vicinity of the area where the station connects to the rack via the umbilical and actuator assemblies. It must be noted, however, that the set of points referred to as the station/rack interface are not coincident with the umbilical and actuator connection points on the station.

Similar reasoning can be used for terms containing the rates of change of the station states given in (m) and (o). From these terms, one obtains the velocity of the N^{th} connection point on the station measured relative to the L frame, which is

$$\vec{V}^L_N = \Delta\dot{\vec{r}}^L_S + \Delta\dot{\vec{\theta}}^L_S \times \vec{D}^L_{oN} \tag{68}$$

The velocity can be rewritten as

$$\Delta\dot{\vec{r}}^L_S + \Delta\dot{\vec{\theta}}^L_S \times \vec{D}^L_{oN} \Rightarrow \Delta\dot{r}^L_{S,i} - \mathbf{D}^L_{oN,ij}\,\Delta\dot{\theta}^L_{S,j} = \Delta\dot{R}^L_{N,i} + \varepsilon_{ijk}\Delta\dot{\theta}^L_{S,j}d^L_{oN,k} \tag{69}$$

where

$$\Delta\dot{R}^L_{N,i} = \Delta\dot{r}^L_{S,i} + \varepsilon_{ijk}\Delta\dot{\theta}^L_{S,j}\left(D^L_{oN,k} - d^L_{oN,k}\right) = V^L_{N,i} - \varepsilon_{ijk}\Delta\dot{\theta}^L_{S,j}d^L_{oN,k} \tag{70}$$

From a practical standpoint, the difference between the velocity represented by the vector $\Delta\dot{\vec{R}}^L_N$ and that represented by $\vec{V}^L_N$ is negligible. By substituting the relation given in Eq. (69) into the equations of motion, however, the mathematics associated with system damping is simplified because the damping matrix associated with the station states can be made identical to the damping matrix associated with the rack states (see Eq. (73)). To determine the elements of the aggregate damping matrix, it has been assumed

that the damping matrix is orthogonal to the modeshapes associated with the rigid body motion of the undamped system. Given an estimation for the modal damping factors, the physical damping matrix can then be calculated (see Appendix D). The ramification of assuming equal damping quantities on the right- and left-hand sides of the equations of motion is that the off-board environment, assumed known at some point on the station, must be mapped to the station/rack interface before it can be used as an input to the equations.

In this section a two-step process is used to map the off-board motion to the station/rack interface. The off-board environment is assumed known at the center of mass of the station and Eqs. (65) and (68) are utilized to map the motion at the station CM to motion at the umbilical and actuator connection points. In the second step, the calculated motion at the connection points ($\Delta X^L_{N,i}$ and $V^L_{N,i}$) is used in Eqs. (67) and (70) to solve for the motion at the station/rack interface.

In actuality the local motion of the station (at the umbilical and actuator connection points) is due to flexure in the structural components of the station as well as the rigid body contribution given in Eqs. (65) and (68). If the local structural behavior of the station is assumed to be unaffected by the motion of the rack, then the local displacements of the station can be assumed to include this structural behavior as well. Generalizing the local station motion to include structural motion also means that the vector quantity $\Delta\bar{\theta}_S$ must be interpreted as the local rotational motion in the vicinity of the connection points. Since low frequency global structural modes look like rigid body motion locally, the station is assumed to be locally rigid and the rotational motion is

assumed to be the same about all of the connection points. From this standpoint, the rack becomes a six degree-of-freedom, harmonic oscillator, connected to a wall of infinite mass via a system of spring/damper elements. The translational and rotational motion of the station at the umbilical and actuator connection points is then treated as a predetermined forcing function to the system, and it can be simulated by the correct combination of translational and rotational inputs at the station/rack interface.

7.2 Rotational Equations of Motion

The derivation of the rotational equations of motion is obtained by the application of Eq. (1) to the Lagrangian and the dissipative function shown in Appendix A. These equations of motion are

$$\frac{d}{dt}\left(\frac{\partial L}{\partial \Delta\dot{\theta}^{R}_{R,\lambda}}\right) - \frac{\partial L}{\partial \Delta\theta^{R}_{R,\lambda}} + \frac{\partial F}{\partial \Delta\dot{\theta}^{R}_{R,\lambda}} = 0 \tag{71}$$

where all torques acting on the rack are assumed to be derivable from the Lagrangian and the dissipative function.

Carrying out Eq. (71) yields the following terms

$$\frac{d}{dt}\left(\frac{\partial L}{\partial \Delta\dot{\theta}^{R}_{R,\lambda}}\right) - \frac{\partial L}{\partial \Delta\theta^{R}_{R,\lambda}} + \frac{\partial F}{\partial \Delta\dot{\theta}^{R}_{R,\lambda}} =$$

$$\begin{aligned}
&I_{x''}\Delta\ddot{\theta}_{x''} - I_{x''y''}\Delta\ddot{\theta}_{y''} - I_{x''z''}\Delta\ddot{\theta}_{z''} \\
&+ I_{x''}\dot{\Omega}_{x'} + \dot{\Omega}_{y'}\left(I_{x''} - I_{y''}\right)\Delta\theta_{z''} + \dot{\Omega}_{z'}\left(I_{z''} - I_{x''}\right)\Delta\theta_{y''} \\
&+ \left[\Omega^2_{y'}\left(I_{y''} - I_{z''}\right) + \Omega^2_{z'}\left(I_{z''} - I_{y''}\right)\right]\Delta\theta_{x''} \\
&+ \Omega_{x'}\Omega_{y'}\left(I_{z''} - I_{x''}\right)\Delta\theta_{y''} + \Omega_{x'}\Omega_{z'}\left(I_{y''} - I_{x''}\right)\Delta\theta_{z''} \\
&+ \Omega_{y'}\left(I_{x''} + I_{z''} - I_{y''}\right)\Delta\dot{\theta}_{z''} + \Omega_{z'}\left(I_{z''} - I_{x''} - I_{y''}\right)\Delta\dot{\theta}_{y''} \\
&- \Omega_{y'}\Omega_{z'}\left(I_{y''} - I_{z''}\right)
\end{aligned}$$

(a) For $\lambda = 1$ only

Permute indices for $\lambda = 2$ and $\lambda = 3$

Orbital coupling terms involving cross moments of inertia have been omitted

$$+\sum_{P} m_P \varepsilon_{\lambda tr} r^R_{P,t} l^{RE/L}_{ri} \left(\ddot{r}^L_{CM,i} + \varepsilon_{ijk} \dot{\Omega}_j r^L_{CM,k} + 2\varepsilon_{ijk} \Omega_j \dot{r}^L_{CM,k} + \varepsilon_{imn} \Omega_m \varepsilon_{njk} \Omega_j r^L_{CM,k} \right) \quad \text{(b)}$$

$$+\sum_{P} m_P \varepsilon_{\lambda tr} r^R_{P,t} l^{RE/L}_{ri} \left(\varepsilon_{ijk} \dot{\Omega}_j r^L_{RE,k} + \varepsilon_{imn} \Omega_m \varepsilon_{njk} \Omega_j r^L_{RE,k} \right) \quad \text{(c)}$$

$$+\sum_{P} m_P \varepsilon_{\lambda tr} r^R_{P,t} l^{RE/L}_{ri} \left(\Delta\ddot{r}^L_{R,i} + \varepsilon_{ijk} \dot{\Omega}_j \Delta r^L_{R,k} + 2\varepsilon_{ijk} \Omega_j \Delta\dot{r}^L_{R,k} + \varepsilon_{imn} \Omega_m \varepsilon_{njk} \Omega_j \Delta r^L_{R,k} \right) \quad \text{(d)}$$

$$+\sum_{P} m_P \varepsilon_{\lambda tr} r^R_{P,t} \left(\ddot{r}^R_{P,r} + \varepsilon_{rmk} \Delta\ddot{\theta}^R_{R,m} r^R_{P,k} + 2\varepsilon_{rmk} \Delta\dot{\theta}^R_{R,m} \dot{r}^R_{P,k} + \varepsilon_{rmk} \Delta\theta^R_{R,m} \ddot{r}^R_{P,k} \right) \quad \text{(e)}$$

+ Additional torques on rack due to coupling between orbital motion and motion of disturbers relative to the rack center of mass. (f)

$$+\sum_{N} \text{KTOR}^R_{N,\lambda i} (\Delta\theta^R_{R,i} - \Delta\theta^R_{S,i}) \quad \text{(g)}$$

$$+\sum_{N} l^{RE/L}_{\lambda i} d^L_{oN,ij} \text{KTRN}^L_{N,jk} \left(\Delta r^L_{R,k} - \Delta r^L_{S,k} \right) \quad \text{(h)}$$

$$-\sum_{N} l^{RE/L}_{\lambda i} d^L_{oN,ij} \text{KTRN}^L_{N,jk} d^L_{oN,km} l^{L/RE}_{mn} \Delta\theta^R_{R,n} \quad \text{(i)}$$

$$+\sum_{N} l^{RE/L}_{\lambda i} d^L_{oN,ij} \text{KTRN}^L_{N,jk} D^L_{oN,km} l^{L/SE}_{mn} \Delta\theta^S_{S,n} \quad \text{(j)}$$

$$+\sum_{N} l^{RE/L}_{\lambda i} d^L_{oN,ij} \text{KTRN}^L_{N,jk} \Delta L^L_{oN,k} \quad \text{(k)}$$

$$+\sum_{N} \text{KTOR}^R_{N,\lambda i} \Delta\theta^R_{oN,i} \quad \text{(l)}$$

$$+\sum_{N} \text{CTOR}^R_{N,\lambda i} (\Delta\dot{\theta}^R_{R,i} - \Delta\dot{\theta}^R_{S,i}) \quad \text{(m)}$$

$$+\sum_{N} l^{RE/L}_{\lambda i} d^L_{oN,ij} \text{CTRN}^L_{N,jk} \left(\Delta\dot{r}^L_{R,k} - \Delta\dot{r}^L_{S,k} \right) \quad \text{(n)}$$

$$-\sum_{N} l^{RE/L}_{\lambda i} d^L_{oN,ij} \text{CTRN}^L_{N,jk} d^L_{oN,km} l^{L/RE}_{mn} \Delta\dot{\theta}^R_{R,n} \quad \text{(o)}$$

$$+\sum_{N} l^{RE/L}_{\lambda i} d^L_{oN,ij} \text{CTRN}^L_{N,jk} D^L_{oN,km} l^{L/SE}_{mn} \Delta\dot{\theta}^S_{S,n} \quad \text{(p)}$$

$$+\frac{\mu_E \sum_{P} m_P \varepsilon_{\lambda tr} r^R_{P,t} l^{RE/L}_{ri} r^L_{CM,i}}{\left| \bar{r}_{CM} \right|^3} \quad \text{(q)}$$

$$+\frac{\mu_E \sum_{P} m_P \varepsilon_{\lambda tr} r^R_{P,t} \left(l^{RE/L}_{ri} \left(r^L_{RE,i} + \Delta r^L_{R,i} \right) - 2\left(r^R_{P,r} + \varepsilon_{rmk} \Delta\theta^R_{R,m} r^R_{P,k} \right) \right)}{\left| \bar{r}_{CM} \right|^3} \quad \text{(r)}$$

$$-\frac{3\mu_E \sum_{P} m_P \varepsilon_{\lambda tr} r^R_{P,t} l^{RE/L}_{r3} \left(r^L_{RE,z} + \Delta r^L_{R,z} \right)}{\left| \bar{r}_{CM} \right|^3} \quad \text{(s)}$$

Discussion of Terms

In discussing the terms in the rotational equations of motion, the vector and matrix equivalents are not given as they were for the translational equations of motion. For the most part, the same forces (with the same vector and matrix equivalents) appear in the rotational equations of motion, but they are subsequently transformed to torques via a cross product operation. The reason is that the line of action of the various forces in the system do not generally run through the rack CM and, as a result, various moments are induced about the CM.

(a)

$$
\begin{aligned}
&I_{x''}\Delta\ddot{\theta}_{x''} - I_{x''y''}\Delta\ddot{\theta}_{y''} - I_{x''z''}\Delta\ddot{\theta}_{z''} \\
&+ I_{x''}\dot{\Omega}_{x'} + \dot{\Omega}_{y'}\left(I_{x''} - I_{y''}\right)\Delta\theta_{z''} + \dot{\Omega}_{z'}\left(I_{z''} - I_{x''}\right)\Delta\theta_{y''} \\
&+ \left[\Omega_{y'}^2\left(I_{y''} - I_{z''}\right) + \Omega_{z'}^2\left(I_{z''} - I_{y''}\right)\right]\Delta\theta_{x''} \\
&+ \Omega_{x'}\Omega_{y'}\left(I_{z''} - I_{x''}\right)\Delta\theta_{y''} + \Omega_{x'}\Omega_{z'}\left(I_{y''} - I_{x''}\right)\Delta\theta_{z''} \\
&+ \Omega_{y'}\left(I_{x''} + I_{z''} - I_{y''}\right)\Delta\dot{\theta}_{z''} + \Omega_{z'}\left(I_{z''} - I_{x''} - I_{y''}\right)\Delta\dot{\theta}_{y''} \\
&- \Omega_{y'}\Omega_{z'}\left(I_{y''} - I_{z''}\right)
\end{aligned}
$$

This represents the inertial time rate of change of the angular momentum of the rack transformed to the rack body-fixed frame. The equation is presented for rotational motion about the x'' axis only ($\lambda = 1$). The equations of motion about the y'' and z'' axes can be easily obtained by cyclically permuting the indices of (a).

For the purpose of presenting the equations of motion, orbital coupling terms involving cross moments of inertia have been omitted. This representation is sufficient to show that

only the first three terms in (a) need to be retained in the equations of motion for rotation about the x″ axis. The largest coefficients of the components of $\Delta\bar{\theta}_R$, appearing in (a), are many times smaller than the stiffness coefficients given in terms (g) and (i) of the rotational equations of motion and therefore have little impact on the dynamic model. The coefficients of the components of $\Delta\dot{\bar{\theta}}_R$, given in (a), are compared to the damping coefficients given in terms (m) and (o). The coefficients appearing in (a) are found to be approximately one order of magnitude less than the smallest eigenvalue of the damping matrices given in (m) and (o). These findings suggest that the umbilical and actuator assemblies induce torques on the rack that are considerably more significant than the torques induced by orbital coupling terms. Therefore, the orbital coupling terms are not included in the final equations of motion for the rack. Since the off-diagonal elements of the moment of inertia matrix are smaller than those of the diagonal, orbital coupling terms involving cross moments of inertia are also omitted from the final equations of motion. The conclusions presented in this discussion are also valid for the equations of motion for rotation about the y″ and z″ axes.

(b)

$$\sum_P m_P \varepsilon_{\lambda\pi} r^R_{P,t} I^{RE/L}_{ri} \left(\ddot{r}^L_{CM,i} + \varepsilon_{ijk}\dot{\Omega}_j r^L_{CM,k} + 2\varepsilon_{ijk}\Omega_j \dot{r}^L_{CM,k} + \varepsilon_{imn}\Omega_m \varepsilon_{njk}\Omega_j r^L_{CM,k} \right)$$

These terms represent the moment of the time rate of change of linear momentum (due to orbital motion) of the disturbers about the center of mass of the rack. This torque is nearly canceled by the torque induced by the action of the gravity force in (q).

(c)

$$\sum_{P} m_P \varepsilon_{\lambda tr} r^R_{P,t} l^{RE/L}_{ri} \left(\varepsilon_{ijk} \dot{\Omega}_j r^L_{RE,k} + \varepsilon_{imn} \Omega_m \varepsilon_{njk} \Omega_j r^L_{RE,k} \right)$$

This is the torque induced about the center of mass of the rack due to the quasi-steady tangential- and centripetal-type forces acting on the disturber masses. These torques are negligible in comparison to the first term of (e) below and are, therefore, omitted from the dynamic model.

(d)

$$\sum_{P} m_P \varepsilon_{\lambda tr} r^R_{P,t} l^{RE/L}_{ri} \left(\Delta \ddot{r}^L_{R,i} + \varepsilon_{ijk} \dot{\Omega}_j \Delta r^L_{R,k} + 2\varepsilon_{ijk} \Omega_j \Delta \dot{r}^L_{R,k} + \varepsilon_{imn} \Omega_m \varepsilon_{njk} \Omega_j \Delta r^L_{R,k} \right)$$

As the rack moves, it carries with it the disturber masses. Since the disturber masses are not located at the rack CM, this perturbed rack motion induces torques about the rack CM, which are represented in (d). These terms are negligible in comparison to the first term of (e).

(e)

$$\sum_{P} m_P \varepsilon_{\lambda tr} r^R_{P,t} \left(\ddot{r}^R_{P,r} + \varepsilon_{rmk} \Delta \ddot{\theta}^R_{R,m} r^R_{P,k} + 2\varepsilon_{rmk} \Delta \dot{\theta}^R_{R,m} \dot{r}^R_{P,k} + \varepsilon_{rmk} \Delta \theta^R_{R,m} \ddot{r}^R_{P,k} \right)$$

The terms in (e) represent the time rate of change of the angular momentum of the disturber masses about the rack center of mass due to their acceleration relative to the rack CM. The terms in parentheses are identical to those presented in terms (g) of the translational equations of motion. Consistent with the discussion of terms (g), the second

and third terms in (e) (the tangential and Coriolis terms respectively) are omitted from the final equations of motion presented in this paper. A comparison between the coefficients of the components of $\Delta\bar{\theta}_R^R$ given in the last term in (e) and the eigenvalues of the stiffness matrices given in terms (g) and (i) of the rotational equations of motion reveals that the ratio between the largest coefficient in (e) and the smallest eigenvalue of (g) and (i) is 0.07. For this reason, the last term in (e) is omitted from the final equations of motion as well.

(f)

Additional torques on rack due to coupling between orbital motion and motion of the disturbers relative to the rack center of mass.

The set of torques described in (f) are due to the forces described in term (h) of the translational equations of motion. The relative positions between the disturber masses and the rack center of mass act as moment arms so that forces at the disturber mass locations result in torques about the rack CM. Just as the force terms in (h) of the translational equations are negligible, the torques described in term (f) are also negligible.

(g)

$$\sum_N \text{KTOR}^R_{N,\lambda i}(\Delta\theta^R_{R,i} - \Delta\theta^R_{S,i})$$

The expression (g) is the restoring torque induced in the umbilical and actuator assemblies due to relative angular displacements between the rack and the station.

(h)

$$\sum_{N} l_{\lambda i}^{RE/L} \mathbf{d}_{oN,ij}^{L} \, KTRN_{N,jk}^{L} \left(\Delta r_{R,k}^{L} - \Delta r_{S,k}^{L} \right)$$

Since the elastic elements tethering the rack to the station are not connected to the rack center of mass, relative linear displacements between the rack and the station induce moments about the rack CM, which are represented by (h).

(i)

$$-\sum_{N} l_{\lambda i}^{RE/L} \mathbf{d}_{oN,ij}^{L} \, KTRN_{N,jk}^{L} \mathbf{d}_{oN,km}^{L} l_{mn}^{L/RE} \Delta\theta_{R,n}^{R}$$

When the rack undergoes angular displacements about its center of mass, translational displacements of the umbilical and actuator connection points result. These displacements induce restoring forces at the connection points and torques about the rack center of mass given in (i).

(j)

$$\sum_{N} l_{\lambda i}^{RE/L} \mathbf{d}_{oN,ij}^{L} \, KTRN_{N,jk}^{L} \mathbf{D}_{oN,km}^{L} l_{mn}^{L/SE} \Delta\theta_{S,n}^{S}$$

The expression (j) is similar to expression (i) but applies to the angular displacement of the station about its center of mass.

(k)

$$\sum_{N} l_{\lambda i}^{RE/L} d_{oN,ij}^{L} KTRN_{N,jk}^{L} \Delta L_{oN,k}^{L}$$

When the system is in the equilibrium configuration, the quasi-steady forces, which are assumed to act at the center of mass of the rack, result in a small translational displacement of the rack from the unstretched position. This displacement results in restoring forces in the umbilical and actuator assemblies that induces small torques, (k), about the center of mass of the rack.

(l)

$$\sum_{N} KTOR_{N,\lambda i}^{R} \Delta\theta_{oN,i}^{R}$$

Term (l) represents a restoring torque in the umbilical and actuator assemblies due to the small angular extension of these elastic elements when the system is in the equilibrium configuration.

(m), (n), (o) and (p)

These terms are similar to (g), (h), (i), and (j) but for moments induced by dissipative forces.

(q)

$$\frac{\mu_E \sum_P m_P \varepsilon_{\lambda t r} r^R_{P,t} l^{RE/L}_{ri} r^L_{CM,i}}{\left|\bar{r}_{CM}\right|^3}$$

The action of the gravitational force on the disturber masses results in a torque about the rack center of mass that is nearly canceled by torque terms given in (b).

(r) and (s)

$$\frac{\mu_E \sum_P m_P \varepsilon_{\lambda t r} r^R_{P,t} \left(l^{RE/L}_{ri} \left(r^L_{RE,i} + \Delta r^L_{R,i} \right) - 2 \left(r^R_{P,r} + \varepsilon_{rmk} \Delta\theta^R_{R,m} r^R_{P,k} \right) \right)}{\left|\bar{r}_{CM}\right|^3}$$

and

$$-\frac{3\mu_E \sum_P m_P \varepsilon_{\lambda t r} r^R_{P,t} l^{RE/L}_{r3} \left(r^L_{RE,z} + \Delta r^L_{R,z} \right)}{\left|\bar{r}_{CM}\right|^3}$$

Expressions (r) and (s) represent torques about the rack center of mass due to gravity gradient forces acting on the disturber masses. These torques are negligible due to the small mass of the disturbers.

Rewriting the Rotational Equations of Motion

As in the case of the translational equations of motion, the force per unit mass relation given in vector Eq. (38) may be utilized to combine terms from the rotational equations of motion. The terms in (b) along with the terms given in (q) can be combined to give

$$\sum_P m_P \varepsilon_{\lambda ir} r^R_{P,t} l^{RE/L}_{ri} \left(\ddot{r}^L_{CM,i} + \varepsilon_{ijk} \dot{\Omega}_j r^L_{CM,k} + 2\varepsilon_{\lambda jk} \Omega_j \dot{r}^L_{CM,k} + \varepsilon_{imn} \Omega_m \varepsilon_{njk} \Omega_j r^L_{CM,k} \right)$$

$$+ \frac{\mu_E \sum_P m_P \varepsilon_{\lambda ir} r^R_{P,t} l^{RE/L}_{ri} r^L_{CM,i}}{\left| \bar{r}_{CM} \right|^3} \qquad (72)$$

$$= \frac{\sum_P m_P}{M_{TOTAL}} \varepsilon_{\lambda ir} r^R_{P,t} l^{RE/L}_{ri} F^L_{EXT,i}$$

where $\varepsilon_{\lambda ir} r^R_{P,t} l^{RE/L}_{ri} F^L_{EXT,i}$ is recognized as a small quasi-steady torque about the rack's center of mass.

In the equilibrium force balance for the system, the orbitally induced forces on the small disturber masses are negligible because the accelerations induced in the rack due to these forces are several orders smaller than the micro-g level. A similar assumption is made concerning the orbitally induced torques on the disturber masses. This assumption leads to the omission of the small quasi-steady torque term on the right-hand side of Eq. (72) as well as the torques represented in terms (c), (d) and (f) of the rotational equations of motion. The torques given in terms (k) and (l), along with the last term in (a) (where indices are permuted to get the appropriate y- and z- direction term), are then assumed to cancel each other in the rotational equations of motion, so that an equilibrium torque balance can be formulated for the system.

The rationale used in mapping the station motion to the station/rack interface can be used in the rotational equations of motion as well. The station displacements from terms (h) and (j) can be combined (as can the station rates from terms (n) and (p)) to reflect motion at the interface. Just as in the case of the translational equations of motion, the off-board environment, assumed known at some point on the station, must be mapped to the station/rack interface before it can be used as an input to the equations.

7.3 Equations of Motion in Matrix Form

The primary frame of reference up to this point in the development has been the local orbital frame. This frame was chosen because of the practical relations of its axes to the orbital motion and the intuitive form of the gravity gradient terms. Since the objective of this research is to build a simulation capability for the ARIS, the rack body-fixed frame provides a more suitable frame in which to write the final form of these equations. The reason is that the RF is local to the rack motion and because ARIS controller hardware, such as the accelerometers and actuator pushrods, are assumed fixed relative to this frame.

The vector and tensor quantities given in the translational and rotational equations of motion in Sections 7.1 and 7.2 may be transformed to the REF through the time-invariant transformation matrix $\left[l^{RE/L}\right]$. In the subsequent transformation from the REF to the RF, the small-angle correction terms are omitted because these terms result in small second-order terms in the equations of motion. Under this condition, the translational and rotational equations of motion can be represented in the matrix form to be given in Eq. (73). In this equation, all rack and station states are measured relative to the REF but resolved along the RF. As for the disturber mass motion, $\left[r_P^R\right]$ is the matrix representing the antisymmetric second order tensor associated with the position vector $\bar{r}_P^R$ and is used to calculate the vector cross product of $\bar{r}_P^R$ and $\ddot{\bar{r}}_P^R$.

Eq. (73) reflects the assumption that the coupling effects between the orbital motion of the system and the perturbed motion of the rack are negligible so that the locally observed motion is approximated as that exhibited by the equivalent inertially-

based system. Although quasi-steady orbital-induced accelerations must still be added in order to compute the inertial acceleration of the rack, these accelerations can be assumed independent of the local perturbed motion of the rack. The resulting equation of motion in matrix form is

$$
\begin{bmatrix} M_R & 0 \\ 0 & I_R^R \end{bmatrix} \begin{Bmatrix} \Delta\ddot{r}_R \\ \Delta\ddot{\theta}_R \end{Bmatrix}
$$

$$
+ \begin{bmatrix} \sum_N [CTRN_N^R] & \sum_N [CTRN_N^R][d_N^R]^T \\ \sum_N [d_N^R][CTRN_N^R] & \sum_N [d_N^R]^T [CTRN_N^R][d_N^R] + \sum_N [CTOR_N^R] \end{bmatrix} \begin{Bmatrix} \Delta\dot{r}_R \\ \Delta\dot{\theta}_R \end{Bmatrix}
$$

$$
+ \begin{bmatrix} \sum_N [KTRN_N^R] & \sum_N [KTRN_N^R][d_N^R]^T \\ \sum_N [d_N^R][KTRN_N^R] & \sum_N [d_N^R]^T [KTRN_N^R][d_N^R] + \sum_N [KTOR_N^R] \end{bmatrix} \begin{Bmatrix} \Delta r_R \\ \Delta\theta_R \end{Bmatrix}
$$

$$
= \begin{bmatrix} \sum_N [CTRN_N^R] & \sum_N [CTRN_N^R][d_N^R]^T \\ \sum_N [d_N^R][CTRN_N^R] & \sum_N [d_N^R]^T [CTRN_N^R][d_N^R] + \sum_N [CTOR_N^R] \end{bmatrix} \begin{Bmatrix} \Delta\dot{R}_N \\ \Delta\dot{\theta}_S \end{Bmatrix}
$$

$$
+ \begin{bmatrix} \sum_N [KTRN_N^R] & \sum_N [KTRN_N^R][d_N^R]^T \\ \sum_N [d_N^R][KTRN_N^R] & \sum_N [d_N^R]^T [KTRN_N^R][d_N^R] + \sum_N [KTOR_N^R] \end{bmatrix} \begin{Bmatrix} \Delta R_N \\ \Delta\theta_S \end{Bmatrix}
$$

$$
- \sum_P m_P \begin{Bmatrix} \{\ddot{r}_P^R\} \\ [r_P^R]\{\ddot{r}_P^R\} \end{Bmatrix}
$$

(73)

7.4 Calculation of Inertial Acceleration

The equations of motion given in Eq. (73) are written in terms of accelerations and velocities measured relative to the REF. From the standpoint of maintaining a microgravity environment inside the rack, the accelerations must be known in the inertial frame because the physical processes associated with the various microgravity experiments are affected by the total inertial acceleration. The inertial acceleration is

$$\bar{a}_I = \bar{a}_{RE} + \bar{a}_{R/RE} \tag{74}$$

where $\bar{a}_I$ is the total inertial acceleration of the rack center of mass, $\bar{a}_{RE}$ is the inertial acceleration of the point RE, and $\bar{a}_{R/RE}$ is the inertially measured acceleration of the rack center of mass relative to the point RE.

The total acceleration of the point RE is

$$\bar{a}_{RE} = \bar{a}_{EXT} + \bar{a}_{CENT} + \bar{a}_{GG} \tag{75}$$

where $\bar{a}_{EXT}$ is the acceleration due to the external forces, $\bar{a}_{CENT}$ is the centripetal acceleration due to the once per orbit rotation of the point RE about the composite center of mass, and $\bar{a}_{GG}$ is the acceleration due to the gravity gradient effect. The tangential acceleration is not included because it is negligible. The centripetal, gravity gradient, and external forces were derived in the equations of motion for the rack and discussed in Section 7.1.

The acceleration of point RE due to the action of external forces is

$$\bar{a}_{EXT} = \frac{\bar{F}_{EXT}}{M_{TOTAL}} \tag{76}$$

where $\frac{\bar{F}_{EXT}}{M_{TOTAL}}$ is the same quantity given on the right-hand side of Eq. (38). Although the components of the vector $\bar{a}_{EXT}$ are assumed to be known (resolved) in the REF, they must be resolved along the rack body-fixed frame if they are to be added directly to the acceleration components computed in Eq. (73). For the purpose of this study, the small-angle correction terms resulting from the transformation of the quasi-steady accelerations from the REF to the RF are negligible because changes in orientation of the rack result in restoring forces in the umbilical and actuator assemblies that are much greater than those resulting from the small correction of the quasi-steady force terms.

The centripetal acceleration of point RE is given in term (b) of the translational equations of motion as

$$\bar{a}_{CENT} = \bar{\Omega} \times \left(\bar{\Omega} \times \bar{r}_{RE} \right) \tag{77}$$

where the components are again assumed to be resolved along the REF axes. Just as in the case of $\bar{a}_{EXT}$, small angle correction terms in the transformation of the centripetal acceleration from the REF to the RF are negligible.

The gravity gradient acceleration, resolved along the REF, can be computed from

$$\left\{ a_{GG}^{RE} \right\} = \left[l^{RE/L} \right] \begin{Bmatrix} a_{GG,x} \\ a_{GG,y} \\ a_{GG,z} \end{Bmatrix} \tag{78}$$

where $a_{GG,x}$, $a_{GG,y}$, and $a_{GG,z}$ are the components of the gravity gradient acceleration resolved along local orbital frame. These components are taken directly from terms (p) and (q) of the translational equations of motion and are

$$a_{GG,x} = \frac{\mu_E r_{RE,x}}{\left|\vec{r}_{CM}\right|^3}$$

$$a_{GG,y} = \frac{\mu_E r_{RE,y}}{\left|\vec{r}_{CM}\right|^3} \tag{79}$$

$$a_{GG,z} = -\frac{2\mu_E r_{RE,z}}{\left|\vec{r}_{CM}\right|^3}$$

As in the case of $\vec{a}_{EXT}$ and $\vec{a}_{CENT}$, correction terms in the transformation of the components of the gravity gradient acceleration from the REF to the RF are omitted in the calculation of the inertial acceleration of the rack.

Consistent with the discussion in Section 7.1, the orbital coupling terms between the orbital motion and the perturbed rack motion (given in (c) of the translational equations of motion) as well as the gravity gradient acceleration arising from the small displacement of the rack from its equilibrium position (given in (p) and (q) of the translational equations) are considered negligible. The inertial acceleration of the rack relative to the point RE is approximated as

$$\vec{a}_{R/RE} \approx \Delta\ddot{\vec{r}}_R^{RE} \tag{80}$$

The approximation given in Eq. (80) states that the inertially measured acceleration of rack, relative to the point RE, is approximated by the locally observed, perturbed acceleration.

Given the assumptions above, the difference between the locally observed perturbed acceleration of the rack (computed from the equations of motion given in Eq. (73)) and that pertinent to the inertial acceleration is the simple addition of a group of quasi-steady acceleration terms that are not functions of the generalized coordinates and

can be considered predetermined functions of time. Since small-angle correction terms in the transformation of the quasi-steady accelerations are negligible, knowledge of the quasi-steady accelerations resolved along the REF is sufficient for this study. The quasi-steady accelerations are considered constant in magnitude and direction over the time interval of interest. These accelerations are then added directly to the perturbed accelerations from Eq. (73) so that the total inertial acceleration can be computed.

8. SIMULINK Version of the Simulation

The purpose of this chapter is to present the SIMULINK version of the ARIS simulation and to show the predicted attenuation performance of the ARIS using results from this simulation. SIMULINK is software for use with MATLAB, a mathematics software package sold by The MathWorks, Inc. (The MathWorks, Inc., *SIMULINK Users Guide*, 1992). SIMULINK provides an environment for the modeling of dynamic systems and controllers. The convenience of SIMULINK derives from its graphical user interface, which allows the building of simulations using block diagrams in conjunction with a variety of pull-down menus. These menus also provide the user with a variety of analytical tools. Additional analysis can be carried out from the MATLAB environment with MATLAB executable files or directly from the command line.

Section 8.1 shows the implementation of the rigid body equations of motion for the rack (Eq. (73)) in the SIMULINK environment. Block diagrams from the SIMULINK simulation are presented that show the simulation architecture and information flow. In Section 8.2 results from the simulation presented in Section 8.1 are discussed. These results apply only to the passive system (ARIS controller inactive). Section 8.3 details the ARIS controller simulation and shows integration of the controller simulation with the rigid body model presented in Section 8.1. Section 8.4 presents results for the closed-loop system (ARIS active).

8.1 Block Diagrams of the Rigid Body Rack Model

The equations of motion given in Eq. (73) are conveniently represented in block diagram form and shown in Figure 10 and Figure 11. The high-level block diagram of Figure 10 shows the complete simulation for the rigid body rack. Multiplexer (Mux) and Demultiplexer (Demux) blocks are utilized to reduce the number of connections needed, therefore reducing the complexity of the diagram. The bold lines represent the transmission of vector information. In this case, the bold lines represent the flow of vector information having six elements, one for each degree of freedom of the rack. Complexity can be further reduced by the use of superblocks, in which a number of individual blocks can be grouped together. Examples of these superblocks are the *Station Interface* block and the *Rigid Rack* block.

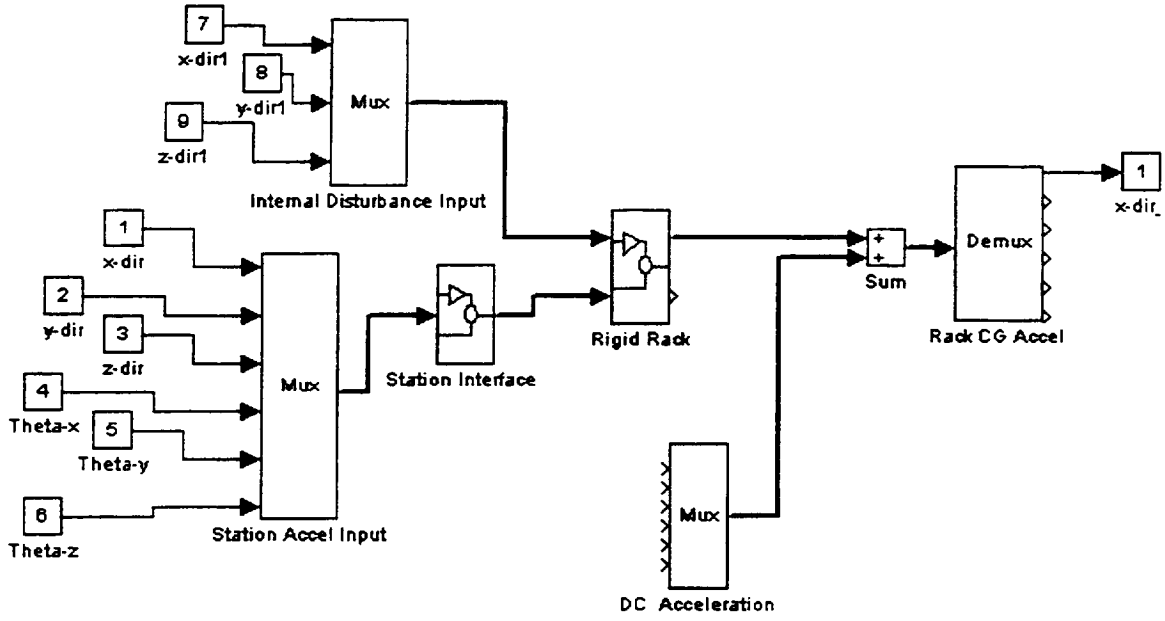

Figure 10: High-Level Block Diagram for Rigid Body Rack Dynamics

The block diagram of Figure 11 shows the blocks that are part of the *Rigid Rack* superblock. Figure 11 is the wiring diagram that carries out the matrix operations on the left-hand side of Eq. (73). In this figure, a number of statespace blocks are used, and these blocks all carry the label

$$x' = Ax + Bu$$
$$y = Cx + Du$$

For the simulation presented in this paper the statespace blocks are used to carry out matrix multiplication by setting the elements of the A, B, and C matrices to zero and setting D equal to the matrix that is multiplied by the vector input. In the block labeled *Stiffness*, the D matrix is set equal to the aggregate 6x6 stiffness matrix. Therefore the statespace blocks actually have no states associated with them. The output of the *Rigid Rack* superblock is the perturbed acceleration of the rack, measure relative to the REF and resolved along the rack body-fixed frame. The stiffness, damping and mass parameters needed to run the simulation are generated in the MATLAB executable file SIM_BSLN.m, which is presented in Appendix F.

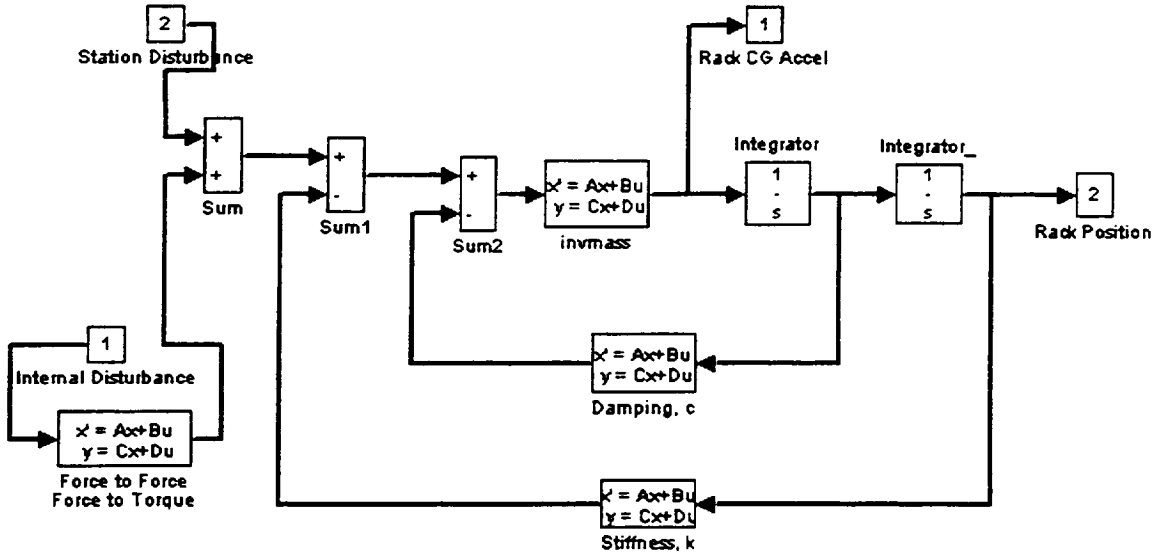

Figure 11: Sub-Level Diagram of the *Rigid Rack* Superblock

The *Station Interface* superblock, shown in the high-level diagram of Figure 10, converts station accelerations at the station/rack interface into force inputs to the rack. Upon entering the *Station Interface* block, the station acceleration signal is directed along two different paths. Along one of the paths the signal is integrated twice to calculate the station displacement vector and this displacement vector is subsequently multiplied by the aggregate stiffness matrix to produce a force input. Along the other path the station acceleration signal is integrated once to compute the local station velocity and this velocity vector is multiplied with the aggregate damping matrix. These force inputs are then added together and routed into the *Rigid Rack* superblock.

8.2 Results for the Passive System

The first results to be presented from the rack model are those for the passive system response. The passive response is defined as the response of the system to various inputs when the umbilical assembly is the only connection between the rack and the

station. The actuators are assumed not to be connected to the rack and the ARIS controller is therefore rendered inactive. All of the results presented in this section are those for the baseline heavy rack with a full set of umbilicals. The physical parameters of this system are given in Appendix B.

Off-Board Disturbance Response

Figures 12 and 13 are transfer functions that show the response of the system due to acceleration disturbances at the station/rack interface. The transfer functions show the gain in decibels of the rack acceleration output to the station acceleration input. In generating the transfer function in Figure 12, the station input is assumed to be an x-directional acceleration input (in the rack body-fixed frame). This assumption is equivalent to setting the components of $\Delta\bar{\theta}_S$ and $\Delta\dot{\bar{\theta}}_S$ to zero in Eqs. (67) and (70). These equations show that a purely x-direction input at the station/rack interface is also equivalent to a purely x-direction input at the umbilical connection points on the station. The output for the transfer function in Figure 12 is the x-direction rack acceleration.

Although the station is assumed to be locally rigid, the environment at the umbilical connection points is assumed to be the result of structural motion of the station as well as rigid body motion. The collection of umbilicals are taken as one aggregate assembly, possessing an aggregate stiffness, with the vector $\bar{d}_{oN\ (N=1\ only)}$ pointing to the centroid of the assembly connections. The reason for this is the translational and torsional stiffness parameters used by the simulation to generate the 6x6 stiffness matrix are supplied by the ARIS developers as total stiffness quantities for the entire assembly.

Figure 12 reveals that resonant peaks exist at certain points in the frequency spectrum at which the off-board acceleration environment is amplified. These resonances are associated with the rigid body motion of the rack as it oscillates on the umbilical assembly. The first resonant peak occurs in the vicinity of 0.07 Hz and results in an amplification of the station environment by a factor of (approximately) thirty. Multiple resonances occur because the rack is a multi-degree-of-freedom system. If the resonant behavior of the system is not controlled, the microgravity environment inside the rack will not meet the microgravity requirement shown in Figure 2. At frequencies lower than the first resonant frequency a unity transmissibility (zero db) is predicted between the rack output and station input. Because of sway-space concerns, this is a desirable response because, if the input and output signals are in phase, the rack motion will track the station motion and the swayspace will be maintained. At frequencies above the highest resonant frequency (approximately 0.5 Hz) the gain decreases, at a rate of about 40 db/decade up to 20 Hz, then at a rate of approximately 20 db/decade beyond this point. This change in slope is due to the damping property of the umbilical assembly.

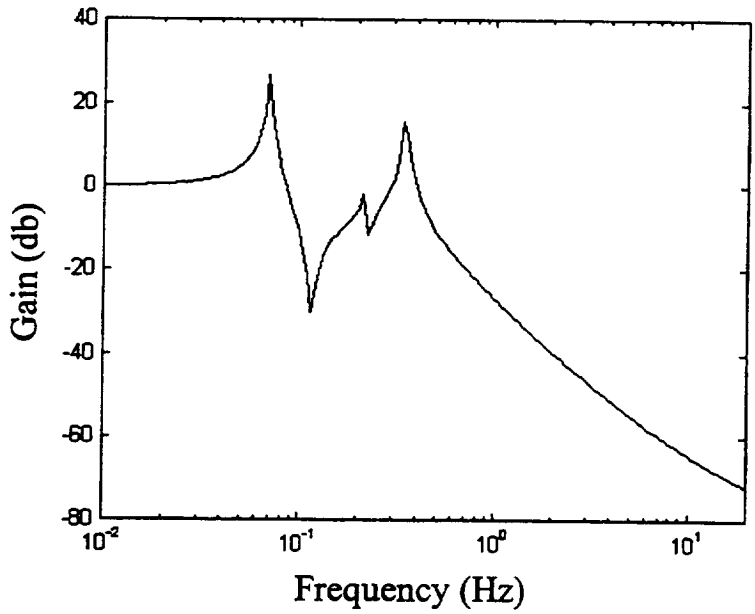

Figure 12: Onboard Response to Off-Board Acceleration: x-Direction

Figure 13 is a plot of the rack response due to a combination of translational and rotational acceleration inputs at the station/rack interface. This combination of inputs has been chosen to simulate a pure rotational acceleration input at the centroid of the array of umbilical connections on the station. The simulated rotational input is a unidirectional rotation about the x axis of the rack body-fixed frame. The plot represents the gain ratio of the angular acceleration of the rack about the x axis to the angular acceleration of the station about the x axis. The station disturbance is transmitted to the rack via the torsional stiffness property of the umbilical assembly. As in Figure 12, resonant peaks can be seen at certain points in the frequency spectrum. These resonances are associated with the (rotational) rigid body motion of the rack. At higher frequencies the transfer function decreases with a slope that becomes shallower with increasing frequency. Just as in Figure 12, this change in slope is due to the damping property of the umbilical assembly.

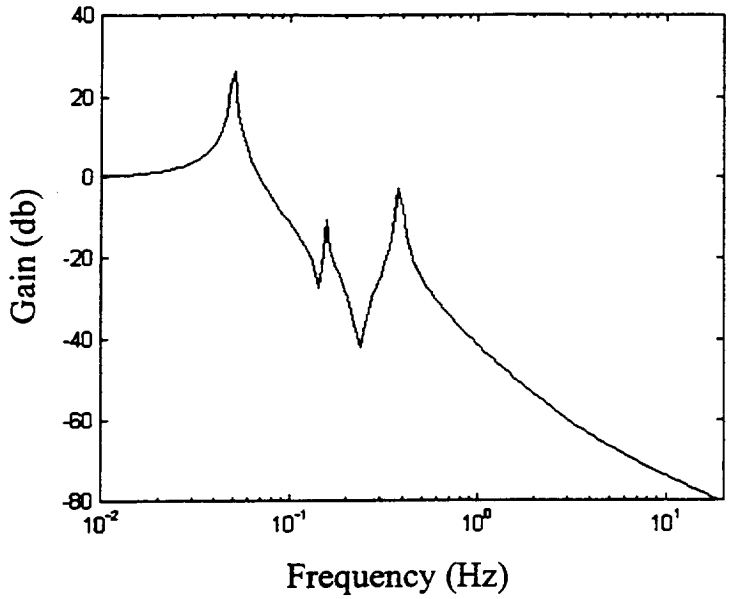

Figure 13: Onboard Response to Off-Board Acceleration: Theta-x Direction

Onboard Disturbance Response

To illustrate the passive response of the system to an onboard disturbance source, the onboard forcing function given in Eq. (73) is assumed to be an oscillatory signal originating from hardware mounted on the microgravity rack. In order to maximize the torque input, the location of the disturbance source is chosen as the extreme upper corner of the rack. Figure 14 shows the ratio of the magnitude of the x-direction acceleration of the center of mass of the rack (the output in units of ft/sec^2) to the magnitude of the x-direction onboard force (the input in units of lbf) as a function of forcing frequency.

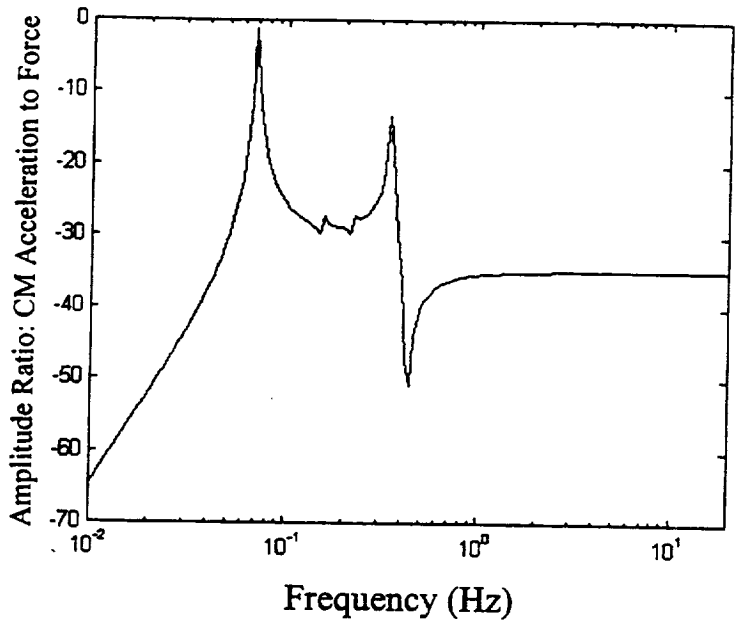

Figure 14: Onboard Acceleration Response to Onboard Force

In the low frequency ranges, the presence of the umbilical assembly helps to isolate the rack from the acceleration effects of the onboard force. Between the frequency ranges of 0.06 Hz and 0.4 Hz, the system undergoes resonant behavior associated with the rigid body translation of the rack. The peak amplitude ratio occurs at approximately 0.07 Hz and nearly reaches the 0 db level. At frequencies above 1 Hz, the amplitude of the rack CM acceleration is a factor of 35 dB less than that of the onboard force amplitude, corresponding to the inverse of the mass of the baseline rack. Therefore, at forcing frequencies above approximately 1 Hz the rack behaves as a free body in space.

8.3 ARIS Baseline Controller Simulation

The ARIS baseline controller simulation presented in this section was constructed from a number of different sources. For the most part, the latest control law was pieced together from information presented at the ARIS Critical Design Review (CDR), held at the Marshall Spaceflight Center, in November, 1996. Other information on the controller was obtained through communications with the ARIS developers and by reviewing documents from previous design reviews and Technical Interchange Meetings (TIM's). Although the controller design undergoes seemingly continuous changes, the controller presented in this section is known to be quite current. The controller versions used for the ARIS Risk Mitigation Experiment (RME) are discussed in Chapter 9 and these versions differ from the baseline version presented in this chapter. The ARIS controller is a state-of-the-art control system that employs a combination of acceleration, position, and stiffness compensation control loops to maintain a microgravity environment inside of an ISPR. Included in the position control is a non-linear anti-bump algorithm that is not modeled in the simulation presented in this paper.

The block diagram for the baseline ARIS controller simulation is shown in Figure 15. The plant model for the rack (the *Rigid Rack* block) appears in the middle portion of the diagram and is nearly identical to that presented in Section 8.1 and shown in Figure 10. One exception is that the an extra input path has been added to interface the plant model with the ARIS controller. Another difference between the passive plant model and the plant model used in the closed-loop simulation is in the stiffness and damping matrices. In the closed-loop simulation the effect of the passive actuator stiffness and

damping must be added to that of the umbilical assembly. For the purpose of this study, a 6x6 actuator stiffness matrix, computed in a MATRIX-X executable file provided by the ARIS developers, has been utilized. MATRIX-X is a mathematics software package that can be used to carry out the matrix calculations needed to generate all of the parameters used in the ARIS simulation (Integrated Systems Inc., *MATRIX-X CORE,* Document Number MDG014-010, 1990). The executable file was converted to MATLAB format and has been included in the code in Appendix F. Since the time this code was supplied by The Boeing Company, the geometry of the lower external actuator pair was changed slightly in the baseline design to eliminate an interference problem. This change is expected to have minimal effect on the aggregate stiffness and system performance, but future work should include obtaining the updated stiffness model and exact geometry of the actuator assembly. As in the case of the umbilical stiffness matrix, the actuator stiffness is referenced to the rack body-fixed coordinate system and to inputs at the station/rack interface.

Two separate outputs are taken from the plant model. The upper output is directed into block *Sum1* and is the predicted acceleration of the center of mass of the rack. The acceleration signal is sent through the acceleration feedback loop (uppermost loop) and operated on by the acceleration compensator. The lower output from the plant model is a rack position measurement. In block *Sum2* the perturbed displacement between the rack and the station/rack interface is calculated. This relative displacement information is required by the position control loop (lowest most loop) which maintains proper swayspace between the rack shell and the wall of the station. The relative position

measurement is also utilized by the stiffness compensation feedforward loop (middle loop).

When the computed acceleration of the rack center of mass enters block *Sum1*, it is added to the DC (quasi-steady) acceleration signal. As explained earlier, the quasi-steady acceleration of the rack is considered independent of the rack states and constant in magnitude over the time interval of interest. The total computed acceleration of the rack center of mass is then forwarded to block *Txtow* which computes the accelerations at the accelerometer head locations. The accelerations measured at the accelerometer locations are different from those experienced at the center of mass of the rack because the angular acceleration of the rack induces an additional translational acceleration component at these locations.

Just as in the block diagram presented in Figure 11, the controller simulation uses a number of statespace blocks, of which block *Txtow* is an example. As described in Section 8.1, these blocks are used to carry out matrix multiplication and have no states associated with them. For the most part, the matrix contained in the block in the actual simulation is the same as the name placed under the block, and these matrices are generated by the MATLAB code in Appendix F.

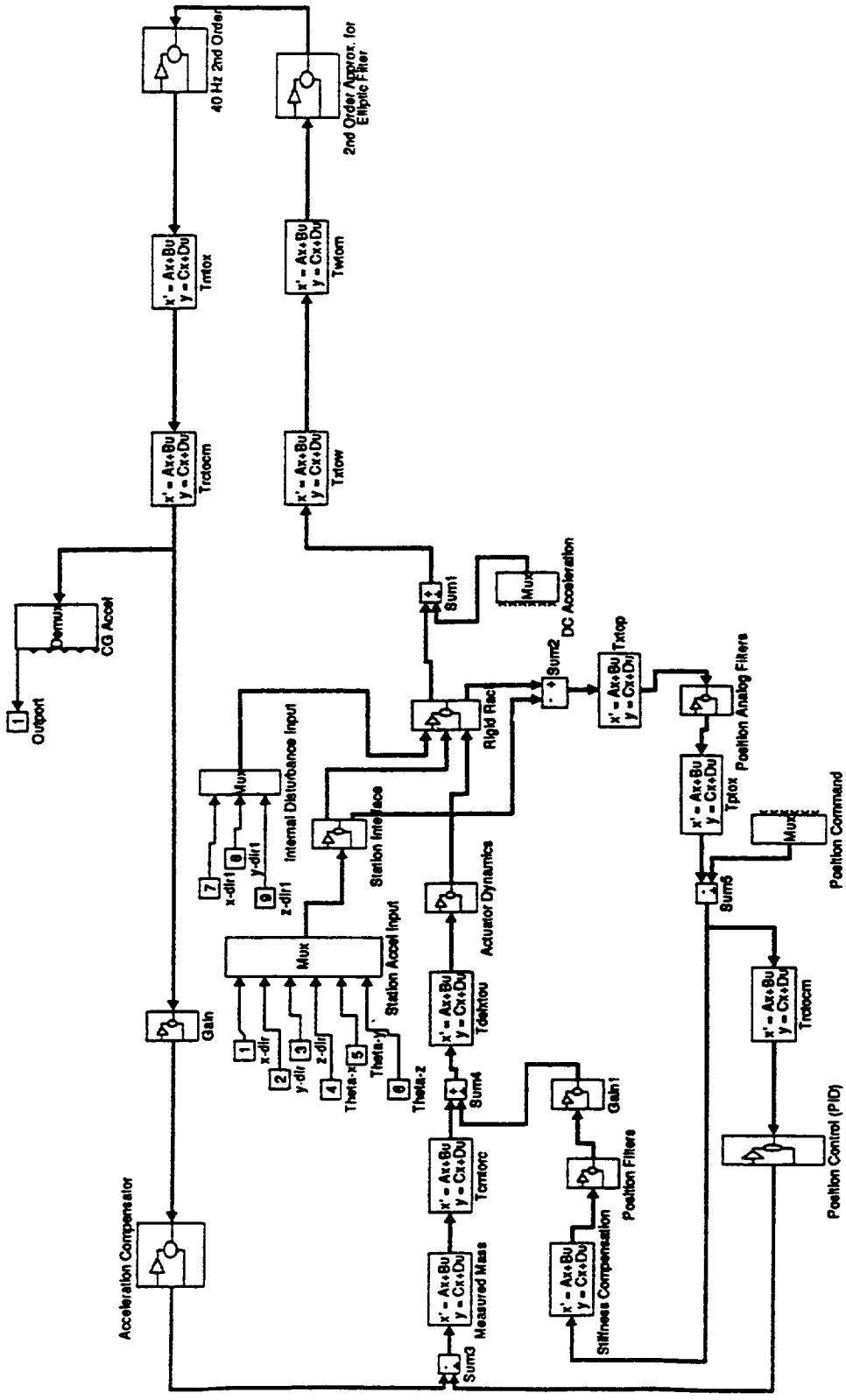

Figure 15: The Closed-Loop ARIS Simulation

After the acceleration signal is passed through block *Txtow*, the acceleration signals (now at the accelerometer head locations) are resolved along the accelerometer orientations to simulate the measurement of the total acceleration. This procedure is carried out in block *Twtom*. The computer code used to calculate the accelerometer location and geometry parameters was supplied by the ARIS developers. Since the time at which this code was supplied, a change has occurred in the location of the upper accelerometer assembly. Furthermore, since the time the code was supplied, an additional accelerometer has been added to the production ARIS bringing the total number of accelerometers to nine. Although there seems to be minimal impact to the system performance, future work should include obtaining the latest code for generating the accelerometer parameters in light of this design change.

The next block downstream in the acceleration feedback loop represents the elliptic filter elements. The simulation utilizes a 2^{nd} order filter to simulate the real elliptic-type filter that is wired into the ARIS controller. The 2^{nd} order filter is a good approximator of the elliptic filter response up to about 10 Hz, at which point the transfer function for the approximator diverges from that of the elliptic filter. The baseline ARIS controller also utilizes an adjustable second order filter that is planned to have a natural frequency set to 40 Hz when the ARIS is operational on the station. The block simulating this element appears downstream from the elliptic filter block.

The acceleration compensator operates on the acceleration signal of the rack center of mass resolved along the rack body-fixed frame so that the accelerations measured by the accelerometers must be resolved back along this frame. This

transformation is accomplished in a two-step process. Firstly, in block *Tmtox,* the eight accelerometer signals are resolved along the *rack center frame*, which is a reference frame with an origin at the geometric center of the rack. In the next step the signal is sent into block *Trctocm* in which a small correction is made to the acceleration signal to transform it from the origin of the rack center frame to the rack center of mass (the origin of the rack body-fixed frame). In the simulation the *Trctocm* block contains the 6x6 matrix *ctm*, which is generated by the code in Appendix F. In the actual ARIS controller the parameter *ctm* can be updated from measurements made by the payload evaluator (see Section 3.2). Since the acceleration at the center of mass of the rack is a quantity of interest, this signal is forwarded to an outport via a demultiplexer block that separates the acceleration signal into its various components. The signal is also forwarded to the *Gain* block, where the loop gain is set, and then forwarded to the acceleration compensator.

The *Acceleration Compensator* block consists of six identical cascade compensators, each of which operates on one of the rack acceleration components. One set of compensators is shown in Figure 16. The compensator has five other branches (one for each translational and rotational acceleration component) and they are all identical to the one shown in Figure 16. The control methodology employed in the acceleration compensator is single input single output (SISO)-type control.

The output signal from the acceleration compensator block is added to the signal from the position control loop in block *Sum3* and the combined signal is multiplied with the full 6x6 mass matrix to produce a set of force and torque commands. The signal is then transformed back to the rack center frame in the block *Tcmtorc.* The *Tcmtorc* block contains the matrix *ctmi* (generated by the code in Appendix F). The force commands are

then transformed to actuator commands in block *Tdelxtou* (the parameters of which are referenced to the rack center frame). Before being forwarded to the plant as a controller input, the signal is sent through the *Actuator Dynamics* block. In the current simulation the ARIS actuators are assumed to be perfect actuators that force the rack in precisely the manner instructed by the controller. In the actual system this approximation is probably only valid within a limited frequency range because the actuators are mechanical entities possessing their own dynamic behavior. The *Actuator Dynamics* block serves as a placeholder in the current simulation and contains an 8x8 identity matrix. The actuator force inputs are sent into the *Rigid Rack* block where the actuator signals are converted to force and torque inputs, resolved along the rack body-fixed frame, via the block *Tutox*. This block is not shown in any of the block diagrams but is generated from the code in Appendix F.

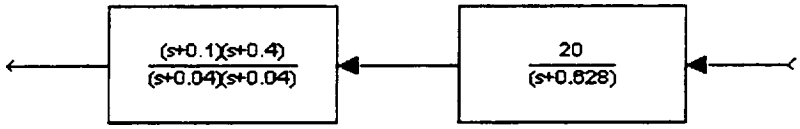

Figure 16: One of Six Cascade Compensators from the *Acceleration Compensator* Block

When the total perturbed displacement between the rack and the station/rack interface is calculated in block *Sum2*, the resulting position vector is forwarded to the block *Txtop*. This block resolves the relative displacement along the direction of the actuator pushrods, which are the locations at which the relative position measurements are made. The signal is then sent through a series of low-pass filters before it is

transformed to a relative displacement vector resolved along the rack center frame. Downstream, the difference between the relative position vector and the position command signal is calculated. At this point the signal is split, and goes to both the position control block and the stiffness compensation block. The position control block employs a proportional, integral, derivative (PID) SISO-type control scheme and is shown in Figure 17. The output from the position controller is then summed with the acceleration feedback signal in block *Sum3* and follows the path, already described above, into the plant.

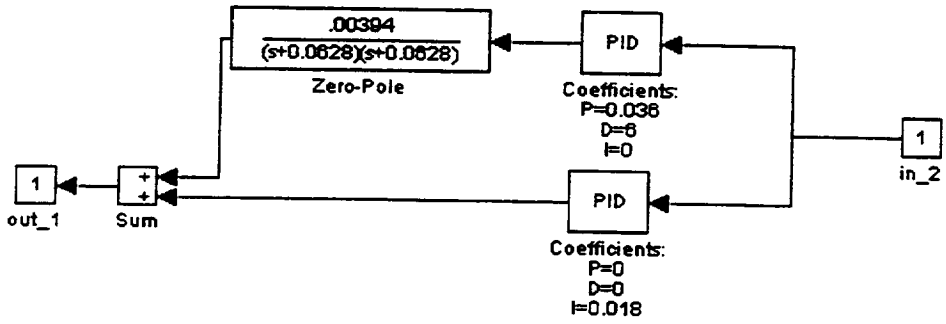

Figure 17: One of Six PID Controllers from the *Position Control* Block

The stiffness compensator is represented in the *Stiffness Compensation* block, which contains *pk*, a 6x6 matrix. One purpose of the stiffness compensation block is to instruct the controller to create forces that negate the coupling effects of the umbilical assembly. Therefore, the off-diagonal elements of *pk* are set equal to the negative value of the off-diagonal elements of the actuator and umbilical aggregate stiffness matrix (as measured by the payload evaluator). The diagonal elements of *pk* are computed such that the natural frequency associated with each degree of freedom of the plant is adjusted

to a predetermined value. The variety of facilities planned for use on ISS will require various umbilical configurations with varying stiffness properties. The stiffness compensation loop will help provide for acceptable isolation performance in the face of changing stiffness parameters. The control inputs from the stiffness compensation loop are intended to make the rack behave as a decoupled system, all the modes of which are equal to a predetermined frequency. Since the output from the stiffness compensation is a force and torque output, the signal is added to the cumulative force and torque signal from the other control loops and is sent directly to the *Tdelxtou* block, then forwarded to the plant as a set of actuator inputs.

8.4 Closed-Loop Results

The results from Section 8.2 show the nature of the problem that exists when the rack is tethered to the station via a passive umbilical assembly. The rack becomes a six degree-of-freedom harmonic oscillator that exhibits resonant behavior at certain frequencies. The results from the ARIS simulation, presented in this section, predict that the ARIS will successfully counteract the resonant behavior of the passive system.

The results presented in this section serve as examples of the predicted attenuation performance of the ARIS. The results are presented on a SISO basis, meaning that only one input/output combination is considered at a time. However, taken as a collective, the SISO results can provide a good understanding of the ability of the ARIS to attenuate various classes of disturbances. The plant model used in generating all plots is the baseline heavy ISPR with a full complement of umbilicals. The equations of motion used in the plant model are taken from Eq. (73) and, as mentioned before, the plant model used

in the closed-loop simulation is very similar to that presented in Section 8.1. The presentation of results begins with the response of the system to off-board disturbances (a class of disturbances against which the ARIS was specifically designed to isolate) and concludes with the response of the system to onboard disturbances.

Off-board Disturbance Attenuation

Figure 18 shows the transfer function between off-board translational accelerations (the inputs) in the rack's body-fixed x, y, and z directions and the x-direction acceleration of the rack CM (the output). Figure 19 shows the phase angle between the off-board acceleration inputs and the rack CM acceleration. The off-board station disturbance inputs are pure translational accelerations at the station/rack interface. According to the transformations given in Eqs. (67) and (70), pure translational inputs at the station/rack interface transform as pure translational inputs at the umbilical and actuator connection points on the off-board side. In Figures 18 and 19 the system performance prediction is shown between the frequencies of 0.001 Hz and 10 Hz. Although outside of the vibratory frequency range, the response of the system at frequencies below 0.01 Hz is shown to illustrate the ability of the ARIS to track station motion in the very low frequency range. Since the second order filter used to approximate the ARIS elliptic filter is a good approximator only up to 10 Hz, the ARIS simulation predictions cannot be considered reliable at frequencies higher than this.

At frequencies below 0.01 Hz a transmissibility ratio of approximately one (zero db) is maintained between the local off-board x-direction acceleration and the x-direction acceleration of the rack center of mass. Furthermore, the phase angle between the off-board x-direction input and the onboard x-direction acceleration is approximately zero

degrees at frequencies below 0.003 Hz. This unity gain and zero phase angle is necessary to maintain the sway space between the rack and the station. Low frequency oscillations result in large relative displacements that could cause bumping between the station and the rack. It should also be noted that the resonant peaks that were characteristic of the passive system (Figure 12) have been eliminated by the ARIS, so that the acceleration environment inside the rack would now satisfy the microgravity requirement, given the predicted ISS environment shown in Figure 3.

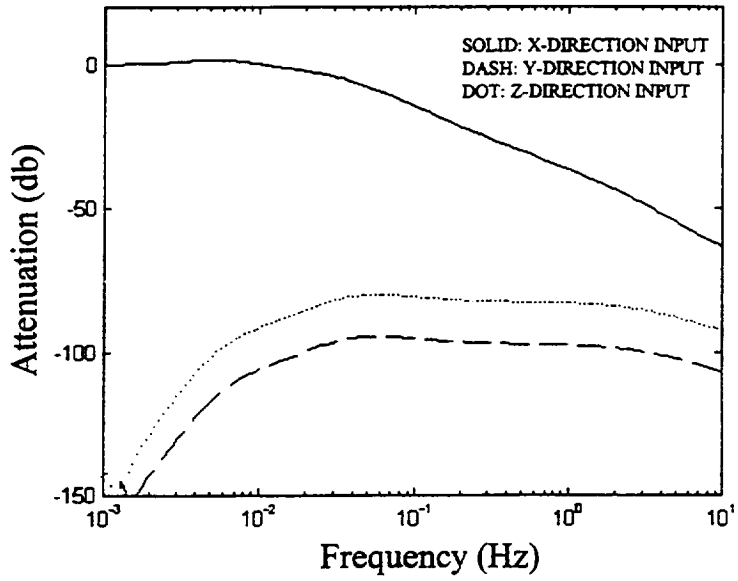

Figure 18: Transfer function between local off-board translational accelerations (inputs), along orthogonal directions, and x-direction acceleration of the rack CM (output).

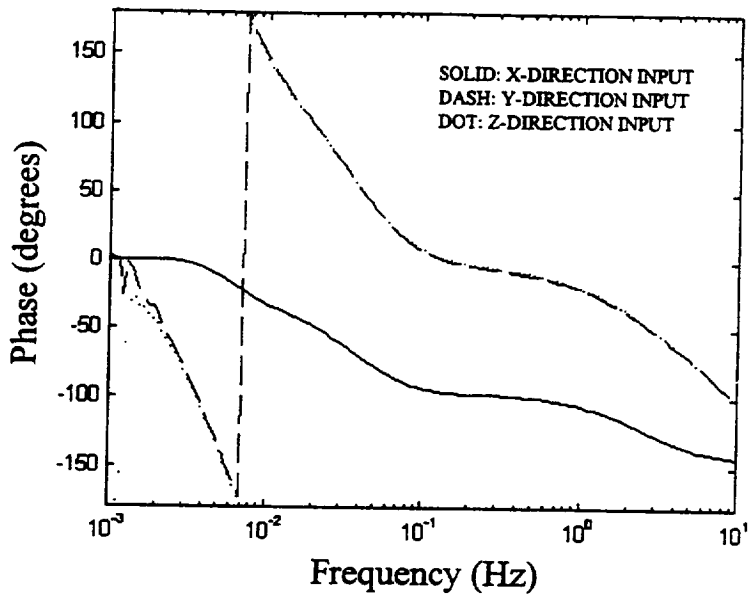

Figure 19: Phase angle between local off-board translational accelerations (inputs), along orthogonal directions, and x-direction acceleration of the rack CM (output).

Also noticeable from Figure 18 is that the coupling between off-board accelerations in the body-fixed y and z directions and the rack CM acceleration in the x-direction is very small in the portion of the frequency spectrum shown. Although coupling mechanisms do exist in the physical system, the ARIS controller minimizes the coupling effects through stiffness compensation. Although Figure 19 shows that the off-board y- and z-direction signals are out of phase with those of the rack x-direction acceleration at most frequencies, the minimal coupling effect and the fact that the inputs are orthogonal to the output means that there is less concern of bumping than with the x-direction off-board input. However, the chances of bumping between the rack and the station are also dependent on the severity of the off-board acceleration environment in a given direction.

The inclusion of the Coriolis coefficients in the equations of motion can have a large impact on the shape of the transfer functions for the y- and z-direction inputs. As a conservative estimate of the effects of the Coriolis acceleration, the components of the orbit rate resolved along the REF were all assumed to have a value of $1.1x10^{-3}$ rad/sec, which is the maximum value of the orbit rate along the y axis of the LVLH frame. The resulting Coriolis coefficients were then put into the simulation for comparison to the simulation results when the Coriolis effect was not included. The differences seen for the transfer function associated with an x-direction input are negligible because the diagonal terms in the translational damping matrix are dominant in comparison to the Coriolis coefficients. However, the differences for the y-direction and z-direction inputs (x-direction output) differ greatly from the results shown in Figure 17. In the frequency range of 0.001 Hz to 10 Hz, the gain is increased by as much as 40 db when the Coriolis coefficients are included. However, the gain was never more than -80 db for the y- and z-direction inputs. The phase comparison shows negligible differences for the x-direction input result shown in Figure 18. However, the phase plots for the y- and z-direction inputs are different by as much as 145 degrees from the results shown in Figure 18. Based on these preliminary studies, it is important to be aware of the Coriolis effect if an in-depth study into coupling, with regard to ARIS performance, is to be carried out.

Although there are nine possible combinations of orthogonal off-board translational acceleration inputs and orthogonal translational accelerations of the rack CM, only three of these combinations are presented. Using the simulation, transfer functions and phase plots between the orthogonal off-board translational acceleration

inputs and the y- and z-direction rack CM accelerations have been generated. These results have similar characteristics to those shown in Figures 18 and 19.

Figure 20 shows the transfer function between angular accelerations at the station/rack interface about the orthogonal directions of the rack's body-fixed frame and the x-direction acceleration of the rack CM. Figure 21 shows the phase angles between this set of inputs and the output. According to Eqs. (67) and (70), rotational inputs at the station/rack interface transform into a combination of translational and rotational inputs at the various umbilical and actuator connection points. Since the station/rack interface is nearly coincident with the position of the rack CM, rotation of the station about the rack body-fixed x and y directions takes advantage of the z-direction moment arm, so that these rotations produce the largest translational inputs at the umbilical and actuator connection points on the station. For this reason, the coupling between the theta-y input and the x-direction output is the most significant.

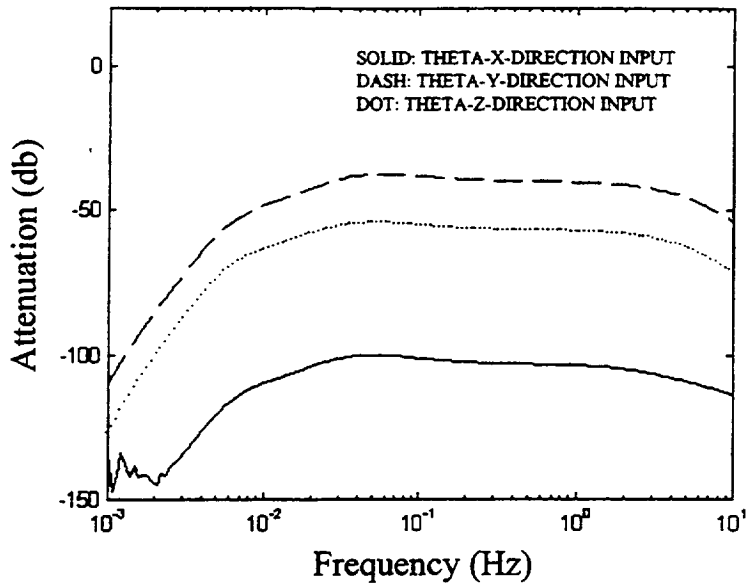

Figure 20: Transfer function between local off-board rotational accelerations (inputs with units rad/sec^2), about orthogonal directions, and the x-direction acceleration of the rack CM (output with units ft/sec^2).

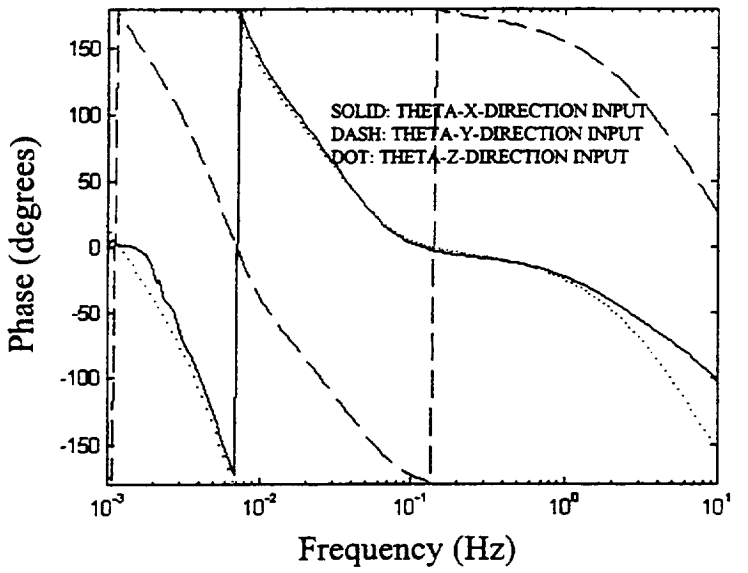

Figure 21: Phase angle between local off-board rotational accelerations (inputs with units rad/sec^2), about orthogonal directions, and the x-direction acceleration of the rack CM (output with units ft/sec^2).

Onboard Disturbance Attenuation

Figure 22 shows the ratio of the magnitude of the x-direction rack CM acceleration to the magnitude of the onboard disturbance forces (in the orthogonal body-fixed directions) as a function of frequency. Just as in the case for the passive system, the onboard disturber is located in the upper corner of the ISPR, a location that maximizes the torque input to the rack. Consideration of the response of the system to an x-direction force input, and comparison of Figure 22 to Figure 14 shows that the resonant peaks characteristic of the result for the passive system have been eliminated by the ARIS controller. At a frequency of about 10 Hz, the transfer function levels out to an attenuation of approximately -35 db, which is the decibel equivalent of the inverse of the rack mass. Therefore, with onboard forcing frequencies in the neighborhood of 10 Hz, the rack responds like a body floating in free space. Figure 22 also shows that the x-direction acceleration of the rack CM is highly decoupled from force inputs in the body-y and body-z directions. The result shown in Figure 22 also typifies the acceleration response of the system in the y and z directions. Although the results are not shown in this paper, the y-direction (z-direction) rack CM acceleration is highly decoupled from force inputs in the x and z (x and y) directions.

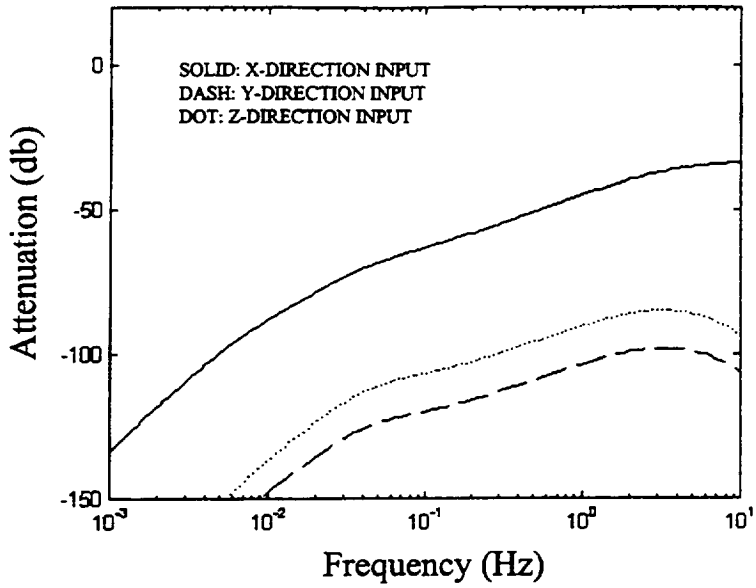

Figure 22: Transfer function between onboard disturber force in orthogonal directions (inputs with units of lbf) and x-direction rack CM acceleration (output with units of ft/sec^2)

9. ARIS Risk Mitigation Experiment

The ARIS Risk Mitigation Experiment (RME) was a flight test of the ARIS carried out during shuttle mission STS-79. The purpose of the RME was to test the functionality of the ARIS with respect to on-orbit operations and performance. A myriad of tests were carried out during the flight and a portion of the data collected during these tests may prove valuable in verifying the results of the ARIS simulation presented in this paper. Therefore, one of the objectives of this research is to simulate the unique ARIS configuration used during the RME so that comparisons between simulation results and test data may be carried out.

The ARIS configuration used during RME differed significantly from the baseline configurations planned for ISS. The most significant differences are as follows:

- The mass of the ISPR was significantly different than that of the various baseline configurations.
- The umbilical assembly was changed during the experiment from a partial umbilical configuration to a minimum umbilical configuration that possesses considerably less translational stiffness.
- The ARIS control laws used during RME were different than the baseline controller planned for use on ISS.
- As a result of anomalous behavior of the ARIS during the RME, one of the eight actuator pushrods was damaged and had to be removed. The ARIS operated with seven pushrods during most of the testing.

The various configuration changes summarized above must be programmed into the simulation if the RME results are to be compared to the results from the ARIS simulation. A listing of the RME configuration parameters is given in Appendix B.

9.1 Verification of the ARIS RME Configuration

Information on the ARIS RME configuration was collected from a number of different sources including various RME written reports (cited parenthetically below) as well as discussions with the ARIS developers and information presented at the latest ARIS CDR (Marshall Spaceflight Center, November, 1996). Given that the ARIS RME simulation was patched together from these various sources, it was considered prudent to attempt to validate the RME simulation architecture to ensure that the correct controller configuration and plant parameters were being used. The validation was carried out through comparison of the results from the current simulation to the results from the ARIS simulation being used by the Boeing Defense and Space Group. The ARIS developers operate this simulation independently, using it to make predictions of system performance for the RME and baseline ARIS configurations.

Several different controller versions were used during the RME and two of these versions are presented in this paper. One type is termed a *baseline robust controller* that utilizes a 2^{nd} order 8 Hz filter in the acceleration feedback loop in addition to the baseline acceleration compensator. Also present in this configuration is an 8^{th} order elliptic filter set at 250 Hz. The second controller type is termed a *high gain controller* in which the gain in the acceleration feedback loop is doubled, the 2^{nd} order filter is set at 40 Hz, and the 8^{th} order elliptic filter is set at 25 Hz. Further, the high gain controller employs an additional lag filter in the acceleration feedback loop.

Figure 23 shows the comparison of the current simulation results to those of the Boeing simulation. The plot shows the predictions for the ARIS RME off-board

attenuation capability as a function of frequency. The gain depicted in the plot is the ratio (in decibels) of the x-direction acceleration of the rack center of mass to the off-board x-direction acceleration at the station/rack interface. This comparison shows that the current simulation is in acceptable agreement with the Boeing simulation and thus the current simulation probably employs the most up-to-date models of the RME controllers for both the high gain and baseline versions.

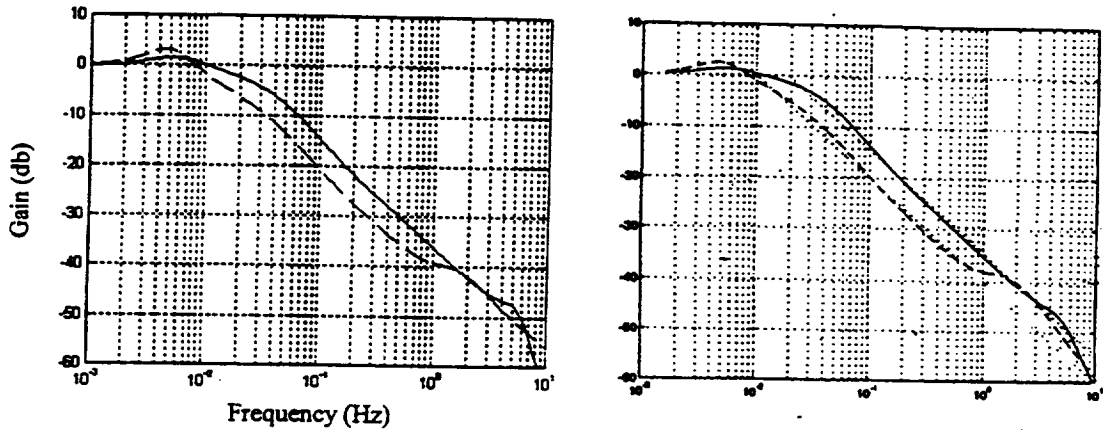

Figure 23: Comparison of current simulation results (left) to Boeing simulation results (right) of ARIS RME off-board attenuation capability. Solid lines are *baseline robust controller* predictions and dashed lines are *high gain controller* predictions.

9.2 Comparison to RME Results

The comparison of simulation results to the results obtained from the RME are currently limited to a small subset of the total data received from the experiment. For the purpose of comparison here, the preprocessed data given in the final RME report were utilized (Boeing Document #SK683-61855-1, *STS-79 Final Report RME-1313/ARIS*, December, 1996). Among a number of other results, the final RME report presented single input single output (SISO) attenuation results from two different isolation tests.

The SISO approach considers only one input/output combination at a time and assumes that the only input that affects a given output is an input in the same direction as that output. For example, it is assumed that the x-direction acceleration of the rack is affected only by an x-direction acceleration onboard the station. Therefore all cross-coupling between the six degrees of freedom is ignored. In reality this assumption is not strictly valid but it does provide for a first-look comparison of results.

The results presented are those from an isolation test run that was carried out on day 5 of the STS-79 mission. The batch file used for the test run was designated B1G_B2.X. Further information on this test is documented in the RME Quick Look Report (Boeing Document #SK683-62235, *ARIS RME-1313 Quick Look Report*, October, 1996) and the final RME report. The test was conducted with the high gain controller configuration active, a minimum umbilical assembly, and the #8 actuator removed. Furthermore, during this test run the ISPR was fully loaded with food logistics for MIR. All of these conditions have been simulated for comparison to the test results.

Figures 24, 25, and 26 show comparisons between the predicted attenuation levels of off-board disturbances and the isolation levels measured during the RME. Because the isolation results were presented in the final RME report as average isolation levels across 1/3 octave band intervals, the predicted isolation levels from the current simulation have been averaged over the same 1/3 octave bands. The average predicted attenuation levels are plotted at the center frequencies of the various 1/3 octaves so that direct comparisons between the prediction and the flight data can be made for each interval.

Valid isolation data from the RME were limited to a certain bandwidth because the acceleration environment present on the Space Shuttle during STS-79 was below the

noise floor of the accelerometers in portions of the frequency spectrum. The region of the spectrum in which the data are believed to be valid is taken to be the same for all three directions, and ranges from approximately 0.04 Hz to 1.2 Hz. No comparisons were made outside of this bandwidth.

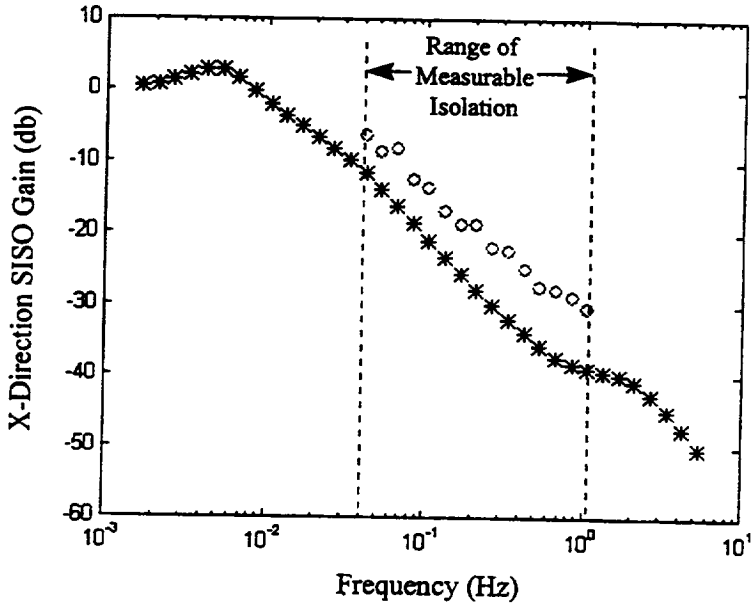

Figure 24: Comparison of current simulation x-direction SISO isolation prediction (asterisk) to RME x-direction SISO isolation results (open symbol):

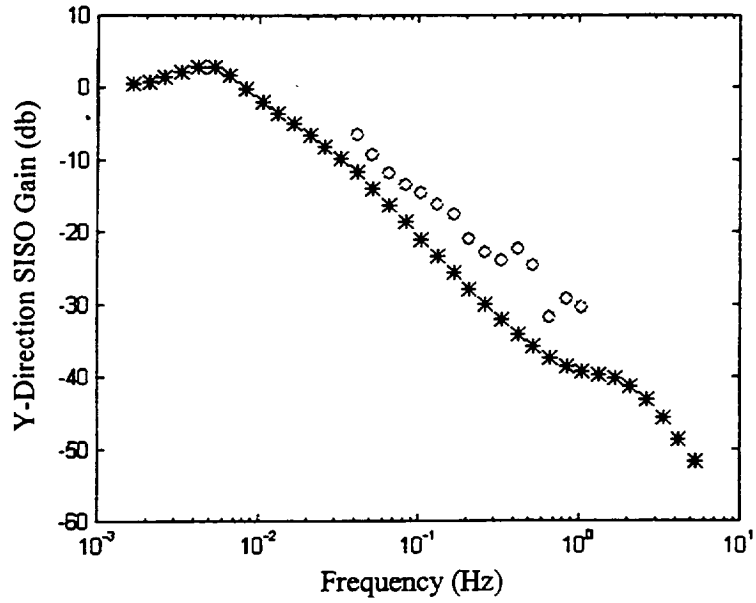

Figure 25: Comparison of current simulation y-direction SISO isolation prediction (asterisk) to RME y-Direction SISO isolation results (open symbol).

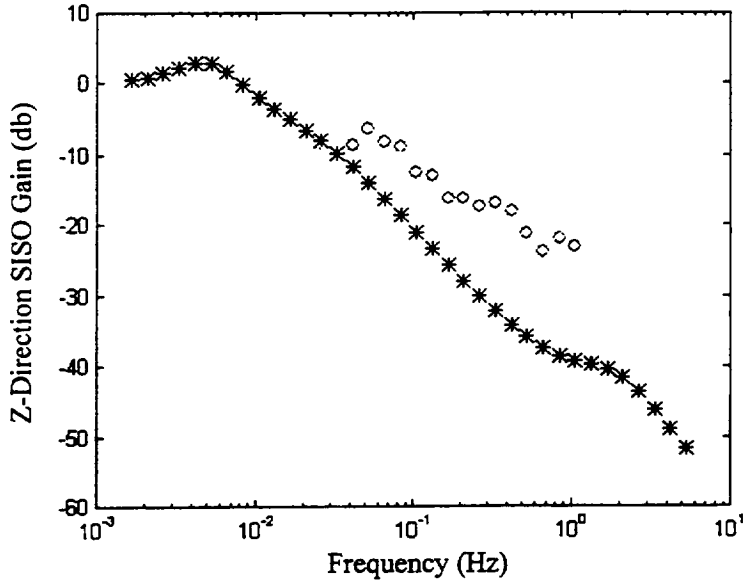

Figure 26: Comparison of current simulation z-direction SISO isolation prediction (asterisk) to RME z-direction SISO isolation results (open symbol).

The x- and y-direction SISO predictions follow the trend of the flight data, but the prediction and results diverge more and more with increasing frequency. Further, the z-direction isolation during RME was not as good as that in the x and y directions and the

simulation over-predicts the isolation by a considerable amount. For the case of the x- and y-direction plots, some of the differences between the flight data and the prediction are attributed to coupling from station inputs in other directions. This coupling effect can be shown to become stronger with increasing frequency. The large differences between the z-direction isolation levels measured during the RME and the z-direction isolation predictions of the current simulation are not fully understood. In a communication from The Boeing Company, it was suggested that the large differences may be accounted for by the variation in stiffness of the umbilicals throughout their range of motion. The effective stiffness of the umbilicals in small amplitude motion is larger than that associated with large amplitude motion, and this behavior is not accounted for in the current simulation.

Further details on ARIS test results are given in Reference 11. This is also an excellent reference for details on ARIS design studies, control methodology and hardware configuration. The reference was authored by the ARIS developers from the Boeing Defense and Space Group.

10. Concluding Remarks

This paper details the development of a simulation capability for a microgravity rack integrated with an ARIS kit. The current simulation is based on a Boeing simulation capability for the ARIS. The computer-based model presented in this paper represents an important first step in building a simulation tool, at the NASA Langley Research Center, that may be utilized to augment technical knowledge of the ARIS and to make attenuation performance predictions for various microgravity facility configurations. In the hands of payload developers and microgravity scientists, this combination of technical knowledge and quantitative predictions may lead to a higher level of science return from the International Space Station.

The research documented in this paper is highly comprehensive in that it details the effect of the orbital motion on the microgravity environment inside the rack while also confronting the dynamics resulting from the umbilical and actuator assemblies, disturbance sources internal to the rack, and the station environment at the station/rack interface. Starting with a basic description of the Space Station and ISPR in orbit, an energy-based method is applied to derive rigid-body equations of motion. By eliminating second-order terms in the orbital equations of motion for the center of mass of the composite system, it is found that the well known equations of motion for the two-body problem can be realized. A forcing function appears on the right-hand side of these equations due to external forces that are acting on the system. Based on this familiar result, the orbital parameters of the system are considered known functions of time, eliminating the need to integrate the orbital equations of motion. Furthermore, the

external forces acting on the system are assumed to be constant in magnitude and direction over the time interval of interest.

For the purpose of this study, the perturbed motion of station is assumed to be predetermined because of the large mass ratio between the station and the rack. Using a suitable set of generalized coordinates and the proper transformations, the perturbed equations of motion for the microgravity rack are derived and the rack states used in these equations are those measured by an observer fixed with respect to the system orbit. Numerous terms are derived in the perturbed equations of motion, and many of these represent orbitally-induced forces on the rack. This paper identifies, and describes in detail, the various forces and torques acting on the microgravity rack. Furthermore, order of magnitude studies are used to identify those terms that may have a significant impact on the microgravity environment inside the rack. For the most part, the coupling terms between the bulk orbital motion of the system and the perturbed motion of the rack are shown to be negligible on the microgravity scale. However, these terms could be significant in the study of coupling effects between the various perturbed rack states.

The derivations presented in this paper are significant in that they establish a firm understanding of the dynamical behavior of the rack in the context of its orbital motion and its locally observed perturbed motion. If coupling terms between the orbital motion and the local perturbed motion of the rack are omitted (and a quasi-equilibrium condition is employed) then the locally observed motion is approximated by equations of motion representing the equivalent inertial-based system. Significant quasi-steady, orbital-induced accelerations are then added to the local perturbed acceleration to calculate the total inertial acceleration of the rack.

Using the equations of motion derived for the microgravity rack, a computer-based simulation was developed in the SIMULINK environment. This environment allowed the ARIS controller simulation to be interfaced easily with the rack model so that a simulation of the entire closed-loop system could be constructed. With the ARIS disconnected, the predicted response of the rack to both onboard and off-board disturbances showed resonant behavior at various frequencies. This behavior will result in noncompliance of the rack environment with the microgravity requirement. When the ARIS is activated the simulation results predict that the resonant behavior is eliminated, and a microgravity environment is maintained inside of the rack.

A limited comparison is made between simulation performance predictions and performance results from the ARIS RME. For the sake of comparison the assumption is made that the translational acceleration of the microgravity rack in a certain direction is affected only by off-board inputs in the same direction. The x- and y-direction attenuation predictions are more in agreement with the flight data than that of the z-direction and all comparisons show that further tuning of the current model is necessary.

REFERENCES

1. Nelson, E. S., "An Examination of Anticipated g-jitter on Space Station and its Effects on Materials Processes," NASA Technical Memorandum 103775, Lewis Research Center, Cleveland, May 1991.

2. Hampton, R.D., Knospe, C.R., Allaire, P.E., and Grodsinsky, C.M., "Microgravity Isolation System Design: A Modern Control Synthesis Framework," NASA Technical Memorandum 106805, December, 1994.

3. "Microgravity Control Plan," International Space Station Program Document #SSP 50036, NASA, May, 1994.

4. "Science Requirements and the Environment Definition", NASA Conference Publication 10094, Proceedings of the International Workshop on Vibration Isolation Technology for Microgravity Science Applications, Cleveland, April 23-25, 1991.

5. Boeing Defense and Space Group Missiles and Space Division, "International Space Station Alpha Reference Guide," November, 1994. Database on-line. Accessed June 27, 1997. Available from http://iss-www.jsc.nasa.gov/ss/techdata/ISSAR/ISSAReferenceGuide.html.

6. "Microgravity Environment Countermeasures Panel Discussion", AIAA Paper 97-0351, 35th Aerospace Sciences Meeting and Exhibit, Reno, January 6-10, 1997.

7. Meirovitch, L., Methods of Analytical Dynamics, Mcgraw-Hill, Inc., New York, 1970.

8. Grodsinsky, C.M., "Development and Approach to Low-Frequency Microgravity Isolation Systems," NASA Technical Paper 2984, August, 1990.

9. Battin, R.H., An Introduction to the Mathematics and Methods of Astrodynamics, American Institute of Aeronautics and Astronautics, Inc., New York, 1987.

10. Wells, D.A., Theory and Problems of Lagrangian Dynamics, McGraw-Hill, Inc., New York, 1967.

11. Bushnell, G., Anderson, T.M., Becraft, M.D., and Jacot, D.J., "Active Rack Isolation System Development for the International Space Station", AIAA Paper 97-1203. AIAA/ASME/ASCE/AHS/ASC Structures, Structural Dynamics, and Materials Conference and Exhibit, 38th, and AIAA/ASME/AHS Adaptive Structures Forum, Kissimmee, FL, April 7-10, 1997. Collection of Technical Papers, Pt. 2. p.1500-1513.

12. Aris, R., Vectors, Tensors, and the Basic Equations of Fluid Mechanics, General Publishing Company, Ltd., Toronto, Ontario, 1962.

13. Dimarogonas, A.D. and Haddad, S., Vibration for Engineers, Prentice Hall, Inc., Englewood Cliffs, NJ, 1992.

APPENDIX A

A.1 Overview of Indicial Notation

Indicial notation is a bookkeeping tool for use in vector algebra. The principles given on indicial notation in this appendix lay the groundwork for indicial notation as it applies to this paper. For further information regarding indicial notation see reference 12.

1) If the quantity known as "vector a" is symbolized as $\vec{a}$ and the quantity known as "vector b" is symbolized as $\vec{b}$, then:

- The notation a_i (i=1,2,3) denotes the i^{th} component of $\vec{a}$ and b_i denotes the i^{th} component of $\vec{b}$.

- If the same indicial symbol appears twice in the same term, it is referred to as a *dummy index* and a summation across this index is implied. Therefore, the dot product of $\vec{a}$ and $\vec{b}$ is given indicially as: $\vec{a} \cdot \vec{b} \Rightarrow a_i b_i$

- The indicial symbol ε_{ijk} is introduced as a permutation symbol that takes the value of +1 if the indices ijk are in cyclic order, -1 if they are in acyclic order, and zero if any two of the three indices ijk are equal. The vector cross product can be represented indicially as: $\vec{a} \times \vec{b} \Rightarrow \varepsilon_{ijk} a_j b_k$

2) If the quantity known as "second order tensor A" is symbolized as $\bar{\bar{A}}$, then:

- The tensor $\bar{\bar{A}}$ may be written down as a 3x3 matrix.

$$A = \begin{bmatrix} A_{11} & A_{12} & A_{13} \\ A_{21} & A_{22} & A_{23} \\ A_{31} & A_{32} & A_{33} \end{bmatrix}$$

- The notation A_{ij} denotes the i^{th}, j^{th} component of $\bar{\bar{A}}$, representing the element in the i^{th} row and j^{th} column of the matrix representation for $\bar{\bar{A}}$.

- A second order tensor is symmetric if $A_{ij} = A_{ji}$.

- A second order tensor is antisymmetric if $A_{ii} = 0$ and $A_{ij} = -A_{ji}$.

- For this study, the vector of an antisymmetric tensor $\bar{\bar{B}}$ is defined as a vector with components v_k (k=1,2,3), and $v_k = \frac{1}{2}\varepsilon_{jik}B_{ij}$.

- For this study, the antisymmetric second order tensor of $\bar{v}$ is given as $B_{ij} = \varepsilon_{jik}v_k$. Therefore, if

$$\bar{v} = \begin{Bmatrix} v_1 \\ v_2 \\ v_3 \end{Bmatrix}, \text{ then } \bar{\bar{B}} = \begin{bmatrix} 0 & -v_3 & v_2 \\ v_3 & 0 & -v_1 \\ -v_2 & v_1 & 0 \end{bmatrix}$$

The last two definitions provided above differ from those given in reference 12. In that reference the definition of the components of $\bar{v}$, the vector of an antisymmetric tensor, are of opposite sign than that given above. For this study the definitions provided in this appendix are used because they are better suited to represent the cross-product operation, which is present in many of the developments presented in this paper.

A.2 Final Indicial Form of the Lagrangian and the Dissipation Function

$L=$

$$\frac{1}{2}M_R\left[\dot{r}^L_{CM,i}+\Delta\dot{r}^L_{R,i}+\varepsilon_{ijk}\Omega_j\left(r^L_{CM,k}+r^L_{RE,k}+\Delta r^L_{R,k}\right)\right]\cdot\left[\dot{r}^L_{CM,i}+\Delta\dot{r}^L_{R,i}+\varepsilon_{imn}\Omega_m\left(r^L_{CM,n}+r^L_{RE,n}+\Delta r^L_{R,n}\right)\right]$$

$$+\frac{1}{2}\sum_p m_p\left[\dot{r}^L_{CM,i}+\Delta\dot{r}^L_{R,i}+l^{L/RE}_{ij}\left(\dot{r}^R_{P,j}+\varepsilon_{jmk}\Delta\dot{\theta}^R_{R,m}r^R_{P,k}+\varepsilon_{jmk}\Delta\theta^R_{R,m}\dot{r}^R_{P,k}\right)+\varepsilon_{ijk}\Omega_j\left(r^L_{CM,k}+r^L_{RE,k}+\Delta r^L_{R,k}+l^{L/RE}_{km}r^R_{P,m}+l^{L/RE}_{km}\varepsilon_{mnp}\Delta\theta^R_{R,n}r^R_{P,p}\right)\right]\cdot$$
$$\left[\dot{r}^L_{CM,i}+\Delta\dot{r}^L_{R,i}+l^{L/RE}_{ir}\left(\dot{r}^R_{P,r}+\varepsilon_{rst}\Delta\dot{\theta}^R_{R,s}r^R_{P,t}+\varepsilon_{rst}\Delta\theta^R_{R,s}\dot{r}^R_{P,t}\right)+\varepsilon_{irs}\Omega_r\left(r^L_{CM,s}+r^L_{RE,s}+\Delta r^L_{R,s}+l^{L/RE}_{st}r^R_{P,t}+l^{L/RE}_{st}\varepsilon_{tvu}\Delta\theta^L_{R,v}r^R_{P,u}\right)\right]$$
$$+\Omega_{y'}\Omega_{z'}\left(I_{y''}-I_{z''}\right)\Delta\theta_{x''}+\Omega_{x'}\Omega_{z'}\left(I_{z''}-I_{x''}\right)\Delta\theta_{y''}$$
$$+\Omega_{x'}\Omega_{y'}\left(I_{x''}-I_{y''}\right)\Delta\theta_{y''}$$
$$+\frac{1}{2}\left(\Omega^2_{y'}-\Omega^2_{z'}\right)\left(I_{z''}-I_{y''}\right)\Delta\theta^2_{x''}+\frac{1}{2}\left(\Omega^2_{z'}-\Omega^2_{x'}\right)\left(I_{x''}-I_{z''}\right)\Delta\theta^2_{y''}$$
$$+\frac{1}{2}\left(\Omega^2_{x'}-\Omega^2_{y'}\right)\left(I_{y''}-I_{x''}\right)\Delta\theta^2_{z''}$$
$$+\Omega_{y'}\Omega_{z'}\left(I_{x''}-I_{z''}\right)\Delta\theta_{x''}\Delta\theta_{y''}+\Omega_{x'}\Omega_{z'}\left(I_{x''}-I_{y''}\right)\Delta\theta_{x''}\Delta\theta_{z''}$$
$$+\Omega_{y'}\Omega_{z'}\left(I_{y''}-I_{x''}\right)\Delta\theta_{y''}\Delta\theta_{z''}$$
$$+\Omega_{x'}I_{x''}\Delta\dot{\theta}_{x''}+\Omega_{y'}I_{y''}\Delta\dot{\theta}_{y''}+\Omega_{z'}I_{z''}\Delta\dot{\theta}_{z''}$$
$$+\Omega_{z'}I_{y''}\Delta\dot{\theta}_{y''}\Delta\theta_{x''}-\Omega_{y'}I_{z''}\Delta\dot{\theta}_{z''}\Delta\theta_{x''}$$
$$+\Omega_{z'}\left(I_{z''}-I_{x''}\right)\Delta\dot{\theta}_{x''}\Delta\theta_{y''}+\Omega_{x'}I_{z''}\Delta\dot{\theta}_{z''}\Delta\theta_{y''}$$
$$+\Omega_{y'}\left(I_{x''}-I_{y''}\right)\Delta\dot{\theta}_{x''}\Delta\theta_{z''}+\Omega_{x'}\left(I_{x''}-I_{y''}\right)\Delta\dot{\theta}_{y''}\Delta\theta_{z''}$$
$$+\frac{1}{2}\Delta\dot{\theta}^R_{R,i}I^R_{R,ij}\Delta\dot{\theta}^R_{R,j}$$
$$-\frac{1}{2}\sum_N\left(\Delta r^L_{R,i}+d^L_{oN,ij}l^{L/RE}_{jk}\Delta\theta^R_{R,k}-\Delta r^L_{S,i}-D^L_{oN,ij}l^{L/SE}_{jk}\Delta\theta^S_{R,k}+\Delta L^L_{oN,i}\right)\cdot KTRN^L_{N,im}\cdot$$
$$\left(\Delta r^L_{R,m}+d^L_{oN,mn}l^{L/RE}_{np}\Delta\theta^R_{R,p}-\Delta r^L_{S,m}-D^L_{oN,mn}l^{L/SE}_{np}\Delta\theta^S_{R,p}+\Delta L^L_{oN,m}\right)$$

$$-\frac{1}{2}\sum_N\left(\Delta\theta^R_{R,i}-\Delta\theta^R_{S,i}+\Delta\theta^R_{oN,i}\right)\cdot KTOR^R_{N,ij}\cdot\left(\Delta\theta^R_{R,j}-\Delta\theta^R_{S,j}+\Delta\theta^R_{oN,j}\right)$$

$$-\mu_E M_R\left[r^L_{CM,i}r^L_{CM,i}+r^L_{RE,i}r^L_{RE,i}+\Delta r^L_{R,i}\Delta r^L_{R,i}+2r^L_{CM,i}r^L_{RE,i}+2r^L_{CM,i}\Delta r^L_{R,i}+2r^L_{RE,i}\Delta r^L_{R,i}\right]^{-\frac{1}{2}}$$

$$-\mu_E\sum_P m_P\left[r^L_{CM,i}r^L_{CM,i}+r^L_{RE,i}r^L_{RE,i}+\Delta r^L_{R,i}\Delta r^L_{R,i}+l^{L/RE}_{ij}\left(r^R_{P,j}+\varepsilon_{kjm}\Delta\theta^R_{R,m}r^R_{P,k}\right)l^{L/RE}_{in}\left(r^R_{P,n}+\varepsilon_{pnq}\Delta\theta^R_{R,q}r^R_{P,p}\right)\right.$$
$$+2r^L_{CM,i}r^L_{RE,i}+2r^L_{CM,i}\Delta r^L_{R,i}+2r^L_{CM,i}l^{L/RE}_{ij}\left(r^R_{P,j}+\varepsilon_{kjm}\Delta\theta^R_{R,m}r^R_{P,k}\right)+2r^L_{RE,i}\Delta r^L_{R,i}$$
$$\left.+2r^L_{RE,i}l^{L/RE}_{ij}\left(r^R_{P,j}+\varepsilon_{kjm}\Delta\theta^R_{R,m}r^R_{P,k}\right)+2\Delta r^L_{R,i}l^{L/RE}_{ij}\left(r^R_{P,j}+\varepsilon_{kjm}\Delta\theta^R_{R,m}r^R_{P,k}\right)\right]^{-\frac{1}{2}}$$

(A-1)

F =

$$\frac{1}{2}\sum_N\left(\Delta\dot r^L_{R,i}+\mathbf{d}^L_{oN,ij}l^{L/RE}_{jk}\Delta\dot\theta^R_{R,k}-\Delta\dot r^L_{S,i}-\mathbf{D}^L_{oN,ij}l^{L/SE}_{jk}\Delta\dot\theta^S_{R,k}\right)\cdot\mathrm{CTRN}^L_{N,im}\cdot$$
$$\left(\Delta\dot r^L_{R,m}+\mathbf{d}^L_{oN,mn}l^{L/RE}_{np}\Delta\dot\theta^R_{R,p}-\Delta\dot r^L_{S,m}-\mathbf{D}^L_{oN,mn}l^{L/SE}_{np}\Delta\dot\theta^S_{R,p}\right)$$

$$+\frac{1}{2}\sum_N\left(\Delta\dot\theta^R_{R,i}-\Delta\dot\theta^R_{S,i}\right)\mathrm{CTOR}^R_{N,ij}\left(\Delta\dot\theta^R_{R,j}-\Delta\dot\theta^R_{S,j}\right)$$

(A-2)

APPENDIX B

Summary of System Parameters

Baseline Heavy Rack

Estimated Mass: $M_R = 54.9$ slugs (1768 lbm)

Estimated Moment of Inertia Matrix (slug-ft^2):

$$\left[I_R^R\right] = \begin{bmatrix} 183.00 & 0 & 0.12 \\ 0 & 194.99 & -7.15 \\ 0.12 & -7.15 & 81.27 \end{bmatrix}$$

Estimated Translational Umbilical Stiffness (lbf/ft) (no coupling predicted):

$$\left[KTRN_{UMB}^R\right] = \begin{bmatrix} 86.4 & 0 & 0 \\ 0 & 104.4 & 0 \\ 0 & 0 & 104.4 \end{bmatrix}$$

Estimated Torsional Umbilical Stiffness (lbf-ft/rad) (no coupling predicted):

$$\left[KTOR_{UMB}^R\right] = \begin{bmatrix} 53.17 & 0 & 0 \\ 0 & 109.27 & 0 \\ 0 & 0 & 78.6 \end{bmatrix}$$

RME Rack

Mass (measured on orbit with full load of logistics): $M_R = 27.6$ slugs (888.72 lbm)

Measured Moment of Inertia Matrix (slug-ft^2):

$$\left[I_R^R\right] = \begin{bmatrix} 113.0 & 2.7 & 2.0 \\ 2.7 & 123 & 5.7 \\ 2.0 & 5.7 & 47 \end{bmatrix}$$

Translational Umbilical Stiffness (on-orbit measurement) (lbf/ft):

$$\left[\mathrm{KTRN}^{R}_{UMB}\right] = \begin{bmatrix} 60.0 & 3.6 & 2.6 \\ 0 & 47.2 & 0 \\ 2.6 & 0 & 44.3 \end{bmatrix}$$

Torsional Umbilical Stiffness (estimated from on-orbit measurement) (lbf-ft/rad):

$$\left[\mathrm{KTOR}^{R}_{UMB}\right] = \begin{bmatrix} 145.3 & -25.7 & -12.2 \\ -4.6 & 269.2 & 40.4 \\ -15.1 & -37.3 & 49.9 \end{bmatrix}$$

APPENDIX C

A Model for Rotating Equipment Disturbance

The majority of the oscillatory disturbances onboard the rack are due to the operation of rotating equipment. The force and torque inputs to the rack are due to mass imbalances in the machinery that result in a time rate of change of the linear and angular momentum vector associated with the rotating motion. Figure C-1 shows the diagram used in developing the model for this class of disturbance.

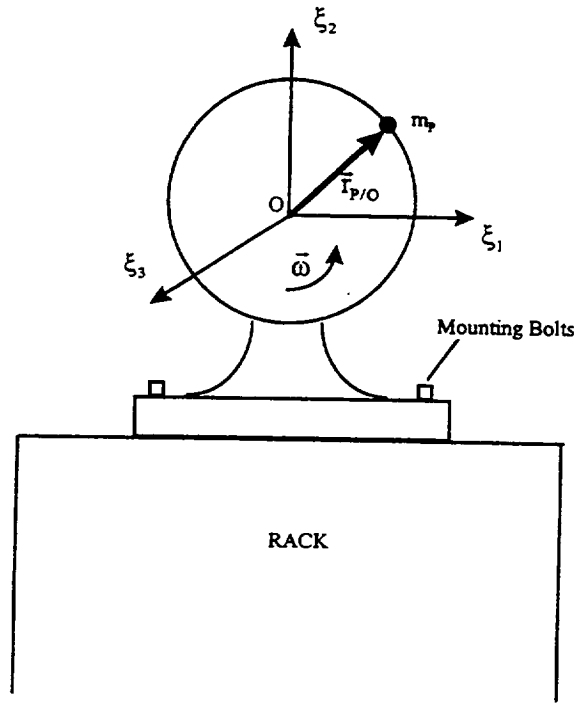

Figure C-1: Diagram of the Rotating Mass Imbalance Model

The model assumes that the total rotating mass imbalance is represented by the point mass m_P, which rotates about an axis through point O. An axis system is assigned so that the axes ξ_1 and ξ_2 lie in the plane of rotation while the axis ξ_3 is normal to the plane of rotation and parallel to the angular velocity vector $\bar{\omega}$. The equipment is

assumed to be hard-mounted to the rack and the axes ξ_1, ξ_2, and ξ_3 are assumed fixed relative to the rack body-fixed frame.

The total acceleration of the disturber mass relative to the rack center of mass is

$$\vec{a}_{m_P} = \vec{a}_O + \vec{\alpha} \times \vec{r}_{P/O} + \vec{\omega} \times \left(\vec{\omega} \times \vec{r}_{P/O}\right) \tag{C-1}$$

where $\vec{\alpha}$ is the angular acceleration vector of the rotating mass about ξ_3 and $\vec{a}_O$ is the acceleration of point O relative to the rack center of mass. The rotating equipment is assumed to be operating in a steady-state condition so that $\vec{\alpha} = \vec{0}$. Furthermore, the relative acceleration $\vec{a}_O$ is considered small compared to the centripetal acceleration term. Therefore, the only term retained is the centripetal acceleration term.

With respect to any rack body-fixed axis, the force input due to rotating imbalances is oscillatory, with a frequency of $f = \dfrac{|\vec{\omega}|}{2\pi}$ Hz. If the magnitude of the position vector $\vec{r}_{P/O}$ is designated as *e*, the maximum possible amplitude of the force input along any body-fixed axis is

$$m_P \left|\ddot{\vec{r}}_P^R\right|_{MAX} = m_P e |\vec{\omega}|^2 \tag{C-2}$$

In a document produced under contract for the Space Station program it is suggested that the disturber mass m_P be assigned a value of 0.5% of the total mass of the rotating part and the imbalance radius, *e*, be given as 0.5% of the radius of the rotating part (Boeing Missiles and Space Division and NASA, Boeing Document #D683-28702-1, *Microgravity Disturbance Forcing Functions Issue A*, 1996). As a final note, the vector $\ddot{\vec{r}}_P^R$ is the same as that represented by the column vector $\left\{\ddot{r}_P^R\right\}$ given on the right hand side of Eq. (73).

APPENDIX D

Approximation for Umbilical and Actuator Damping

The damping matrices given in Eq. (73) pose a problem from a practical standpoint because of the difficulty of making approximations for these quantities. As a first approximation, information on the damping quantity supplied by the ARIS developers is utilized. The only information provided thus far is the value of ζ_j, the modal damping coefficient associated with the j^{th} mode. To utilize this information, an algebraic expression for the modal form of the equations must be derived so that the physical damping quantity can then be backed out of the modal information provided. Many of the developments in this appendix are informed by reference 13.

The general form of Eq. (73) can be interpreted as the equations of motion for a damped harmonic oscillator subjected to base motion excitation as well as directly applied disturbing forces. The condensed form of the equations for this system is

$$[M]\{\ddot{x}\} + [C]\{\dot{x}\} + [K]\{x\} = [C]\{\dot{y}\} + [K]\{y\} + \{F_{INTERNAL}\} \qquad \text{(D-1)}$$

where the column vector $\{x\}$ and its time derivatives are rack states and $\{y\}$ and its time derivative are station states.

The modal development begins with a consideration of the natural, undamped equations of motion, given as

$$[M]\{\ddot{x}\} + [K]\{x\} = \{0\} \qquad \text{(D-2)}$$

A linear transformation of the form

$$\{x\} = [Z]\{q\} \tag{D-3}$$

is substituted into Eq. (D-2), which is then rewritten as

$$\{\ddot{q}\} + [Z]^{-1}[M]^{-1}[K][Z]\{q\} = \{0\} \tag{D-4}$$

If the columns of $[Z]$ are assumed to be the eigenvectors of the matrix product $[M]^{-1}[K]$, then the eigenvalue problem of the following form is realized,

$$\det\left([K] - \lambda_j[M]\right) = \{0\} \tag{D-5}$$

where λ_j is the eigenvalue associated with the j^{th} eigenvector (j^{th} column of $[Z]$).

The orthogonality relation for the natural modes implies that the mass matrix can be diagonalized with the j^{th} eigenvector in the following fashion

$$\{z_j\}^T[M]\{z_i\} = 0 \tag{D-6}$$

and

$$\{z_j\}^T[M]\{z_j\} = m_j \tag{D-7}$$

For convenience the eigenvectors are normalized as

$$\{\phi_j\} = \frac{\{z_j\}}{(m_j)^{\frac{1}{2}}} \tag{D-8}$$

where ϕ_j is the j^{th} column of a normalized eigenvector matrix $[\phi]$.

For the purpose of this study, it is assumed that the modal matrix diagonalizes the damping matrix as well, so that

$$[\phi]^T[C][\phi] = \text{diag}[2\zeta_j\omega_j] \tag{D-9}$$

The ARIS developers assigned the damping factors a value of 0.015 for all modes. This is the value currently used in the simulation presented in this paper and the damping matrix is calculated in physical coordinates using

$$[C] = \left(\left[\phi\right]^T\right)^{-1} \mathrm{diag}\left[2\zeta_j\omega_j\right]\left[\phi\right]^{-1} \tag{D-10}$$

Eq. (D-10) has certain implications regarding the form of the physical damping matrix. If an aggregate 6x6 stiffness matrix, incorporating translational and torsional stiffness elements, is used to generate the eigenvalues and eigenvectors then the physical damping matrix realized through Eq. (D-10) is not of the same form as that given in Eq. (73). The reason for this is that although the torsional stiffness quantity is confined to the lower right-hand minor of the aggregate stiffness matrix, it effects all of the eigenvalues and eigenvectors obtained from the eigenvalue problem in Eq. (D-5). Therefore, all of the terms in the physical damping matrix are affected when the physical damping is approximated using Eq. (D-10). Although the validity of the assumption in Eq. (D-9) (and therefore Eq. (D-10)) is in question no matter which form of the stiffness matrix is used, it was decided to approximate damping using the eigenvalues and eigenvectors from the undamped, unforced system incorporating the aggregate 6x6 stiffness matrix, which is the summation of all actuator and umbilical stiffnesses, both translational and torsional.

To maintain the same form of the 6x6 damping matrix given in Eq. (73), a different approach is needed. In this approach, 2N equations of the form given in Eq. (D-2) would be written. In each equation, the stiffness matrix would be different, and represent the stiffness for one of the N elastic elements. For each elastic element, there

would be two equations - one incorporating a 6x6 stiffness matrix for the translational stiffness and one incorporating the torsional stiffness. Damping matrices would be generated for each element individually using eigenvalues and eigenvectors unique to that particular element. The 2N physical damping matrices generated through Eq. (D-10) would then be added together to from an aggregate damping matrix for all of the elements. Although this approach may be more intuitive, the validity of this approximation over that described in the last paragraph is questionable.

APPENDIX E

Transfer Functions of the ARIS Control Elements

Many of the control elements presented in the ARIS block diagram in Figure 15 are represented by superblocks, in which a number of individual blocks are grouped together. In the case of such control elements as the *Acceleration Compensator* or the *40 Hz Second Order Filter* the superblocks consist of an array of compensators. In the *Acceleration Compensator* block there are six identical cascade compensator branches (paths) and each of these operates on one of the translational or rotational acceleration signals. The *40 Hz Second Order Filter* block consists of eight identical compensator branches, one for each of the eight accelerometer signals. In the following listing, the transfer functions found in each of the ARIS controller elements, for the baseline production and RME versions, are presented. The block name is given along with the number of control branches and the block-diagram form of the transfer functions within the control element. In every case, the compensator for each branch or path in the given control element is identical.

Table E-1: Simulation Blocks for Baseline Production ARIS Controller Elements

Name of Block	Number of Branches	Transfer Function and Configuration (All Branches Identical)
2nd Order Approx. for Elliptic Filter (This approximating filter was supplied by Boeing Product Group 3 (PG-3).)	8	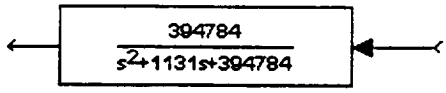
40 Hz 2nd Order	8	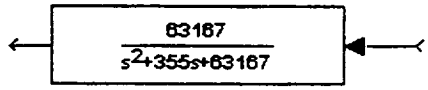
Acceleration Compensator	6	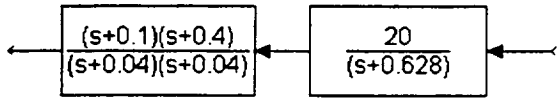
Position Analog Filters	8	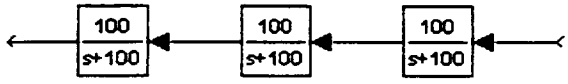
Position Filters	6	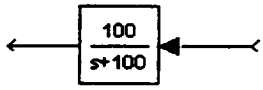
Position Control	6	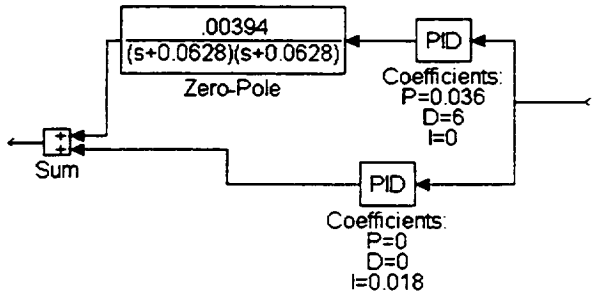

The ARIS controllers employed during the RME differed from the baseline production controller shown above in several respects. With regard to the controller elements considered in this appendix, the *baseline robust controller* used during the RME utilized an 8 Hz second order filter in place of the 40 Hz second order filter used in the baseline production controller. Furthermore, the *baseline robust controller* utilized a 250 Hz elliptic filter instead of the 25 Hz elliptic filter used in the production version. With regard to the controller elements presented in this appendix, the RME *high gain controller* differs from the ARIS production controller in that it incorporates an additional lag filter in the acceleration feedback loop, downstream of the acceleration compensation. Furthermore, the acceleration feedback loop gain is double the gain in the baseline production version. Instead of using a second order filter to approximate the elliptic filter elements, as is done in the simulation presented in Section 8.3, the RME simulations use the full 8^{th} order transfer functions to simulate the elliptic controller elements. All of the RME controller element variations described here are presented below. With the exception of controller element variations described here, the RME controllers are assumed to utilize controller elements identical to those presented for the baseline production controller given above.

Table E-2: RME *Baseline Robust Controller* Variations

Name of Block	Number of Branches	Transfer Function and Configuration (All Branches Identical)
8 Hz Second Order	8	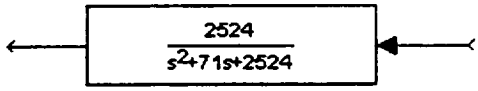
250 Hz Elliptic	8	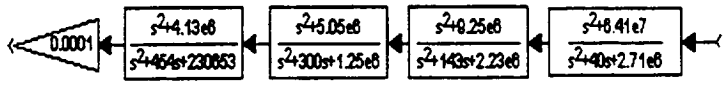

Table E-3: RME *High Gain Controller* Variations

Name of Block	Number of Branches	Transfer Function and Configuration (All Branches Identical)
Analog Filter 2 (Lag Filter)	8	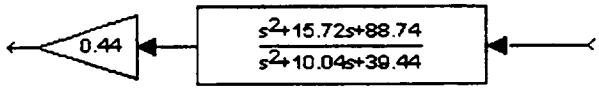
25 Hz Elliptic	8	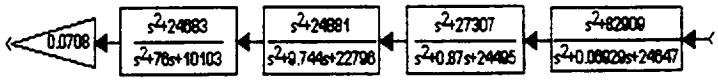

APPENDIX F

MATLAB Code for Generating Simulation Parameters

The MATLAB code given in this appendix is mainly composed of several different executable files received from The Boeing Company in October, 1995. Since the time at which this code was supplied, several ARIS design changes have taken place. Therefore, the code should be considered applicable to the baseline design from late 1995 and must be corrected or modified in order to simulate specific ARIS racks currently planned for use on the Space Station.

```
% THIS PROGRAM GENERATES PARAMETERS FOR USE IN THE ARIS SIMULATION

%*****************************************************************************
%                        RACK BASELINE MASS PROPERTIES
%*****************************************************************************


% MASS (SLUGS)

MR=54.916;


% MOMENT OF INERTIA (SLUG-FT^2)

IR=[183, -0.0076831, 0.11565;
        -0.0076831, 194.99, -7.1478;
        0.11565, -7.1478, 81.279];


% AGGREGATE MASS MATRIX

massmat=zeros(6);
massmat(1:3,1:3)=[MR,0,0;0,MR,0;0,0,MR];
massmat(1:3,4:6)=zeros(3);
massmat(4:6,1:3)=zeros(3);
massmat(4:6,4:6)=IR;

invmass=inv(massmat);

%*****************************************************************************
%                        BASELINE UMBILICAL STIFFNESS PROPERTIES
%                        (No Translational Coupling Predicted)
%*****************************************************************************


kx=86.4;
ky=104.4;
kz=104.4;
kxy=0;
kxz=0;
kyz=0;

%POSITION VECTOR OF THE CENTROID OF THE UMBILICAL CONNECTION, MEASURED
%RELATIVE TO THE CENTER OF MASS OF THE RACK, IN RACK EQUILIBRIUM
%COORDINATES (FT)

dvect=[-0.363, -0.342, -2.42];


% SECOND ORDER TENSOR ASSOCIATED WITH dvect

dtens=[0 -dvect(3) dvect(2); dvect(3) 0 -dvect(1); -dvect(2) dvect(1) 0];
```

```
% CONSTRUCT 3X3 (UPPER LEFT) MINOR OF THE STIFFNESS MATRIX

Ktr=zeros(3);
Ktr(1,1)=kx;
Ktr(2,2)=ky;
Ktr(3,3)=kz;


% TORSIONAL STIFFNESS (CALCULATED FROM BOEING-SUPPLIED INFORMATION)

Ktor=zeros(3);
Ktor(1,1)=53.17;
Ktor(2,2)=109.27;
Ktor(3,3)=78.56;


% CONSTRUCT 6X6 STIFFNESS MATRIX

Kumb=zeros(6);
Kumb(1:3,1:3)=Ktr;
Kumb(1:3,4:6)=Ktr*dtens';
Kumb(4:6,1:3)=dtens*Ktr;
Kumb(4:6,4:6)=dtens'*Ktr*dtens+Ktor;


%*********************************************************************************************
%       EIGENVALUES AND EIGENVECTORS OF SYSTEM WITH UMBILICALS ONLY
%                                       AND
%       APPROXIMATION OF PHYSICAL DAMPING MATRIX FOR UMBILICALS
%*********************************************************************************************


[Vumb,Dumb]=eig(invmass*Kumb);

%NORMALIZED EIGENVECTORS

massdiag=zeros(6);
massdiag=Vumb'*massmat*Vumb;

for i=1:6
phi_umb(:,i)=Vumb(:,i)/(massdiag(i,i))^0.5;
end

%APPROXIMATION FOR UMBILICAL DAMPING IN PHYSICAL COORDINATES

Cumb=inv(phi_umb')*2*0.015*Dumb.^0.5*inv(phi_umb);

% Check on umbilical damping geometry

Cumbc=zeros(6);
Ctr=Cumb(1:3,1:3);
Cumbc(1:3,1:3)=Ctr;
Cumbc(1:3,4:6)=Ctr*dtens';
```

```
Cumbc(4:6,1:3)=dtens*Ctr;
Cumbc(4:6,4:6)=dtens'*Ctr*dtens;


%*****************************************************************************************
%                          ACCELEROMETER GEOMETRY
%                  (THIS SECTION PROVIDED BY ARIS DEVELOPERS)
%*****************************************************************************************

%clear msv
centocg=[0,0,0];
rhead1=[-17.7 14.1 27.9]-centocg;
rhead2=[-17.7 11.2 -31.5]-centocg;
rhead3=[17.7 11.2 -31.5]-centocg;
racc1=(rhead1)/12;
racc2=(rhead1)/12;
racc3=(rhead2)/12;
racc4=(rhead2)/12;
racc5=(rhead2)/12;
racc6=(rhead3)/12;
racc7=(rhead3)/12;
racc8=(rhead3)/12;

phia=0;
phib=pi/4;
phic=-pi/4;

cp=cos(phia);
sp=sin(phia);
ry=[cp 0 -sp;0 1 0;sp 0 cp];
acc1=[sqrt(2)/2 sqrt(2)/2 0];
acc2=[-sqrt(2)/2 sqrt(2)/2 0];
acc1=(ry*acc1')';
acc2=(ry*acc2')';


cp=cos(phib);
sp=sin(phib);
rz=[cp -sp 0;sp cp 0;0 0 1];
acc3=[sqrt(2)/2 0.5 0.5];
acc4=[-sqrt(2)/2 0.5 0.5];
acc5=[0 -1 1]/sqrt(2);
acc3=(rz*acc3')';
acc4=(rz*acc4')';
acc5=(rz*acc5')';

cp=cos(phic);
sp=sin(phic);
rz=[cp -sp 0;sp cp 0;0 0 1];
acc6=[sqrt(2)/2 0.5 0.5];
acc7=[-sqrt(2)/2 0.5 0.5];
acc8=[0 -1 1]/sqrt(2);
acc6=(rz*acc6')';
acc7=(rz*acc7')';
```

```
acc8=(rz*acc8')';
max1=0;

% ROTACC=[0.7071 -0.7071 0.1464 -0.8536 0.5000 -0.3000 -0.6660 //0.6830;
%  0.7071  0.7071  0.8536 -0.1464 -0.5000  0.8124 -0.5536 //-0.1830;
% 0.0000  0.0000  0.5000  0.5000  0.7071  0.5000  0.5000  //0.7071]
% acc1=(rotacc(:,1))';
% acc2=(rotacc(:,2))';
% acc3=(rotacc(:,3))';
% acc4=(rotacc(:,4))';
% acc5=(rotacc(:,5))';
% acc6=(rotacc(:,6))';
% acc7=(rotacc(:,7))';
% acc8=(rotacc(:,8))';

rot1=cross(racc1,acc1);
rot2=cross(racc2,acc2);
rot3=cross(racc3,acc3);
rot4=cross(racc4,acc4);
rot5=cross(racc5,acc5);
rot6=cross(racc6,acc6);
rot7=cross(racc7,acc7);
rot8=cross(racc8,acc8);
rotacc=[acc1' acc2' acc3' acc4' acc5' acc6' acc7' acc8']
M=[acc1 rot1;
  acc2 rot2;
  acc3 rot3;
  acc4 rot4;
  acc5 rot5;
  acc6 rot6;
  acc7 rot7;
  acc8 rot8];

for l=1:8, ...
b=eye(8,8); ...
b(l,l)=0; ...
mnew=b*M; ...
msv(l)=min(svd(mnew)); ...
end; ...
msv

for k=1:8, ...
for j=1:8, ...
b=eye(8,8); ...
b(k,k)=0; ...
b(j,j)=0; ...
mnew=b*M; ...
minsv(j,k)=min(svd(mnew)); ...
end; ...
end;
failmsv=minsv
minsv(1:2,1:2)=[10 10;10 10]; ...
mminsv=min(minsv);
zro= 0*ones(1,3);
```

```
Twtom= [acc1  zro  zro;
        acc2  zro  zro;
        zro  acc3  zro;
        zro  acc4  zro;
        zro  acc5  zro;
        zro  zro  acc6;
        zro  zro  acc7;
        zro  zro  acc8]


%*****************************************************************************************
%                                    ACTUATOR GEOMETRY
%                        (THIS SECTION PROVIDED BY ARIS DEVELOPERS)
%*****************************************************************************************

lowl_to_nate=[0 -1.008 0];
lowl_to_lpivot=[-1.08 -25.58 1.922];
lpivot_to_modc=[20.5 -45.5 36.2];
nate_to_cg=[19.56 -12.93 38.40];
modtocg = -lpivot_to_modc-lowl_to_lpivot+lowl_to_nate+nate_to_cg;

%pushrod flex joint point on actuator lever arm
r1=([-17.8 47.2 -31.3]-modtocg)/12;
r2=([-18.6 64.2 -29.7]-modtocg)/12;
r3=([17.8 47.2 -31.3]-modtocg)/12;
r4=([18.6 64.2 -29.7]-modtocg)/12;
r5=([13.2 68.6 -42.2]-modtocg)/12;
r6=([-13.2 68.6 -42.2]-modtocg)/12;
r7=([3.9 47.9 39.3]-modtocg)/12;
r8=([-3.9 47.9 39.3]-modtocg)/12;
ract= [r1' r2' r3' r4' r5' r6' r7' r8'];
%
%pushrod flex joint point at end of pushrod
re1=([-17.8 67.5 -42.6]-modtocg)/12;
re2=([-18.6 48.4 -42.4]-modtocg)/12;
re3=([17.8 67.5 -42.6]-modtocg)/12;
re4=([18.6 48.4 -42.4]-modtocg)/12;
re5=([0.9 59.6 -40.2]-modtocg)/12;
re6=([-0.9 59.6 -40.2]-modtocg)/12;
re7=([10.7 72.4 39.3]-modtocg)/12;
re8=([-10.7 72.4 39.3]-modtocg)/12;
rend= [re1' re2' re3' re4' re5' re6' re7' re8'];
%
rd= rend - ract;
%
% pushrod unit vectors in rack coordinates
rd1norm=rd(:,1)/norm(rd(:,1));
rd2norm=rd(:,2)/norm(rd(:,2));
rd3norm=rd(:,3)/norm(rd(:,3));
rd4norm=rd(:,4)/norm(rd(:,4));
rd5norm=rd(:,5)/norm(rd(:,5));
rd6norm=rd(:,6)/norm(rd(:,6));
rd7norm=rd(:,7)/norm(rd(:,7));
rd8norm=rd(:,8)/norm(rd(:,8));
```

```
rdnorm=[rd1norm rd2norm rd3norm rd4norm rd5norm rd6norm rd7norm rd8norm];
%
% lever arm unit vector direction in rack coordinates
rarm1=[0 -1.1 -2.8]'/3.00832;
rarm2=[0 1.5 -2.6]'/3.0017;
rarm3=[0 -1.1 -2.8]'/3.00832;
rarm4=[0 1.5 -2.6]'/3.0017;
rarm5=[1.3 -2.7 0]'/2.99666;
rarm6=[-1.3 -2.7 0]'/2.99666;
rarm7=[-2.8 1.2 0]'/3.0463;
rarm8=[2.8 1.2 0]'/3.0463;
%
% cg to actuator hinge point vector
r=3/12;
r1o=r1-r*rarm1';
r2o=r2-r*rarm2';
r3o=r3-r*rarm3';
r4o=r4-r*rarm4';
r5o=r5-r*rarm5';
r6o=r6-r*rarm6';
r7o=r7-r*rarm7';
r8o=r8-r*rarm8';
%
% complete the right handed coordinate system
rz1=cross(rarm1',rd1norm');
rz2=cross(rarm2',rd2norm');
rz3=cross(rarm3',rd3norm');
rz4=cross(rarm4',rd4norm');
rz5=cross(rarm5',rd5norm');
rz6=cross(rarm6',rd6norm');
rz7=cross(rarm7',rd7norm');
rz8=cross(rarm8',rd8norm');
%
% compute the transformation maping vectors in local actuator
% centered coordinates to center of mass coordinates
rot1=[rarm1 rd1norm rz1'];
rot2=[rarm2 rd2norm rz2'];
rot3=[rarm3 rd3norm rz3'];
rot4=[rarm4 rd4norm rz4'];
rot5=[rarm5 rd5norm rz5'];
rot6=[rarm6 rd6norm rz6'];
rot7=[rarm7 rd7norm rz7'];
rot8=[rarm8 rd8norm rz8'];


zero= 0*ones(3);
t1= [rot1' zero;zero rot1'];
t2= [rot2' zero;zero rot2'];
t3= [rot3' zero;zero rot3'];
t4= [rot4' zero;zero rot4'];
t5= [rot5' zero;zero rot5'];
t6= [rot6' zero;zero rot6'];
t7= [rot7' zero;zero rot7'];
t8= [rot8' zero;zero rot8'];
```

```
wr= [r1o' r2o' r3o' r4o' r5o' r6o' r7o' r8o'];
wt= [t1 t2 t3 t4 t5 t6 t7 t8];
m= 0;...
bigx= 0*ones(48,6);
bigxt= 0*ones(6,48);
%
for j= 1:8,...
rc(1,1)= 0;...
rc(2,2)= 0;...
rc(3,3)= 0;...
rc(1,2)= -wr(3,j);...
rc(1,3)= wr(2,j);...
rc(2,3)= -wr(1,j);...
rc(2,1)= -rc(1,2);...
rc(3,1)= -rc(1,3);...
rc(3,2)= -rc(2,3);...
c= [eye(3) -rc;zero eye(3)];...
for k= 1:6;...
for l= 1:6;...
t(k,l)= wt(k,l+m);...
end,...
end,...
x= t*c;...
xt= x';...
for k= 1:6,...
for l= 1:6,...
bigx(k+m,l)= x(k,l);...
bigxt(k,l+m)= xt(k,l);...
end,...
end,...
m= m+6;...
end

%*****************************************************************************************
%                    STIFFNESS MATRICES FOR ACTUATORS IN LOCAL COORDINATES
%                                (THIS SECTION PROVIDED BY ARIS DEVELOPERS)
%*****************************************************************************************

l1=23.3/12;l2=20.2/12;l3=23.3/12;l4=20.2/12;
l5=15.4/12;l6=15.4/12;l7=25.4/12;l8=25.4/12;
%
k1= .5/12;
k3= .5/12;
k4= .5/12;
kp= .5/12;
%
ks133= (k3+k4)/(l1*l1)+kp/(r*r);...
ks1=[(k3+k4)/(l1*l1), k3/r/l1,  0,    0,    0,    0
    k3/r/l1, (k1+k3)/(r*r),   0,    0,    0,   k1/r
     0,    0,    ks133 , k3/l1,   -r*(k3+k4)/(l1*l1)+kp/r,  0
     0,    0,    k3/l1,        k3,       -r*k3/l1,      0
     0,    0, -r*(k3+k4)/(l1*l1)+kp/r, -r*k3/l1, (r*r)*(k3+k4)/(l1*l1)+kp, 0
     0,   k1/r,      0,        0,        0,          k1];
```

```
gam1= [-(k3+k4)/(l1*l1),    0,      0,          0,      0,  k4/l1
       -k3/(r*l1),   -k1/(r*r),  0,          0,      0,   0
         0,           0   -(k3+k4)/(l1*l1),  k4/l1,  -kp/r,   0
         0,           0,   -k3/l1,        0,      0,   0
         0,           0, r*(k3+k4)/(l1*l1),-r*k4/l1,  -kp    0
         0,         -k1/r,    0,          0,      0,   0];

ks233= (k3+k4)/(l2*l2)+kp/(r*r);...

ks2=[(k3+k4)/(l2*l2), k3/r/l2,   0,    0,    0,    0
    k3/r/l2, (k1+k3)/(r*r),   0,    0,    0,   k1/r
     0,    0,    ks233,   k3/l2,   -r*(k3+k4)/(l2*l2)+kp/r, 0
     0,    0,    k3/l2,         k3,       -r*k3/l2,       0
     0,    0, -r*(k3+k4)/(l2*l2)+kp/r, -r*k3/l2, (r*r)*(k3+k4)/(l2*l2)+kp, 0
     0,   k1/r,       0,         0,         0,          k1];

gam2= [-(k3+k4)/(l2*l2),    0,      0,          0,      0,  k4/l2
       -k3/(r*l2),   -k1/(r*r),  0,          0,      0,   0
         0,           0   -(k3+k4)/(l2*l2),  k4/l2,  -kp/r,   0
         0,           0,   -k3/l2,        0,      0,   0
         0,           0, r*(k3+k4)/(l2*l2),-r*k4/l2,  -kp    0
         0,         -k1/r,    0,          0,      0,   0];


ks333= (k3+k4)/(l3*l3)+kp/(r*r);...

ks3=[(k3+k4)/(l3*l3), k3/r/l3,   0,    0,    0,    0
    k3/r/l3, (k1+k3)/(r*r),   0,    0,    0,   k1/r
     0,    0,    ks333,   k3/l3,   -r*(k3+k4)/(l3*l3)+kp/r, 0
     0,    0,    k3/l3,         k3,       -r*k3/l3,       0
     0,    0, -r*(k3+k4)/(l3*l3)+kp/r, -r*k3/l3, (r*r)*(k3+k4)/(l3*l3)+kp, 0
     0,   k1/r,       0,         0,         0,          k1];

gam3= [-(k3+k4)/(l3*l3),    0,      0,          0,      0,  k4/l3
       -k3/(r*l3),   -k1/(r*r),  0,          0,      0,   0
         0,           0   -(k3+k4)/(l3*l3),  k4/l3,  -kp/r,   0
         0,           0,   -k3/l3,        0,      0,   0
         0,           0, r*(k3+k4)/(l3*l3),-r*k4/l3,  -kp    0
         0,         -k1/r,    0,          0,      0,   0];

ks433= (k3+k4)/(l4*l4)+kp/(r*r);...

ks4=[(k3+k4)/(l4*l4), k3/r/l4,   0,    0,    0,    0
    k3/r/l4, (k1+k3)/(r*r),   0,    0,    0,   k1/r
     0,    0,    ks433,   k3/l4,   -r*(k3+k4)/(l4*l4)+kp/r, 0
     0,    0,    k3/l4,         k3,       -r*k3/l4,       0
     0,    0, -r*(k3+k4)/(l4*l4)+kp/r, -r*k3/l4, (r*r)*(k3+k4)/(l4*l4)+kp, 0
     0,   k1/r,       0,         0,         0,          k1];

gam4= [-(k3+k4)/(l4*l4),    0,      0,          0,      0,  k4/l4
       -k3/(r*l4),   -k1/(r*r),  0,          0,      0,   0
         0,           0   -(k3+k4)/(l4*l4),  k4/l4,  -kp/r,   0
         0,           0,   -k3/l4,        0,      0,   0
         0,           0, r*(k3+k4)/(l4*l4),-r*k4/l4,  -kp    0
```

```
          0,        -k1/r,     0,          0,      0,    0];

 ks533= (k3+k4)/(15*15)+kp/(r*r);...

 ks5=[(k3+k4)/(15*15), k3/r/15,  0,    0,    0,    0
     k3/r/15, (k1+k3)/(r*r),   0,    0,    0,   k1/r
      0,    0,   ks533,   k3/15,   -r*(k3+k4)/(15*15)+kp/r, 0
      0,    0,   k3/15,        k3,       -r*k3/15,       0
      0,    0, -r*(k3+k4)/(15*15)+kp/r, -r*k3/15, (r*r)*(k3+k4)/(15*15)+kp, 0
      0,  k1/r,       0,        0,        0,          k1];

 gam5= [-(k3+k4)/(15*15),    0,      0,          0,      0,  k4/15
        -k3/(r*15),   -k1/(r*r),  0,          0,      0,    0
          0,           0  -(k3+k4)/(15*15),  k4/15,  -kp/r,   0
          0,           0,   -k3/14,        0,      0,    0
          0,           0, r*(k3+k4)/(15*15),-r*k4/15,  -kp    0
          0,         -k1/r,     0,          0,      0,    0];

 ks633= (k3+k4)/(16*16)+kp/(r*r);...

 ks6=[(k3+k4)/(16*16), k3/r/16,  0,    0,    0,    0
     k3/r/16, (k1+k3)/(r*r),   0,    0,    0,   k1/r
      0,    0,   ks633,   k3/16,   -r*(k3+k4)/(16*16)+kp/r, 0
      0,    0,   k3/16,        k3,       -r*k3/16,       0
      0,    0, -r*(k3+k4)/(16*16)+kp/r, -r*k3/16, (r*r)*(k3+k4)/(16*16)+kp, 0
      0,  k1/r,       0,        0,        0,          k1];

 gam6= [-(k3+k4)/(16*16),    0,      0,          0,      0,  k4/16
        -k3/(r*16),   -k1/(r*r),  0,          0,      0,    0
          0,           0  -(k3+k4)/(16*16),  k4/16,  -kp/r,   0
          0,           0,   -k3/16,        0,      0,    0
          0,           0, r*(k3+k4)/(16*16),-r*k4/16,  -kp    0
          0,         -k1/r,     0,          0,      0,    0];

 ks733= (k3+k4)/(17*17)+kp/(r*r);...

 ks7=[(k3+k4)/(17*17), k3/r/17,  0,    0,    0,    0
     k3/r/17, (k1+k3)/(r*r),   0,    0,    0,   k1/r
      0,    0,   ks733,   k3/17,   -r*(k3+k4)/(17*17)+kp/r, 0
      0,    0,   k3/17,        k3,       -r*k3/17,       0
      0,    0, -r*(k3+k4)/(17*17)+kp/r, -r*k3/17, (r*r)*(k3+k4)/(17*17)+kp, 0
      0,  k1/r,       0,        0,        0,          k1];

 gam7= [-(k3+k4)/(17*17),    0,      0,          0,      0,  k4/17
        -k3/(r*17),   -k1/(r*r),  0,          0,      0,    0
          0,           0  -(k3+k4)/(17*17),  k4/17,  -kp/r,   0
          0,           0,   -k3/17,        0,      0,    0
          0,           0, r*(k3+k4)/(17*17),-r*k4/17,  -kp    0
          0,         -k1/r,     0,          0,      0,    0];

 ks833= (k3+k4)/(18*18)+kp/(r*r);...

 ks8=[(k3+k4)/(18*18), k3/r/18,  0,    0,    0,    0
     k3/r/18, (k1+k3)/(r*r),   0,    0,    0,   k1/r
```

```
    0,   0,   ks833,   k3/l8,   -r*(k3+k4)/(l8*l8)+kp/r, 0
    0,   0,   k3/l8,      k3,      -r*k3/l8,      0
    0,   0, -r*(k3+k4)/(l8*l8)+kp/r, -r*k3/l8, (r*r)*(k3+k4)/(l8*l8)+kp, 0
    0,  k1/r,      0,       0,       0,          k1];

gam8= [-(k3+k4)/(l8*l8),    0,     0,         0,      0,  k4/l8
       -k3/(r*l8),   -k1/(r*r),  0,         0,      0,   0
         0,           0   -(k3+k4)/(l8*l8),  k4/l8,  -kp/r,   0
         0,           0,   -k3/l8,         0,      0,   0
         0,           0, r*(k3+k4)/(l8*l8),-r*k4/l8,  -kp    0
         0,         -k1/r,    0,          0,      0,   0];



%*********************************************************************************
%                AGGREGATE ACTUATOR STIFFNESS IN CENTER OF MASS COORDINATES
%                          (THIS SECTION PROVIDED BY ARIS DEVELOPERS)
%*********************************************************************************

zro= 0*ones(6);...
bigk= [ks1 zro zro zro zro zro zro zro;
    zro ks2 zro zro zro zro zro zro;
    zro zro ks3 zro zro zro zro zro;
    zro zro zro ks4 zro zro zro zro;
    zro zro zro zro ks5 zro zro zro;
    zro zro zro zro zro ks6 zro zro;
    zro zro zro zro zro zro ks7 zro;
    zro zro zro zro zro zro zro ks8];

ks= bigxt*bigk*bigx;

gamx= gam1*t1+gam2*t2+gam3*t3+gam4*t4+gam5*t5+gam6*t6+gam7*t7+gam8*t8;

%*********************************************************************************
%EIGENVALUES AND EIGENVECTORS OF SYSTEM WITH UMBILICALS AND ACTUATORS
%                                  AND
%APPROXIMATION OF PHYSICAL DAMPING MATRIX FOR UMBILICALS AND ACTUATORS
%*********************************************************************************

%TOTAL STIFFNESS: UMBILICALS AND ACTUATORS

K=Kumb+ks;

[V,D]=eig(invmass*K);

%NORMALIZED EIGENVECTORS

massdiag=V'*massmat*V;

for i=1:6
phi(:,i)=V(:,i)/(massdiag(i,i))^0.5;
end
```

```
%APPROXIMATION FOR UMBILICAL AND ACTUATOR DAMPING IN PHYSICAL
COORDINATES

C=inv(phi')*2*0.015*D.^0.5*inv(phi);

%*****************************************************************************************
%TRANSFORMATION FROM CONTROL INPUTS TO FORCE COMPONENTS
%FOR EXCITING FLEXIBLE MODES
%                (THIS SECTION PROVIDED BY ARIS DEVELOPERS)
%*****************************************************************************************

zro= 0*ones(3,1);
Tutow= [rd1norm  zro    zro    zro    zro    zro    zro  zro;
        zro  rd2norm  zro    zro    zro    zro    zro  zro
        zro    zro  rd3norm  zro    zro    zro    zro  zro;
        zro    zro    zro  rd4norm  zro    zro    zro  zro
        zro    zro    zro    zro  rd5norm  zro    zro  zro
        zro    zro    zro    zro    zro  rd6norm  zro  zro
        zro    zro    zro    zro    zro    zro  rd7norm  zro
        zro    zro    zro    zro    zro    zro    zro rd8norm]



%*****************************************************************************************
%RESOLVE ACTUATOR FORCE DIRECTIONS ALONG RACK COORDINATES TO COMPUTE
%FORCEAND TORQUE INPUTS FROM THE ACTUATORS
%                          (THIS SECTION PROVIDED BY ARIS DEVELOPERS)
%*****************************************************************************************

[u1,x]= crossudf(ract(:,1)',rd1norm');
[u2,x]= crossudf(ract(:,2)',rd2norm');
[u3,x]= crossudf(ract(:,3)',rd3norm');
[u4,x]= crossudf(ract(:,4)',rd4norm');
[u5,x]= crossudf(ract(:,5)',rd5norm');
[u6,x]= crossudf(ract(:,6)',rd6norm');
[u7,x]= crossudf(ract(:,7)',rd7norm');
[u8,x]= crossudf(ract(:,8)',rd8norm');
Tutox= [rd1norm rd2norm rd3norm rd4norm rd5norm rd6norm rd7norm rd8norm;
     u1'   u2'    u3'   u4'   u5'   u6'   u7'   u8'  ]

%Simulate removal of #8 actuator on baseline

%Tutox(:,7)=zeros(6,1);


%*****************************************************************************************
%                RESOLVE RIGID BODY MOTION ALONG THE ACTUATOR PUSHRODS
%                          (THIS SECTION PROVIDED BY ARIS DEVELOPERS)
%*****************************************************************************************

[x,y,rc1]= crossudf(zro',ract(:,1)');
[x,y,rc2]= crossudf(zro',ract(:,2)');
[x,y,rc3]= crossudf(zro',ract(:,3)');
[x,y,rc4]= crossudf(zro',ract(:,4)');
```

```
[x,y,rc5]= crossudf(zro',ract(:,5)');
[x,y,rc6]= crossudf(zro',ract(:,6)');
[x,y,rc7]= crossudf(zro',ract(:,7)');
[x,y,rc8]= crossudf(zro',ract(:,8)');
Txa1= [eye(3) -rc1];
Txa2= [eye(3) -rc2];
Txa3= [eye(3) -rc3];
Txa4= [eye(3) -rc4];
Txa5= [eye(3) -rc5];
Txa6= [eye(3) -rc6];
Txa7= [eye(3) -rc7];
Txa8= [eye(3) -rc8];
Txtop= Tutow'*[Txa1;Txa2;Txa3;Txa4;Txa5;Txa6;Txa7;Txa8]
xp= Txtop;
Tptox= inv(xp'*xp)*xp'
xp=Txtop;
Tptox=inv(xp'*xp)*xp';

%*****************************************************************************
%              MAP RIGID BODY ACCELERATION TO ACCELEROMTER LOCATIONS
%                        (THIS SECTION PROVIDED BY ARIS DEVELOPERS)
%*****************************************************************************

    rc1= [ -17.7 14.1 27.9 ]/12;
    rc2= [ -17.7 11.2 -31.5]/12;
    rc3= [ 17.7 11.2 -31.5 ]/12;
[x,y,rcc1]= crossudf(rc1,rc1);
[x,y,rcc2]= crossudf(rc2,rc2);
[x,y,rcc3]= crossudf(rc3,rc3);
Txtow= [eye(3) -rcc1;
     eye(3) -rcc2;
     eye(3) -rcc3]
Twtom
Txtom= Twtom*Txtow
Tmtox= pinv(Txtom)
checkXtoX= Tmtox*Txtom


%*****************************************************************************
%       TRANSFORMATION OF ACCELERATION COMMANDS TO ACTUATOR COMMANDS
%                        (THIS SECTION PROVIDED BY ARIS DEVELOPERS)
%*****************************************************************************

[tor1,x1,x2]=  crossudf(ract(:,1)',rd(:,1)');
[tor2,x1,x2]=  crossudf(ract(:,2)',rd(:,2)');
[tor3,x1,x2]=  crossudf(ract(:,3)',rd(:,3)');
[tor4,x1,x2]=  crossudf(ract(:,4)',rd(:,4)');
[tor5,x1,x2]=  crossudf(ract(:,5)',rd(:,5)');
[tor6,x1,x2]=  crossudf(ract(:,6)',rd(:,6)');
[tor7,x1,x2]=  crossudf(ract(:,7)',rd(:,7)');
[tor8,x1,x2]=  crossudf(ract(:,8)',rd(:,8)');
ttor= [tor1' tor2' tor3' tor4' tor5' tor6' tor7' tor8'];
for i= 1:8,...
  mag= norm(ttor(:,i));...
```

```
  ttoru(:,i)= ttor(:,i)/mag;...
end
Tdelxtou= [rd1norm' ttoru(:,1)'/norm(ract(:,1));
        rd2norm' ttoru(:,2)'/norm(ract(:,2));
        rd3norm' ttoru(:,3)'/norm(ract(:,3));
        rd4norm' ttoru(:,4)'/norm(ract(:,4));
        rd5norm' ttoru(:,5)'/norm(ract(:,5));
        rd6norm' ttoru(:,6)'/norm(ract(:,6));
        rd7norm' ttoru(:,7)'/norm(ract(:,7));
        rd8norm' ttoru(:,8)'/norm(ract(:,8))];
Tdelxtou= pinv(Tutox)
checkxtox= Tutox*Tdelxtou

%*************************************************************************************
%                                  AUXILLIARY PARAMETERS
%*************************************************************************************


twozeta=0.03*eye(6);
intoft=0.08333*eye(9);

cgx=0;
cgy=0;
cgz=0;


idm=massmat;
ctm=eye(6,6);
ctmi=eye(6,6);
ctmcg=[0, cgz,-cgy;
    -cgz,0,cgx;
    cgy,-cgx,0];

ctm(1:3,4:6)=ctmcg;
ctmi(4:6,1:3)=-ctmcg;

pk=zeros(6);
pk=-K;
w2=1.4;
for i=1:6
pk(i,i)=w2*w2*massmat(i,i)-K(i,i);
end

Gain=1*eye(6);
Gain1=1*eye(6);

%Position vector of the pth disturber, relative to the rack center of mass
rpvect=[1.75,1.59,3.17];
rptens=[0,-rpvect(1,3),rpvect(1,2);
          rpvect(1,3),0,-rpvect(1,1);
          -rpvect(1,2),rpvect(1,1),0];


%*************************************************************************
```

```
%                          PLOTTING ROUTINE
%*****************************************************************************

% Set up Frequency vector from 0.001 to 20 Hz

wmax=10*6.28;
wmin=0.001*6.28;
wmin_pow=log10(wmin);
wmax_pow=log10(wmax);
w=logspace(wmin_pow,wmax_pow,300);
whz=w/6.28;

%disp('rack_ol')
%[Aol,Bol,Col,Dol]=linmod('rack_ol');
%[mag,phase]=bod1(Aol,Bol,Col,Dol,7,w);
%magl(:,1)=log10(mag);
%semilogx(whz,20*magl(:,1));
%axis([.001 10 -80 40])



for i=1:3
[Acl,Bcl,Ccl,Dcl]=linmod('aris_cl');
[mag,phase]=bode(Acl,Bcl,Ccl,Dcl,i,w);
magl(:,i)=log10(mag);
PHASE(:,i)=phase
end
semilogx(whz,20*magl(:,1),'y',whz,20*magl(:,2),'y--',whz,20*magl(:,3),'y.');
axis([.001 10 -150 40]);
%figure
%semilogx(whz,PHASE(:,1),'y',whz,PHASE(:,2),'y--',whz,PHASE(:,3),'y.');
%axis([.001 10 -180 180]);



%[Acl,Bcl,Ccl,Dcl]=linmod('aris_cl');
%[mag,phase]=bode(Acl,Bcl,Ccl,Dcl,2,w);
%magl(:,2)=log10(mag);
%PHASE(:,1)=phase
%semilogx(whz,20*magl(:,1),'.',whz,20*magl(:,2));
%axis([.001 20 -80 20]);
%figure
%semilogx(whz,PHASE(:,1));
%axis([.001 20 -500 360])



%****************************** END OF FILE ********************************
```

```
% THIS M-FILE GENERATES PHYSICAL PARAMETERS FOR THE ARIS RME RACK

%*************************************************************************
%                          RACK RME MASS PROPERTIES
%*************************************************************************

% MEASURED MASS IN SLUGS (RSA LOGISTICS INCLUDED)

MR=27.6;


% MEASURED MOMENT OF INERTIA TENSOR (SLUG-FT^2)
% THIS IS FOR RACK WITH RSA LOGISTICS

IR=[113, 2.7, 2;
        2.7, 123, 5.7;
        2, 5.7, 47];


% AGGREGATE MASS MATRIX

massmat=zeros(6);
massmat(1:3,1:3)=[MR,0,0;0,MR,0;0,0,MR];
massmat(1:3,4:6)=zeros(3);
massmat(4:6,1:3)=zeros(3);
massmat(4:6,4:6)=IR;

invmass=inv(massmat);


%*************************************************************************
%              UMBILICAL AND ACTUATOR STIFFNESS PROPERTIES
%                       (MEASURED ON ORBIT)
%*************************************************************************

% MINIMUM UMBILICAL STIFFNESS TEST RESULTS

Kmu=[64.5,3.6,2.6,4.5,-194,31;
3.6,54.5,0,145,-12,-17;
2.6,0,49.2,-20,11,5;
4.5,145,-20,503,-29,-54;
-194,-12,11,-29,662,-86;
31,-17,5,-54,-86,72.4];


% PARTIAL UMBILICAL STIFFNESS RESULTS

Kpu=[102,7.6,-3.1,9.6,-293,66;
7.6,81.6,-2.9,230,-21,-0.7;
-3.1,-2.9,81.3,-52,5.8,8;
9.6,230,-52,720,-66,-18;
```

```
-293,-21,5.8,-66,923,-181;
66,-0.7,8,-18,-181,106];



%*****************************************************************************************
%                              ACCELEROMETER GEOMETRY
%                        (THIS SECTION PROVIDED BY ARIS DEVELOPERS)
%*****************************************************************************************

%clear msv
centocg=[0,0,0];
rhead1=[-17.7 14.1 27.9]-centocg;
rhead2=[-17.7 11.2 -31.5]-centocg;
rhead3=[17.7 11.2 -31.5]-centocg;
racc1=(rhead1)/12;
racc2=(rhead1)/12;
racc3=(rhead2)/12;
racc4=(rhead2)/12;
racc5=(rhead2)/12;
racc6=(rhead3)/12;
racc7=(rhead3)/12;
racc8=(rhead3)/12;

phia=0;
phib=pi/4;
phic=-pi/4;

cp=cos(phia);
sp=sin(phia);
ry=[cp 0 -sp;0 1 0;sp 0 cp];
acc1=[sqrt(2)/2 sqrt(2)/2 0];
acc2=[-sqrt(2)/2 sqrt(2)/2 0];
acc1=(ry*acc1')';
acc2=(ry*acc2')';


cp=cos(phib);
sp=sin(phib);
rz=[cp -sp 0;sp cp 0;0 0 1];
acc3=[sqrt(2)/2 0.5 0.5];
acc4=[-sqrt(2)/2 0.5 0.5];
acc5=[0 -1 1]/sqrt(2);
acc3=(rz*acc3')';
acc4=(rz*acc4')';
acc5=(rz*acc5')';

cp=cos(phic);
sp=sin(phic);
rz=[cp -sp 0;sp cp 0;0 0 1];
acc6=[sqrt(2)/2 0.5 0.5];
acc7=[-sqrt(2)/2 0.5 0.5];
acc8=[0 -1 1]/sqrt(2);
acc6=(rz*acc6')';
```

```
acc7=(rz*acc7')';
acc8=(rz*acc8')';
max1=0;

% ROTACC=[0.7071  -0.7071  0.1464 -0.8536  0.5000  -0.3000  -0.6660  //0.6830;
%  0.7071   0.7071   0.8536  -0.1464  -0.5000   0.8124  -0.5536  //-0.1830;
% 0.0000   0.0000   0.5000   0.5000   0.7071   0.5000   0.5000  //0.7071]
% acc1=(rotacc(:,1))';
% acc2=(rotacc(:,2))';
% acc3=(rotacc(:,3))';
% acc4=(rotacc(:,4))';
% acc5=(rotacc(:,5))';
% acc6=(rotacc(:,6))';
% acc7=(rotacc(:,7))';
% acc8=(rotacc(:,8))';

rot1=cross(racc1,acc1);
rot2=cross(racc2,acc2);
rot3=cross(racc3,acc3);
rot4=cross(racc4,acc4);
rot5=cross(racc5,acc5);
rot6=cross(racc6,acc6);
rot7=cross(racc7,acc7);
rot8=cross(racc8,acc8);
rotacc=[acc1' acc2' acc3' acc4' acc5' acc6' acc7' acc8']
M=[acc1 rot1;
  acc2 rot2;
  acc3 rot3;
  acc4 rot4;
  acc5 rot5;
  acc6 rot6;
  acc7 rot7;
  acc8 rot8];

for l=1:8, ...
b=eye(8,8); ...
b(l,l)=0; ...
mnew=b*M; ...
msv(l)=min(svd(mnew)); ...
end; ...
msv

for k=1:8, ...
for j=1:8, ...
b=eye(8,8); ...
b(k,k)=0; ...
b(j,j)=0; ...
mnew=b*M; ...
minsv(j,k)=min(svd(mnew)); ...
end; ...
end;
failmsv=minsv
minsv(1:2,1:2)=[10 10;10 10]; ...
mminsv=min(minsv);
```

```
zro= 0*ones(1,3);
Twtom= [acc1  zro   zro;
        acc2  zro   zro;
        zro   acc3  zro;
        zro   acc4  zro;
        zro   acc5  zro;
        zro   zro   acc6;
        zro   zro   acc7;
        zro   zro   acc8]


%*****************************************************************************************
%                                  ACTUATOR GEOMETRY
%                        (THIS SECTION PROVIDED BY ARIS DEVELOPERS)
%*****************************************************************************************

lowl_to_nate=[0 -1.008 0];
lowl_to_lpivot=[-1.08 -25.58 1.922];
lpivot_to_modc=[20.5 -45.5 36.2];
nate_to_cg=[19.56 -12.93 38.40];
modtocg = -lpivot_to_modc-lowl_to_lpivot+lowl_to_nate+nate_to_cg;

%pushrod flex joint point on actuator lever arm
r1=([-17.8 47.2 -31.3]-modtocg)/12;
r2=([-18.6 64.2 -29.7]-modtocg)/12;
r3=([17.8 47.2 -31.3]-modtocg)/12;
r4=([18.6 64.2 -29.7]-modtocg)/12;
r5=([13.2 68.6 -42.2]-modtocg)/12;
r6=([-13.2 68.6 -42.2]-modtocg)/12;
r7=([3.9 47.9 39.3]-modtocg)/12;
r8=([-3.9 47.9 39.3]-modtocg)/12;
ract= [r1' r2' r3' r4' r5' r6' r7' r8'];
%
%pushrod flex joint point at end of pushrod
re1=([-17.8 67.5 -42.6]-modtocg)/12;
re2=([-18.6 48.4 -42.4]-modtocg)/12;
re3=([17.8 67.5 -42.6]-modtocg)/12;
re4=([18.6 48.4 -42.4]-modtocg)/12;
re5=([0.9 59.6 -40.2]-modtocg)/12;
re6=([-0.9 59.6 -40.2]-modtocg)/12;
re7=([10.7 72.4 39.3]-modtocg)/12;
re8=([-10.7 72.4 39.3]-modtocg)/12;
rend= [re1' re2' re3' re4' re5' re6' re7' re8'];
%
rd= rend - ract;
%
% pushrod unit vectors in rack coordinates
rd1norm=rd(:,1)/norm(rd(:,1));
rd2norm=rd(:,2)/norm(rd(:,2));
rd3norm=rd(:,3)/norm(rd(:,3));
rd4norm=rd(:,4)/norm(rd(:,4));
rd5norm=rd(:,5)/norm(rd(:,5));
rd6norm=rd(:,6)/norm(rd(:,6));
rd7norm=rd(:,7)/norm(rd(:,7));
```

```
rd8norm=rd(:,8)/norm(rd(:,8));
rdnorm=[rd1norm rd2norm rd3norm rd4norm rd5norm rd6norm rd7norm rd8norm];
%
% lever arm unit vector direction in rack coordinates
rarm1=[0 -1.1 -2.8]'/3.00832;
rarm2=[0 1.5 -2.6]'/3.0017;
rarm3=[0 -1.1 -2.8]'/3.00832;
rarm4=[0 1.5 -2.6]'/3.0017;
rarm5=[1.3 -2.7 0]'/2.99666;
rarm6=[-1.3 -2.7 0]'/2.99666;
rarm7=[-2.8 1.2 0]'/3.0463;
rarm8=[2.8 1.2 0]'/3.0463;
%
% cg to actuator hinge point vector
r=3/12;
r1o=r1-r*rarm1';
r2o=r2-r*rarm2';
r3o=r3-r*rarm3';
r4o=r4-r*rarm4';
r5o=r5-r*rarm5';
r6o=r6-r*rarm6';
r7o=r7-r*rarm7';
r8o=r8-r*rarm8';
%
% complete the right handed coordinate system
rz1=cross(rarm1',rd1norm');
rz2=cross(rarm2',rd2norm');
rz3=cross(rarm3',rd3norm');
rz4=cross(rarm4',rd4norm');
rz5=cross(rarm5',rd5norm');
rz6=cross(rarm6',rd6norm');
rz7=cross(rarm7',rd7norm');
rz8=cross(rarm8',rd8norm');
%
% compute the transformation maping vectors in local actuator
% centered coordinates to center of mass coordinates
rot1=[rarm1 rd1norm rz1'];
rot2=[rarm2 rd2norm rz2'];
rot3=[rarm3 rd3norm rz3'];
rot4=[rarm4 rd4norm rz4'];
rot5=[rarm5 rd5norm rz5'];
rot6=[rarm6 rd6norm rz6'];
rot7=[rarm7 rd7norm rz7'];
rot8=[rarm8 rd8norm rz8'];


zero= 0*ones(3);
t1= [rot1' zero;zero rot1'];
t2= [rot2' zero;zero rot2'];
t3= [rot3' zero;zero rot3'];
t4= [rot4' zero;zero rot4'];
t5= [rot5' zero;zero rot5'];
t6= [rot6' zero;zero rot6'];
t7= [rot7' zero;zero rot7'];
```

```
t8= [rot8' zero;zero rot8'];
wr= [r1o' r2o' r3o' r4o' r5o' r6o' r7o' r8o'];
wt= [t1 t2 t3 t4 t5 t6 t7 t8];
m= 0;...
bigx= 0*ones(48,6);
bigxt= 0*ones(6,48);
%
for j= 1:8,...
rc(1,1)= 0;...
rc(2,2)= 0;...
rc(3,3)= 0;...
rc(1,2)= -wr(3,j);...
rc(1,3)= wr(2,j);...
rc(2,3)= -wr(1,j);...
rc(2,1)= -rc(1,2);...
rc(3,1)= -rc(1,3);...
rc(3,2)= -rc(2,3);...
c= [eye(3) -rc;zero eye(3)];...
for k= 1:6;...
for l= 1:6;...
t(k,l)= wt(k,l+m);...
end,...
end,...
x= t*c;...
xt= x';...
for k= 1:6,...
for l= 1:6,...
bigx(k+m,l)= x(k,l);...
bigxt(k,l+m)= xt(k,l);...
end,...
end,...
m= m+6;...
end

%*****************************************************************************************
%                    STIFFNESS MATRICES FOR ACTUATORS IN LOCAL COORDINATES
%                                (THIS SECTION PROVIDED BY ARIS DEVELOPERS)
%*****************************************************************************************

l1=23.3/12;l2=20.2/12;l3=23.3/12;l4=20.2/12;
l5=15.4/12;l6=15.4/12;l7=25.4/12;l8=25.4/12;
%
k1= .5/12;
k3=  .5/12;
k4=  .5/12;
kp= .5/12;
%
ks133= (k3+k4)/(l1*l1)+kp/(r*r);...
ks1=[(k3+k4)/(l1*l1), k3/r/l1,  0,    0,    0,    0
    k3/r/l1, (k1+k3)/(r*r),   0,    0,    0,   k1/r
     0,    0,    ks133 , k3/l1,   -r*(k3+k4)/(l1*l1)+kp/r,  0
     0,    0,    k3/l1,         k3,       -r*k3/l1,       0
     0,    0, -r*(k3+k4)/(l1*l1)+kp/r, -r*k3/l1, (r*r)*(k3+k4)/(l1*l1)+kp, 0
     0,   k1/r,       0,         0,         0,          k1];
```

```
gam1= [-(k3+k4)/(l1*l1),    0,      0,          0,      0,  k4/l1
       -k3/(r*l1),   -k1/(r*r),  0,          0,      0,   0
         0,           0   -(k3+k4)/(l1*l1),  k4/l1,  -kp/r,   0
         0,           0,   -k3/l1,        0,      0,    0
         0,           0, r*(k3+k4)/(l1*l1),-r*k4/l1,  -kp    0
         0,         -k1/r,     0,          0,      0,    0];

ks233= (k3+k4)/(l2*l2)+kp/(r*r);...

ks2=[(k3+k4)/(l2*l2), k3/r/l2,   0,    0,    0,    0
    k3/r/l2, (k1+k3)/(r*r),    0,    0,    0,   k1/r
     0,    0,    ks233,   k3/l2,   -r*(k3+k4)/(l2*l2)+kp/r, 0
     0,    0,    k3/l2,         k3,       -r*k3/l2,       0
     0,    0, -r*(k3+k4)/(l2*l2)+kp/r, -r*k3/l2, (r*r)*(k3+k4)/(l2*l2)+kp, 0
     0,   k1/r,       0,         0,         0,          k1];

gam2= [-(k3+k4)/(l2*l2),    0,      0,          0,      0,  k4/l2
       -k3/(r*l2),   -k1/(r*r),  0,          0,      0,   0
         0,           0   -(k3+k4)/(l2*l2),  k4/l2,  -kp/r,   0
         0,           0,   -k3/l2,        0,      0,    0
         0,           0, r*(k3+k4)/(l2*l2),-r*k4/l2,  -kp    0
         0,         -k1/r,     0,          0,      0,    0];


ks333= (k3+k4)/(l3*l3)+kp/(r*r);...

ks3=[(k3+k4)/(l3*l3), k3/r/l3,   0,    0,    0,    0
    k3/r/l3, (k1+k3)/(r*r),    0,    0,    0,   k1/r
     0,    0,    ks333,   k3/l3,   -r*(k3+k4)/(l3*l3)+kp/r, 0
     0,    0,    k3/l3,         k3,       -r*k3/l3,       0
     0,    0, -r*(k3+k4)/(l3*l3)+kp/r, -r*k3/l3, (r*r)*(k3+k4)/(l3*l3)+kp, 0
     0,   k1/r,       0,         0,         0,          k1];

gam3= [-(k3+k4)/(l3*l3),    0,      0,          0,      0,  k4/l3
       -k3/(r*l3),   -k1/(r*r),  0,          0,      0,   0
         0,           0   -(k3+k4)/(l3*l3),  k4/l3,  -kp/r,   0
         0,           0,   -k3/l3,        0,      0,    0
         0,           0, r*(k3+k4)/(l3*l3),-r*k4/l3,  -kp    0
         0,         -k1/r,     0,          0,      0,    0];

ks433= (k3+k4)/(l4*l4)+kp/(r*r);...

ks4=[(k3+k4)/(l4*l4), k3/r/l4,   0,    0,    0,    0
    k3/r/l4, (k1+k3)/(r*r),    0,    0,    0,   k1/r
     0,    0,    ks433,   k3/l4,   -r*(k3+k4)/(l4*l4)+kp/r, 0
     0,    0,    k3/l4,         k3,       -r*k3/l4,       0
     0,    0, -r*(k3+k4)/(l4*l4)+kp/r, -r*k3/l4, (r*r)*(k3+k4)/(l4*l4)+kp, 0
     0,   k1/r,       0,         0,         0,          k1];

gam4= [-(k3+k4)/(l4*l4),    0,      0,          0,      0,  k4/l4
       -k3/(r*l4),   -k1/(r*r),  0,          0,      0,   0
         0,           0   -(k3+k4)/(l4*l4),  k4/l4,  -kp/r,   0
         0,           0,   -k3/l4,        0,      0,    0
```

```
          0,          0, r*(k3+k4)/(l4*l4),-r*k4/l4, -kp    0
          0,       -k1/r,    0,          0,      0,    0];

 ks533= (k3+k4)/(l5*l5)+kp/(r*r);...

 ks5=[(k3+k4)/(l5*l5), k3/r/l5,  0,    0,    0,    0
     k3/r/l5, (k1+k3)/(r*r),   0,    0,    0,   k1/r
      0,    0,   ks533,   k3/l5,   -r*(k3+k4)/(l5*l5)+kp/r, 0
      0,    0,   k3/l5,        k3,       -r*k3/l5,      0
      0,    0, -r*(k3+k4)/(l5*l5)+kp/r, -r*k3/l5, (r*r)*(k3+k4)/(l5*l5)+kp, 0
      0,  k1/r,      0,        0,        0,          k1];

 gam5= [-(k3+k4)/(l5*l5),    0,      0,          0,      0,  k4/l5
        -k3/(r*l5),   -k1/(r*r),  0,          0,      0,    0
          0,          0   -(k3+k4)/(l5*l5),  k4/l5,  -kp/r,   0
          0,          0,   -k3/l4,        0,      0,    0
          0,          0, r*(k3+k4)/(l5*l5),-r*k4/l5,  -kp    0
          0,       -k1/r,    0,          0,      0,    0];

 ks633= (k3+k4)/(l6*l6)+kp/(r*r);...

 ks6=[(k3+k4)/(l6*l6), k3/r/l6,  0,    0,    0,    0
     k3/r/l6, (k1+k3)/(r*r),   0,    0,    0,   k1/r
      0,    0,   ks633,   k3/l6,   -r*(k3+k4)/(l6*l6)+kp/r, 0
      0,    0,   k3/l6,        k3,       -r*k3/l6,      0
      0,    0, -r*(k3+k4)/(l6*l6)+kp/r, -r*k3/l6, (r*r)*(k3+k4)/(l6*l6)+kp, 0
      0,  k1/r,      0,        0,        0,          k1];

 gam6= [-(k3+k4)/(l6*l6),    0,      0,          0,      0,  k4/l6
        -k3/(r*l6),   -k1/(r*r),  0,          0,      0,    0
          0,          0   -(k3+k4)/(l6*l6),  k4/l6,  -kp/r,   0
          0,          0,   -k3/l6,        0,      0,    0
          0,          0, r*(k3+k4)/(l6*l6),-r*k4/l6,  -kp    0
          0,       -k1/r,    0,          0,      0,    0];

 ks733= (k3+k4)/(l7*l7)+kp/(r*r);...

 ks7=[(k3+k4)/(l7*l7), k3/r/l7,  0,    0,    0,    0
     k3/r/l7, (k1+k3)/(r*r),   0,    0,    0,   k1/r
      0,    0,   ks733,   k3/l7,   -r*(k3+k4)/(l7*l7)+kp/r, 0
      0,    0,   k3/l7,        k3,       -r*k3/l7,      0
      0,    0, -r*(k3+k4)/(l7*l7)+kp/r, -r*k3/l7, (r*r)*(k3+k4)/(l7*l7)+kp, 0
      0,  k1/r,      0,        0,        0,          k1];

 gam7= [-(k3+k4)/(l7*l7),    0,      0,          0,      0,  k4/l7
        -k3/(r*l7),   -k1/(r*r),  0,          0,      0,    0
          0,          0   -(k3+k4)/(l7*l7),  k4/l7,  -kp/r,   0
          0,          0,   -k3/l7,        0,      0,    0
          0,          0, r*(k3+k4)/(l7*l7),-r*k4/l7,  -kp    0
          0,       -k1/r,    0,          0,      0,    0];

 ks833= (k3+k4)/(l8*l8)+kp/(r*r);...

 ks8=[(k3+k4)/(l8*l8), k3/r/l8,  0,    0,    0,    0
```

```
    k3/r/l8, (k1+k3)/(r*r),   0,    0,    0,   k1/r
     0,    0,   ks833,    k3/l8,   -r*(k3+k4)/(l8*l8)+kp/r, 0
     0,    0,   k3/l8,        k3,       -r*k3/l8,      0
     0,    0, -r*(k3+k4)/(l8*l8)+kp/r, -r*k3/l8, (r*r)*(k3+k4)/(l8*l8)+kp, 0
     0,  k1/r,      0,        0,        0,          k1];

gam8= [-(k3+k4)/(l8*l8),    0,      0,          0,      0,  k4/l8
       -k3/(r*l8),   -k1/(r*r),  0,          0,      0,    0
         0,           0   -(k3+k4)/(l8*l8),  k4/l8,  -kp/r,   0
         0,           0,   -k3/l8,         0,      0,    0
         0,           0, r*(k3+k4)/(l8*l8),-r*k4/l8,  -kp    0
         0,         -k1/r,     0,          0,      0,    0];


%*************************************************************************************
%                  AGGREGATE ACTUATOR STIFFNESS IN CENTER OF MASS COORDINATES
%                            (THIS SECTION PROVIDED BY ARIS DEVELOPERS)
%*************************************************************************************

zro= 0*ones(6);...
bigk= [ks1 zro zro zro zro zro zro zro;
    zro ks2 zro zro zro zro zro zro;
    zro zro ks3 zro zro zro zro zro;
    zro zro zro ks4 zro zro zro zro;
    zro zro zro zro ks5 zro zro zro;
    zro zro zro zro zro ks6 zro zro;
    zro zro zro zro zro zro ks7 zro;
    zro zro zro zro zro zro zro ks8];

ks= bigxt*bigk*bigx;

gamx= gam1*t1+gam2*t2+gam3*t3+gam4*t4+gam5*t5+gam6*t6+gam7*t7+gam8*t8;


%*************************************************************************************
%TRANSFORMATION FROM CONTROL INPUTS TO FORCE COMPONENTS FOR EXCITING
%FLEXIBLE MODES
%                  (THIS SECTION PROVIDED BY ARIS DEVELOPERS)
%*************************************************************************************

zro= 0*ones(3,1);
Tutow= [rd1norm  zro   zro   zro   zro   zro   zro  zro;
      zro  rd2norm zro   zro   zro   zro   zro  zro
      zro   zro  rd3norm zro   zro   zro   zro  zro;
      zro   zro   zro  rd4norm zro   zro   zro  zro
      zro   zro   zro   zro  rd5norm zro   zro  zro
      zro   zro   zro   zro   zro  rd6norm zro  zro
      zro   zro   zro   zro   zro   zro  rd7norm zro
      zro   zro   zro   zro   zro   zro    zro rd8norm]


%*************************************************************************************
```

```
%RESOLVE ACTUATOR FORCE DIRECTIONS ALONG RACK COORDINATES TO COMPUTE
%FORCE
%                       AND TORQUE INPUTS FROM THE ACTUATORS
%                       (THIS SECTION PROVIDED BY ARIS DEVELOPERS)
%*************************************************************************************

[u1,x]= crossudf(ract(:,1)',rd1norm');
[u2,x]= crossudf(ract(:,2)',rd2norm');
[u3,x]= crossudf(ract(:,3)',rd3norm');
[u4,x]= crossudf(ract(:,4)',rd4norm');
[u5,x]= crossudf(ract(:,5)',rd5norm');
[u6,x]= crossudf(ract(:,6)',rd6norm');
[u7,x]= crossudf(ract(:,7)',rd7norm');
[u8,x]= crossudf(ract(:,8)',rd8norm');
Tutox= [rd1norm rd2norm rd3norm rd4norm rd5norm rd6norm rd7norm rd8norm;
      u1'   u2'    u3'    u4'    u5'    u6'    u7'   u8'  ]

Tutox(:,7)=zeros(6,1);
%*************************************************************************************
%              RESOLVE RIGID BODY MOTION ALONG THE ACTUATOR PUSHRODS
%                       (THIS SECTION PROVIDED BY ARIS DEVELOPERS)
%*************************************************************************************

[x,y,rc1]= crossudf(zro',ract(:,1)');
[x,y,rc2]= crossudf(zro',ract(:,2)');
[x,y,rc3]= crossudf(zro',ract(:,3)');
[x,y,rc4]= crossudf(zro',ract(:,4)');
[x,y,rc5]= crossudf(zro',ract(:,5)');
[x,y,rc6]= crossudf(zro',ract(:,6)');
[x,y,rc7]= crossudf(zro',ract(:,7)');
[x,y,rc8]= crossudf(zro',ract(:,8)');
Txa1= [eye(3) -rc1];
Txa2= [eye(3) -rc2];
Txa3= [eye(3) -rc3];
Txa4= [eye(3) -rc4];
Txa5= [eye(3) -rc5];
Txa6= [eye(3) -rc6];
Txa7= [eye(3) -rc7];
Txa8= [eye(3) -rc8];
Txtop= Tutow'*[Txa1;Txa2;Txa3;Txa4;Txa5;Txa6;Txa7;Txa8]
xp= Txtop;
Tptox= inv(xp'*xp)*xp'
xp=Txtop;
Tptox=inv(xp'*xp)*xp';

%*************************************************************************************
%              MAP RIGID BODY ACCELERATION TO ACCELEROMTER LOCATIONS
%                       (THIS SECTION PROVIDED BY ARIS DEVELOPERS)
%*************************************************************************************

   rc1= [ -17.7 14.1 27.9 ]/12;
   rc2= [ -17.7 11.2 -31.5]/12;
   rc3= [ 17.7 11.2 -31.5 ]/12;
[x,y,rcc1]= crossudf(rc1,rc1);
```

```
[x,y,rcc2]= crossudf(rc2,rc2);
[x,y,rcc3]= crossudf(rc3,rc3);
Txtow= [eye(3) -rcc1;
      eye(3) -rcc2;
      eye(3) -rcc3]
Twtom
Txtom= Twtom*Txtow
Tmtox= pinv(Txtom)
checkXtoX= Tmtox*Txtom


%*****************************************************************************************
%       TRANSFORMATION OF ACCELERATION COMMANDS TO ACTUATOR COMMANDS
%                          (THIS SECTION PROVIDED BY ARIS DEVELOPERS)
%*****************************************************************************************

[tor1,x1,x2]= crossudf(ract(:,1)',rd(:,1)');
[tor2,x1,x2]= crossudf(ract(:,2)',rd(:,2)');
[tor3,x1,x2]= crossudf(ract(:,3)',rd(:,3)');
[tor4,x1,x2]= crossudf(ract(:,4)',rd(:,4)');
[tor5,x1,x2]= crossudf(ract(:,5)',rd(:,5)');
[tor6,x1,x2]= crossudf(ract(:,6)',rd(:,6)');
[tor7,x1,x2]= crossudf(ract(:,7)',rd(:,7)');
[tor8,x1,x2]= crossudf(ract(:,8)',rd(:,8)');
ttor= [tor1' tor2' tor3' tor4' tor5' tor6' tor7' tor8'];
for i= 1:8,...
  mag= norm(ttor(:,i));...
  ttoru(:,i)= ttor(:,i)/mag;...
end
Tdelxtou= [rd1norm' ttoru(:,1)'/norm(ract(:,1));
        rd2norm' ttoru(:,2)'/norm(ract(:,2));
        rd3norm' ttoru(:,3)'/norm(ract(:,3));
        rd4norm' ttoru(:,4)'/norm(ract(:,4));
        rd5norm' ttoru(:,5)'/norm(ract(:,5));
        rd6norm' ttoru(:,6)'/norm(ract(:,6));
        rd7norm' ttoru(:,7)'/norm(ract(:,7));
        rd8norm' ttoru(:,8)'/norm(ract(:,8))];
Tdelxtou= pinv(Tutox)
checkxtox= Tutox*Tdelxtou

%*****************************************************************************************
%       ESTIMATION OF STIFFNESS QUANTITIES FOR THE ENTIRE SYSTEM
%*****************************************************************************************

%POSITION VECTOR OF THE CENTROID OF THE UMBILICAL CONNECTION, MEASURED
%RELATIVE TO THE CENTER OF MASS OF THE RACK, IN RACK EQUILIBRIUM
%COORDINATES (FT)

dvect=[-0.363, -0.342, -2.42];

% SECOND ORDER TENSOR ASSOCIATED WITH dvect

dtens=[0 -dvect(3) dvect(2); dvect(3) 0 -dvect(1); -dvect(2) dvect(1) 0];
```

```
%ESTIMATION OF STIFFNESS PARAMETERS FROM MEASURED STIFFNESS ON ORBIT

%USE MINIMUM UMBILICAL DATA FROM DIAGONAL OF UPPER LEFT MINOR TO COMPUTE
6-DOF STIFFNESS MATRIX
%SUBTRACT ACTUATOR STIFFNESS
kx=Kmu(1,1)-ks(1,1);
ky=Kmu(2,2)-ks(2,2);
kz=Kmu(3,3)-ks(3,3);
kxy=Kmu(1,2)-ks(1,2);
kxz=Kmu(1,3)-ks(1,3);
kyz=Kmu(2,3)-ks(2,3);

Ktr=zeros(3);
Ktr(1,1)=kx;
Ktr(2,2)=ky;
Ktr(3,3)=kz;
Ktr(1,2)=kxy;
Ktr(1,3)=kxz;
Ktr(2,1)=Ktr(1,2);
Ktr(2,3)=kyz;
Ktr(3,1)=Ktr(1,3);
Ktr(3,2)=Ktr(2,3);


Kumb=zeros(6);
Kumb(1:3,1:3)=Ktr;
Kumb(1:3,4:6)=-Ktr*dtens;
Kumb(4:6,1:3)=dtens*Ktr;
Kumb(4:6,4:6)=-dtens*Ktr*dtens;

% COMPUTE ESTIMATED TOTAL UMBILICAL CONTRIBUTION TO LOWER RIGHT MINOR

KLR=Kmu(4:6,4:6)-ks(4:6,4:6);

% COMPUTE ESTIMATED TORSIONAL STIFFNESS OF THE UMBILICALS

Ktor=zeros(3);
Ktor=KLR-Kumb(4:6,4:6);
Kumb(4:6,4:6)=Kumb(4:6,4:6)+Ktor;

%K=Kumb+Ks;



%*************************************************************************
%EIGENVALUES AND EIGENVECTORS OF SYSTEM WITH UMBILICALS AND ACTUATORS
%                                    AND
%APPROXIMATION OF PHYSICAL DAMPING MATRIX FOR UMBILICALS AND ACTUATORS
%*************************************************************************

%TOTAL STIFFNESS: UMBILICALS AND ACTUATORS

K=Kmu;
```

```
[V,D]=eig(invmass*K);

%NORMALIZED EIGENVECTORS

massdiag=V'*massmat*V;

for i=1:6
phi(:,i)=V(:,i)/(massdiag(i,i))^0.5;
end

%APPROXIMATION FOR UMBILICAL AND ACTUATOR DAMPING IN PHYSICAL
COORDINATES

C=inv(phi')*2*0.015*D.^0.5*inv(phi);


%*****************************************************************************
%                              AUXILLIARY PARAMETERS
%*****************************************************************************


twozeta=0.03*eye(6);
intoft=0.08333*eye(9);

%Decoupling Parameters
%These are for the B1G_B2 test
%cg Decoupling (ft)
cgx=0.015;
cgy=0.02;
cgz=0.065;

idm=massmat;
ctm=eye(6,6);
ctmi=eye(6,6);
ctmcg=[0, cgz,-cgy;
    -cgz,0,cgx;
    cgy,-cgx,0];

ctm(1:3,4:6)=ctmcg;
ctmi(4:6,1:3)=-ctmcg;

pk=zeros(6);
pk=-K;
w2=1.4;
for i=1:6
pk(i,i)=w2*w2*massmat(i,i)-K(i,i);
end

% Off-diagonal (rotational) stiffness cancellation matrix
% elements set to zero for RME
pk(4,5)=0;
pk(4,6)=0;
pk(5,4)=0;
pk(5,6)=0;
```

```
pk(6,4)=0;
pk(6,5)=0;

Gain=1*eye(6);
Gain1=1*eye(6);


%Position vector of the pth disturber, relative to the rack center of mass
rpvect=[1.75,1.59,3.17];
rptens=[0,-rpvect(1,3),rpvect(1,2);
        rpvect(1,3),0,-rpvect(1,1);
        -rpvect(1,2),rpvect(1,1),0];


%*************************************************************************
%                          Plotting Routines
%*************************************************************************

% Closed-loop State-space realization: Continuous TF
w=logspace(-3,2,150);
whz=w/6.28;
[Acl,Bcl,Ccl,Dcl]=linmod('rme_clh');
[mag,phase]=bode(Acl,Bcl,Ccl,Dcl,3,w);
maglh=log10(mag)
%semilogx(whz,20*maglh(:,1))
%grid
%axis([.001 10 -60 10])

%[Acl,Bcl,Ccl,Dcl]=linmod('rme_clb');
%[mag,phase]=bode(Acl,Bcl,Ccl,Dcl,1,w);
%maglb=log10(mag);

%semilogx(whz,20*maglh(:,1),'y--',whz,20*maglb(:,1),'y')
%grid
%axis([.001 10 -60 10])



% Set up vector to hold border frequencies of the 1/3
% octave bands.  Start at 6 Hz.
wtob=zeros(13,1);
sz_wtob=size(wtob);
wtob(1)=6.00000000;
%Find starting and ending points for 1/3 octave breakdown
for i=1:sz_wtob(1,1)-1;
wtob(i+1)=wtob(i)/2;
end
%Find border points for the 1/3 octaves over full
%bandwidth
pow_teni=log10(wtob(13));
pow_tenf=log10(wtob(1));

wbord=logspace(pow_teni,pow_tenf,sz_wtob(1,1)*3-2)';
```

```
%Compute center freqencies of 1/3 octave bands
wcf=zeros((sz_wtob-1)*3,1);
for i=1:(sz_wtob-1)*3
wcf(i)=(wbord(i)+wbord(i+1))/2;
end

%Average Transfer Function over 1/3 Octaves
count=zeros((sz_wtob-1)*3,1);
magtot=zeros((sz_wtob-1)*3,1);
magave=zeros((sz_wtob-1)*3,1);

%sort data into 1/3 octave bands and average
for i=1:150
for j=1:(sz_wtob-1)*3
if whz(i)>=wbord(j) & whz(i)<=wbord(j+1)
magtot(j)=magtot(j)+mag(i);
count(j)=count(j)+1;
end
end
end


for j=1:(sz_wtob-1)*3
magave(j)=magtot(j)/count(j);
maglave(j)=log10(magave(j));
end

%x-dir atten. in dB from page 126
gnx=[-6.25,-8.74,-8.125,-12.5,-13.75,-16.9,-18.8,-18.8,-22,-22.5,-25,-27.5,-28.1,-28.8,-30.6];

%y-dir atten. from page 127
gny=[-6.5,-9.4,-11.8,-13.5,-14.7,-16.3,-17.6,-21.2,-22.9,-24.1,-22.4,-24.7,-31.8,-29.4,-30.6];

%z-dir atten. from pg. 128
gnz=[-8.75,-6.25,-8.1,-8.8,-12.5,-13.1,-16.3,-16.3,-17.3,-17,-18.1,-21.3,-23.8,-22,-23.1]

semilogx(wcf,20*maglave,'*',wcf(15:29),gnz,'o');
axis([.001 10 -60 10])


for i=1:3
[Acl,Bcl,Ccl,Dcl]=linmod('rme_clh');
[mag,phase]=bode(Acl,Bcl,Ccl,Dcl,i,w);
magl(:,i)=log10(mag);
PHASE(:,i)=phase
end
semilogx(whz,20*magl(:,1),'y',whz,20*magl(:,2),'y--',whz,20*magl(:,3),'y.');
axis([.001 10 -150 40]);
```

REPORT DOCUMENTATION PAGE

Form Approved
OMB No. 0704-0188

1. AGENCY USE ONLY (Leave blank)	2. REPORT DATE	3. REPORT TYPE AND DATES COVERED
	March 1998	Contractor Report

4. TITLE AND SUBTITLE

Development of a Simulation Capability for the Active Rack Isolation System

5. FUNDING NUMBERS

NCC1-104

963-89-00-01

6. AUTHOR(S)

Terry L. Johnson
Robert H. Tolson

7. PERFORMING ORGANIZATION NAME(S) AND ADDRESS(ES)

The George Washington University
Joint Institute for Advancement of Flight Sciences
NASA Langley Research Center
Hampton, VA 23681-2199

8. PERFORMING ORGANIZATION REPORT NUMBER

9. SPONSORING/MONITORING AGENCY NAME(S) AND ADDRESS(ES)

National Aeronautics and Space Administration
Langley Research Center
Hampton, VA 23681-2199

10. SPONSORING/MONITORING AGENCY REPORT NUMBER

NASA/CR-1998-206942

11. SUPPLEMENTARY NOTES

The information submitted in this report was offered as a thesis by the first author in partial fulfillment of the requirements for the Degree of Master of Science, The George Washington University, JIAFS. Langley Technical Monitor:Dr. M. G. Gilbert

12a. DISTRIBUTION/AVAILABILITY STATEMENT

Unclassified - Unlimited
Subject Category 18
Distribution Nonstandard
Availability: NASA CASI (301) 621-0290

12b. DISTRIBUTION CODE

13. ABSTRACT *(Maximum 200 words)*

To realize quality microgravity science on the International Space Station, many microgravity facilities will utilize the Active Rack Isolation System (ARIS). Simulation capabilities for ARIS will be needed to predict the microgravity environment. This paper discusses the development of a simulation model for use in predicting the performance of the ARIS in attenuating disturbances with frequency content between 0.01 Hz and 10Hz. The derivation of the model utilizes an energy-based approach. The complete simulation includes the dynamic model of the ISPR integrated with the model for the ARIS controller so that the entire closed-loop system is simulated. Preliminary performance predictions are made for the ARIS in attenuating both off-board disturbances as well as disturbances from hardware mounted onboard the microgravity facility. These predictions suggest that the ARIS does eliminate resonant behavior detrimental to microgravity experimentation. A limited comparison is made between the simulation predictions of ARIS attenuation of off-board disturbances and results from the ARIS flight test. These comparisons show promise, but further tuning of the simulation is needed.

14. SUBJECT TERMS

Microgravity, vibration isolation,
Active Rack Isolation System, ARIS,
International Space Station Alpha

15. NUMBER OF PAGES

192

16. PRICE CODE

A09

17. SECURITY CLASSIFICATION OF REPORT	18. SECURITY CLASSIFICATION OF THIS PAGE	19. SECURITY CLASSIFICATION OF ABSTRACT	20. LIMITATION OF ABSTRACT
Unclassified	Unclassified	Unclassified	